MICROBIAL COMMUNITIES IN THE GUANA TOLOMATO MATANZAS NATIONAL ESTUARINE RESEARCH RESERVE: AN ASSESSMENT OF THE RESPONSES OF *SPARTINA ALTERNIFLORA* EPIPHYTES TO NITROGEN ENRICHMENT, AND A CHARACTERIZATION OF BENTHIC CYANOBACTERIAL DIVERSITY

By

Anne Hurley

A thesis submitted to the Department of Biology in partial fulfillment of the requirement for the degree of Master of Science in Biology

University of North Florida

College Of Arts and Science

December 2023

Anne Hurley

Contents

Acknowledgements

Thank you to my advisor, Dr. Dale Casamatta, for encouraging me to seize new and exciting opportunities—whether that meant presenting my research at a conference or isolating cyanobacteria from a strange and unexpected location—and for reading and responding to all of my long, rambling emails. Thank you to my other wonderful committee members, Dr. Nikki Dix and Dr. Samantha Chapman, whose guidance and feedback throughout this process greatly expanded my understanding of salt marsh (and mangrove!) ecosystems, and helped me to see—and appreciate—algae in a new light. Thank you to the Friends of the Guana Tolomato Matanzas National Estuarine Research Reserve for awarding me the Friends of GTMNERR Graduate Fellowship—this research would not have been possible without your generous support, and I am honored to have been given this opportunity to contribute to the extensive body of research that has taken place at GTMNERR. Tremendous thanks to Morgan Mack, Jocelyn Bravo, and Therese Adgie, for allowing me to collect epiphytic algae samples from their experimental plots in GTMNERR, and for helping me find my footing in the marsh. Thank you to Gabriela Canas, for collecting the GTMNERR sediment samples that served as the basis for my benthic cyanobacteria characterization project. Thank you to Veronica at the UTK Genomics Core for going above and beyond to answer my metabarcoding-related questions. Thank you to Skyler Swyers, Hunter Weeks, and Davis Fray, for assisting me with my sample collection endeavors in the marsh. To Callahan McGovern, thank you for answering my countless questions about analyzing metabarcoding data, for inspiring me as a person and as a scientist, for being a wonderful friend, and for so many other things. Thank you to all of the UNF biology graduate students for being so incredibly friendly and welcoming to me from day one. To my roommates,

Laura, Savanna, and Pooja, who literally could not have been any more amazing if I had genetically engineered them in the lab myself. To my dear friends, Margaret, Olivia, and Elizabeth—there are no words to describe how much you mean to me. Thank you to my parents, my sister, and all my family members, who cheered me on and supported me throughout this whole process. And thank you to Yari, who first introduced me to the wonderful of cyanobacteria while I was an undergraduate research assistant at Montclair State University—none of this would have happened without you!

CHAPTER 1:

A DNA METABARCODING ASSESSMENT OF THE IMPACTS OF NITROGEN ENRICHMENT ON EPIPHYTIC MICROBIAL COMMUNITIES ON THE SALT MARSH GRASS *SPARTINA ALTERNIFLORA*

ABSTRACT

Anthropogenic eutrophication poses a serious threat to estuarine ecosystems worldwide. Elevated nitrogen and phosphorus inputs from anthropogenic sources can lead to significant increases in planktonic, benthic, and epiphytic algal biomass, and changes in algal community composition. Epiphytic microalgae on the salt marsh grass *Spartina alterniflora* play an important role in food availability in salt marsh ecosystems, and epiphytic nitrogen-fixing (diazotrophic) prokaryotes, particularly cyanobacteria, can provide an important source of nitrogen for salt marsh consumers. While the impacts of nutrient enrichment on epiphytic algae in coastal ecosystems have been well-studied in the context of seagrasses, few studies have addressed potential nutrient-driven changes to epiphytes on emergent salt marsh plants, such as *S. alterniflora*. This study employed DNA metabarcoding to analyze the impacts of a sediment nitrogen enrichment field experiment on epiphytic cyanobacteria, diatoms, and prokaryotes (all bacteria and archaea) on *S. alterniflora* in the Guana Tolomato Matanzas National Estuarine Research Reserve in northeastern Florida (USA). Statistical analyses of epiphytic community alpha diversity found that nitrogen enrichment resulted in significantly lower diversity of epiphytic cyanobacteria, suggesting that anthropogenic nitrogen input may have consequences for these important diazotrophic communities. Analyses of epiphytic beta diversity also indicated that the overall community structures of all examined epiphytic assemblages differed between creek edge and marsh interior *S. alterniflora* plants, indicating that many taxa within these communities may exhibit habitat specificity.

INTRODUCTION

The persistent flow of nitrogen and phosphorus into aquatic ecosystems from anthropogenic sources is causing an increasing number of freshwater, coastal, and marine aquatic ecosystems to be afflicted by eutrophication (Le Moal et al., 2019; Hallegraeff, 1993; Khan & Ansari, 2005; Smith & Schindler, 2009). Excessive algal growths, or algal blooms, fueled by anthropogenic nitrogen and phosphorus inputs can have a wide range of consequences, including ecosystem degradation, public health risks, and economic damage (Van Dolah, et al., 2001; Bricker et al., 2008; Cheung et al., 2013; Burford et al., 2019; Lapointe et al., 2020). Estuarine ecosystems are particularly threatened by eutrophication, as high population density in coastal areas has resulted in nutrient pollution from wastewater treatment facilities and other anthropogenic sources (Bricker et al., 2008). The elevated nitrogen and phosphorus inputs stemming from these sources can lead not only to significant increases in algal biomass, but also to changes in algal community composition (Armitage et al., 2006; Coleman & Burkholder, 1995), including decreased species diversity (Lemley et al., 2016; Le Moal et al., 2019). Such nutrient-driven disruptions can occur in a variety of estuarine algal assemblages, including planktonic (Lapointe et al., 2020), benthic (Clark et al., 2020), and epiphytic (Armitage et al., 2006) assemblages.

Epiphytic algae live on the surfaces of plants, and can be found on both submerged and emergent aquatic vegetation. On submerged aquatic vegetation, such as seagrasses, nutrient enrichment can lead to increases in epiphytic algal biomass and subsequent harm to host plant populations, as the epiphytic algae may outcompete the host plants for access to sunlight (Wijewardene et al., 2021; Nelson, 2017; Twilley et al., 1985). While the impacts of nutrient enrichment on epiphytic algae in coastal ecosystems have been well-studied with regards to

seagrasses (Nelson, 2017), there is very little research concerning nutrient-driven changes to epiphytes on Spartina alterniflora, an emergent salt marsh macrophyte (Verhulst, 2013). Compared to seagrasses, epiphytic communities on S. alterniflora are shaped by different environmental conditions and different selective pressures, and thus they may exhibit different responses to nutrient enrichment. For instance, unlike seagrass epiphytes, S. alterniflora epiphytes experience alternating periods of desiccation and tidal inundation. Consequently, desiccation likely plays an important role in determining epiphytic community structure, as desiccation tolerance varies among epiphyte taxa (Currin & Paerl, 1998). Additionally, because tidal inundation imports nitrogen from surrounding ecosystems into salt marshes (Tobias & Neubauer, 2019), the responses of benthic algae in salt marshes to nitrogen enrichment may vary with proximity to tidal creeks, as algal communities in the most frequently inundated areas of a marsh may not be nitrogen-limited (Sullivan & Currin, 2002). The responses of S. alterniflora epiphytes to nitrogen enrichment may be similarly dependent upon their proximity to tidal creeks, further indicating that elevated nitrogen input may have different effects on these salt marsh epiphytic communities compared to those in seagrass habitats.

Epiphytic microalgae on S. alterniflora are ingested by salt marsh consumers, such as grass shrimp (Palaemonetes pugio) (Quiñones-Rivera & Fleeger, 2005), brown shrimp (Penaeus aztecus) (Gleason & Zimmerman, 1984), the amphipod Orchestia grillus, and snails, including Melampus bidendatus (Pascal & Fleeger, 2013). Atmospheric nitrogen fixed by cyanobacteria, which have been known to be abundant in epiphytic communities on S. alterniflora (Currin et al., 1995; Verhulst, 2013), also represents a source of nitrogen input which may enter salt marsh food webs through marsh consumers' feeding on epiphytic microalgae (Currin & Paerl, 1998). S. alterniflora epiphytes thus play important roles in nitrogen cycling and food availability in

estuarine ecosystems, which are hosts to commercially valuable species such as oysters (Crassostrea virginica) and blue crabs (Callinectes sapidus), as well as migratory shorebirds (Frazel, 2009). Given the ecological significance of epiphytic communities on S. alterniflora, it is important to characterize the potential impacts that anthropogenic nitrogen enrichment may have on these microbial communities.

The development of environmental DNA (eDNA) metabarcoding, a high-throughput sequencing technique, has enabled the characterization of complex microbial communities without the need to isolate and culture individual constituent taxa (Escobar-Zepeda et al., 2015). Compared to traditional, microscopy-based techniques used to analyze microalgal communities, metabarcoding carries the advantage of providing high taxonomic resolution without requiring time-consuming microscopic assessments performed by highly specialized algal taxonomists (Bailet et al., 2020). Metabarcoding thus enables analysis of changes in species-level community diversity, which may be an indicator of environmental stressors in algal assemblages (Clark et al., 2020), as well as characterization of baseline community diversity at a high level of taxonomic resolution.

The primary goal of this study was to explore the potential impacts of anthropogenic nitrogen enrichment on S. alterniflora epiphytic communities. To that end, eDNA metabarcoding was employed to evaluate the effects of experimental nitrogen enrichment on S. alterniflora epiphytes, and to assess whether these effects differed between experimental plots located along the bank of a tidal creek and those located in the marsh interior. Multiple metabarcoding gene markers, targeting specific taxonomic groups of interest, were employed in order to examine the epiphytic diatom, cyanobacterial, and prokaryotic (archaea and bacteria, including cyanobacteria) communities. Given the paucity of research concerning these epiphytic

communities' responses to nutrient enrichment, this study provides valuable insight into the ways in which salt marsh ecosystems may be impacted by nutrient pollution.

METHODS

SITE DESCRIPTION

The nitrogen enrichment experiment was set up in the Guana Tolomato Matanzas National Estuarine Research Reserve (GTMNERR), in northeastern Florida, USA (Fig. 1a). The experimental field site (29°43' N, 81°14' W) is located in an area of estuarine salt marsh habitat within the southern component of GTMNERR, which is associated with the Matanzas River estuary (Fig. 1a). The site is tidally-influenced, with a tidal creek running through the area that encompasses the experimental plots (Fig. 1b). The site is situated near the northern range limit of mangroves, and lies within a salt marsh-mangrove ecotone, where mangroves are encroaching into herbaceous plant-dominated salt marsh ecosystems (Chapman et al., 2021). *Spartina alterniflora* and *Batis maritima* are the dominant marsh plants at the site, with black mangrove (*Avicennia germinans*) trees dispersed throughout.

FIELD EXPERIMENT

The nitrogen enrichment field experiment that served as the basis for this project was designed and carried out by Morgan Mack, Jocelyn Bravo, and Therese Adgie (Villanova University), as part of a separate research project. All field sampling activities carried out for the purpose of the present study were done so with the express permission of these researchers.

Existing research plots, previously established at the GTMNERR field site as part of the Warming Ecosystem Temperatures in a Florida Ecotone Experiencing Transition (WETFEET; www.wetfeetproject.com) project (Chapman et al., 2021), were utilized for the field experiment.

All WETFEET plots used for the present study were dominated by salt marsh plants (as opposed to mangroves), primarily Spartina alterniflora and Batis maritima, though only the epiphytic microbial communities on stems of S. alterniflora were analyzed for the present study. Each plot was 1.5 x 1.5 m and open on all sides, with plot areas demarcated by PVC piping. Plots were designated as either creekside or interior according to each plot's distance from the bank of the tidal creek, with plots less than 10 m from the bank designated as creekside plots, and plots greater than 10 m from the bank designated as interior plots. A total of twenty plots were included in the present study, with ten plots in each position group (creekside or interior). Five plots within each position group were haphazardly assigned to a nitrogen treatment group, and five were assigned to an untreated (control) group. A schematic representation of the experimental design is show in Fig. 2. Plot coordinates are listed in Table S1. Nitrogen treatment was applied on March 30th, 2022, using slow-release urea pellets. Two sealed mesh bags, each containing 150 g of urea pellets, were separately deposited in two 30-cm deep holes in each nitrogen treatment plot, with the two holes situated on opposite corners of each plot. The determined loading rate of nitrogen received by each treatment plot was 93.2 g m-2 y-1. All aspects of plot position classification and nitrogen treatment application, as described here, were carried out by Morgan Mack, Jocelyn Bravo, and Therese Adgie.

SAMPLE COLLECTION AND PROCESSING

Samples were collected from each plot on April 30th, July 11th, and September 17th, 2022, in order to collect data that spanned the growing season of the epiphytic communities' host plant (*S. alterniflora*). On each sampling trip, segments of three *S. alterniflora* stems were collected from each plot. Each plant was cut directly above its point of contact with the sediment surface, trimmed to a three-inch segment (the lowermost three inches of the plant), and deposited in a 100

mL sterile amber plastic bottle. All plants collected from the same plot were deposited in the same bottle. Scissors and rulers used to cut and measure stem segments were cleaned with isopropyl alcohol wipes in between each plot. Latex gloves were worn while handling plants and were changed in between each plot. On each sampling trip, one field negative sample was collected by handling an empty sample bottle in the same manner as all other samples but without depositing any plant segments in the bottle. Samples were stored on ice in a cooler until arrival and subsequent sample processing at the lab.

Processing of samples to dislodge and collect *S. alterniflora* epiphytes was performed immediately upon return from each sampling trip. Each sample bottle was filled with 100 mL of sterilized distilled water, and epiphytes were dislodged from stem segments by two minutes of vigorous shaking (Borrego-Ramos et al., 2021). 2.25 mL of liquid from each sample were then aliquoted into microcentrifuge tubes and centrifuged at high speed for ten minutes to pellet epiphyte cells. Field negative samples were processed in the same manner as other samples. Pellets were stored at -20°C until DNA extraction.

DNA EXTRACTION, AMPLIFICATION, AND SEQUENCING

Extraction of DNA from pelleted epiphytic material was done using the DNeasy® PowerSoil® Pro Kit (Qiagen), following the manufacturer's instructions. Four gene markers, representing microbial communities of interest, were separately amplified by PCR. The V4-V5 region of the 16S rRNA gene (hereafter referred to as the "16S Universal" gene marker) was selected to represent prokaryotic communities (all Bacteria and Archaea), and was amplified using primers 515F and 926R. The V3-V4 region of the 16S rRNA gene (hereafter referred to as the "16S Cyanobacteria" gene marker) was selected to represent cyanobacterial communities specifically, and was amplified using primers CYA359F and CYA781R (Nübel et al., 1997). The communities

assessed using the 16S Universal and 16S Cyanobacteria gene markers will hereafter be referred to as the "prokaryotic" and "cyanobacterial" communities, respectively, despite the fact that cyanobacterial taxa are also included in the 16S Universal gene marker dataset. Diatom communities were represented by a diatom-specific rbcL gene marker, which was amplified using an equimolar mix of three forward primers (Diat_rbcL_708F_1, Diat_rbcL_708F_2, and Diat_rbcL_708F_3) and an equimolar mix of two reverse primers (Diat_rbcL_R3_1 and Diat_rbcL_R3_2) (Vasselon et al., 2017). Eukaryotic algal and cyanobacterial communities (together) were represented by the Universal Plastid Amplicon (UPA), which was amplified using primers p23SrV_f1 and p23SrV_r1 (Sherwood & Presting, 2007). Illumina MiSeq overhang adapter sequences were appended to all primer sequences. The nucleotide sequences of all primers used are included in Table S2.

Amplicon PCRs for each of the four gene markers were performed in 25 µl reactions, using 2.5 µl of extracted DNA, 5 µl of each forward and reverse primer (1 µM), and 12.5 µl of Q5 High-Fidelity 2X Master Mix (New England BioLabs Inc., Ipswich, MA, USA). One PCR negative control sample was prepared for each set of amplicon PCRs, using nuclease-free water in place of extracted DNA. Thermocycler settings for each amplicon PCR are detailed in Table S3. Amplicon PCRs for each gene marker were performed in duplicate for each sample, and duplicates were pooled together following amplification to yield a total volume of 50 µl of amplicon PCR product per sample. PCR products were then visualized using agarose gel electrophoresis to confirm the presence of amplified gene markers.

The four amplicon PCR products were pooled together by sample prior to shipment to the University of Tennessee, Knoxville (UTK) Genomics Core for additional preparation steps and sequencing. Following the recommendation of the UTK Genomics Core, amplicon PCR products

were pooled according to relative product strength, as determined by visualization with agarose gel electrophoresis. The following volumes of each amplicon PCR product were pooled together for each sample: 5 µl of the 16S universal amplicon PCR product, and 10 µl each of the UPA, 16S cyanobacteria, and rbcL amplicon PCR products. Pooled PCR products were then shipped to UTK for amplicon PCR clean-up using Agencourt AmPure XP beads (Beckman Coulter Inc., Indianapolis, IN, USA), index PCR and clean-up, library quantification, and sequencing. Libraries were loaded with 25% PhiX clustering control and were sequenced on an Illumina MiSeq platform, using the MiSeq V3 reagent kit, to generate 300-bp paired-end reads. Sequence data were demultiplexed at the UTK Genomics Core facility.

BIOINFORMATICS

Sequence reads were sorted by gene marker and primer sequences were trimmed using CUTADAPT version 2.8 (Martin, 2011). Reads from each gene marker dataset were then separately processed using the DADA2 pipeline (Callahan et al., 2016) in RStudio (version 4.2.0). Default options for DADA2 parameters were used except where explicitly stated. Briefly, forward and reverse reads were truncated based on quality (truncLen=c(220,175) for 16S universal data; truncLen=c(190,200) for rbcL data; truncLen=c(175,220) for 16S Cyanobacteria data; truncLen=c(190,200) for UPA data) and filtered using standard filtering parameters (maxN=0, truncQ=2, rm.phix=TRUE, maxEE=c(2,2)) for all but the 16S Universal dataset, in which case the maxEE parameter was adjusted to maxEE=c(2,4). Sequence variants for forward and reverse reads were inferred based on estimated error rates, paired forward and reverse reads were merged to obtain full-length amplicon sequence variants (ASVs), and chimeric ASVs were removed. Taxonomy was then assigned using DADA2, with a different reference sequence database employed for each gene marker. For the 16S Universal dataset, taxonomy was assigned

using a DADA2-formatted SILVA version 138.1 database (Callahan et al., 2016; Quast et al., 2013). For the 16S Cyanobacteria dataset, a DADA2-formatted SILVA version 138.1 database appended with CyanoSeq version 1.1.1 (Lefler et al., 2022) was used. For the rbcL dataset, taxonomy was assigned using a DADA2-formatted Diat.barcode version 10 database (Rimet et al., 2019). For the UPA dataset, the microgreen version 1.1 database (Djemiel et al., 2019) with AlgaeBase (Guiry & Guiry, 2023) taxonomy was downloaded and formatted for use with DADA2.

The resulting ASV abundance data and taxonomic assignments were then imported into the phyloseq R package (McMurdie & Holmes, 2013). Taxonomic assignments of ASVs were then inspected, and non-target taxa were removed from each dataset. ASVs not assigned to class Cyanophyceae were removed from the 16S Cyanobacteria dataset, ASVs not assigned to phylum Bacillariophyta were removed from the rbcL data, ASVs assigned to phylum Bryophyta were removed from the UPA dataset, and ASVs assigned to order "Chloroplast" or family "Mitochondria" were removed from the 16S Universal dataset. ASVs assigned to cyanobacterial taxa in the 16S Universal dataset were not removed from the dataset. Following removal of non-target taxa, singletons and doubletons (ASVs represented by a total of less than three reads across the dataset) were removed, and remaining ASVs detected in the four negative control samples (three field negatives and one PCR negative) were assessed. No reads remained in any of the four negative samples for both the 16S Universal and 16S Cyanobacteria datasets, so no further action was taken to account for ASVs present in negative controls. For the rbcL and UPA datasets, contamination (ASVs present in negative controls) was dealt with using the method described by Bell et al. (2018) and implemented by Clark et al. (2020): for each ASV found in a negative control sample, the maximum number of reads (among negative control samples) was

subtracted from the corresponding ASVs' read count values across all samples. The total number of reads per sample remaining after each stage of the DADA2 pipeline and after each stage of ASV filtering in phyloseq are listed in tables S4-S7.

Rarefaction curves for all samples in each dataset were plotted using the ggrare function in the ranacapa (Kandlikar et al., 2018) R package. For the 16S Universal, 16S Cyanobacteria, and rbcL datasets, rarefaction curves showed observed ASV richness per sample plateauing for all samples (Figs. S1-S3), and all samples were thus retained for downstream analyses. For the UPA dataset, rarefaction curves (Fig. S4) indicated that sequencing depth was insufficient for many of the samples collected in April and July. For this reason, in addition to the poor quality of the taxonomic assignment data (described in the Results section), no further analyses were performed on the UPA dataset.

STATISTICAL ANALYSES

Separate statistical analyses were performed for the rbcL, 16S Universal, and 16S Cyanobacteria datasets. All analyses were done in RStudio (version 4.2.0).

Shannon and Simpson diversity indices were calculated using the estimate_richness function in phyloseq (McMurdie & Holmes, 2013), and the data for each diversity index were tested for normality using the R shapiro.test function. Parametric statistical tests were used for the Shannon diversity index data, which were normally distributed. For the analysis of the Shannon diversity index data, a three-way analysis of variance (ANOVA) was first run, using the R aov function, to test whether the effects of treatment, plot position, or their interaction, varied with respect to sampling month. There were no significant interaction terms involving sampling month, so the data were not separated by sampling month prior to conducting two-way ANOVAs. A two-way ANOVA was then run to test the effects of plot position, nitrogen

treatment, and their interaction on the Shannon diversity index data. There were no significant treatment X position interactions, so the interaction term was removed and the ANOVA was re-run. Non-parametric statistical tests were used for the Simpson diversity index data, which were not normally distributed. For the analysis of the Simpson diversity index data, Scheirer-Ray-Hare tests were first run, using the rcompanion package's scheirerRayHare function, to test whether the effects of plot position or treatment on Simpson diversity varied with respect to sampling month. The interactions between month and position, and between month and treatment, were tested separately using two-factor Scheirer-Ray-Hare tests because the scheirerRayHare function could not incorporate three factors. There were no significant interaction terms involving sampling month, so the data were not separated by month prior to running a two-factor Scheirer-Ray-Hare test of the effects of plot position, treatment, and their interaction on the Simpson diversity index data. Though there were no significant treatment X position interactions, the scheirerRayHare function could not run the tests without including the interaction term, so the tests were not able to be run with the interaction term removed.

The phyloseq (McMurdie & Holmes, 2013) and vegan (Oksanen et al., 2013) packages in R were used to explore differences in overall community structure (beta diversity) between plot positions and nitrogen treatment groups. Read count data were first transformed to proportional abundances using the transform_sample_counts function in phyloseq. A Bray-Curtis distance matrix was then calculated and plotted using Principal Coordinates Analysis (PCoA), using the ordinate and plot_ordination functions in phyloseq. A three-way PERMANOVA test of the Bray-Curtis matrix was then run, using the adonis2 function in vegan, to test whether the effects of treatment, plot position, or their interaction on overall community structure varied with respect to sampling month. If there were significant interaction terms involving sampling month, the data

were separated by month prior to testing the effects of position, treatment, and their interaction. A two-way PERMANOVA test of the Bray-Curtis matrix was then run to test the effects of plot position, nitrogen treatment, and their interaction on overall community structure. If the position X treatment interaction term was insignificant, the interaction term was removed and the PERMANOVA was re-run. Because PERMANOVA assumes equal beta dispersion, beta dispersion values for position groups and treatment groups were separately calculated using the betadisper function in vegan, and were separately tested for homogeneity of multivariate dispersions using the permutest function in vegan. Dispersions were not significantly different between treatment groups or position groups for any dataset, meaning the data did not violate the PERMANOVA assumption of equal beta dispersion, and thus alternative tests were not performed.

Venn diagrams were created (https://bioinformatics.psb.ugent.be/webtools/Venn/) to visualize the number of ASVs shared between edge and interior samples, control and nitrogen samples, and April, July, and September samples. The taxonomic composition of each community was visualized using the phyloseq plot_bar function. The proportional abundance data (not absolute read counts) were used to generate all taxonomic composition figures.

RESULTS

SEQUENCING DATA

The final filtered datasets contained 358,223 paired-end reads for the 16S Cyanobacteria dataset (Table S4), 128,386 paired-end reads for the 16S Universal dataset (Table S5), 4,293,321 paired-end reads for the rbcL (diatoms) dataset (Table S6), and 168,813 paired-end reads for the UPA (eukaryotic algae and cyanobacteria) dataset (Table S7). Rarefaction curves generated for each dataset indicated that sufficient sequencing depth was attained for all samples in the 16S

Cyanobacteria (Fig S1), 16S Universal (Fig S2), and rbcL datasets (Fig S3). Rarefaction curves generated for the UPA dataset (Fig S4), however, indicated that sequencing depth was insufficient for approximately one-third of the samples, including nearly all of the samples collected in April.

Sequencing reads from the 16S Cyanobacteria dataset were assigned to 917 unique amplicon sequence variants (ASVs), of which 882 (96% of all ASVs in the dataset) were assigned taxonomy (i.e., classified) at least to the level of Order (Table S8). 599 ASVs (65%) were assigned taxonomy to the level of Genus, the lowest taxonomic rank included in the reference database (Table S8). Sequencing reads from the 16S Universal dataset were assigned to 3,729 ASVs, all of which were assigned taxonomy through the level of Family, and 2,396 of which (64% of all ASVs in the dataset) were assigned taxonomy to the level of Genus, the lowest taxonomic rank included in the reference database (Table S9). Sequencing reads from the rbcL dataset were assigned to 1,317 ASVs, of which 951 (72% of all ASVs in the dataset) were assigned taxonomy at least to the level of Order (Table S10). 705 ASVs (54%) were assigned taxonomy to the level of Genus, and 422 (32%) were assigned taxonomy to the level of Species, the lowest taxonomic rank included in the reference database (Table S10).

The UPA dataset contained the largest proportion of ASVs not assigned taxonomy at least to the level of Order. Sequencing reads from the UPA dataset were assigned to 1,196 ASVs, of which only 649 (54% of all ASVs in the dataset) were assigned taxonomy at least to the level of Order (Table S11). 504 ASVs (42%) in the dataset were assigned taxonomy at the level of Genus, and 446 (37%) were assigned taxonomy to the level of Species, the lowest taxonomic rank included in the reference database. Due to the insufficient sequencing depth attained for many of the samples in the UPA datasets, in addition to the large proportion of ASVs lacking taxonomic

assignments at higher-order taxonomic ranks, further analysis of the UPA dataset was not pursued.

EFFECTS OF EXPERIMENTAL FACTORS ON THE ALPHA DIVERSITY OF EPIPHYTIC COMMUNITIES

For the 16S Cyanobacteria dataset, there was a significant effect of sampling month on both Shannon and Simpson diversity metrics, but no significant interactions between month and position and/or treatment (Tables S12-214). The two-way ANOVA test of the effects of treatment, position, and their interaction on Shannon diversity found that the treatment X position interaction effect was insignificant (Table S15), and when the interaction term was removed, neither position nor treatment was found to have a significant effect on Shannon diversity (Table 1; Fig. 3). The Scheirer-Ray-Hare test of the effects of treatment, position, and their interaction on Simpson diversity also showed that the effect of position was insignificant, while the effect of treatment was significant ($p<0.05$), with higher diversity in control plots (Table 2; Fig. 3). The treatment X position interaction effect was also insignificant for the Simpson diversity metric (Table 2).

For the rbcL (diatoms) dataset, there was a significant effect of sampling month on both Shannon and Simpson diversity metrics, but no significant interactions between month and position and/or treatment (Tables S12-S14). The two-way ANOVA test of the effects of treatment, position, and their interaction on Shannon diversity found that the treatment X position interaction effect was insignificant (Table S15). When the interaction term was removed, the two-way ANOVA test of the effects of treatment and position on Shannon diversity showed that treatment had no significant effect, while position had a significant effect ($p<0.05$), with greater diversity in edge plots (Table 1; Fig. 4). The Scheirer-Ray-Hare test of the effects of treatment, position, and their interaction on Simpson diversity also showed that treatment had no

significant effect, and that the effect of position was significant ($p<0.05$), with greater diversity in edge plots (Table 2; Fig. 4). The treatment X position interaction effect was also insignificant for the Simpson diversity metric (Table 2).

For the 16S Universal (all prokaryotes) dataset, there was no significant effect of sampling month on either diversity metric, and no significant interactions between month and position and/or treatment (Tables S12-S14). The two-way ANOVA test of the effects of treatment, position, and their interaction on Shannon diversity found that the treatment X position interaction effect was insignificant (Table S15). When the interaction term was removed, the two-way ANOVA test of the effects of treatment and position on Shannon diversity showed that neither position nor treatment had a significant effect (Table 1; Fig. 5). The Scheirer-Ray-Hare test of the effects of treatment, position, and their interaction on Simpson diversity showed that neither treatment nor position had a significant effect (Table 2; Fig. 5). The treatment X position interaction effect was also insignificant for the Simpson diversity metric (Table 2).

EFFECTS OF EXPERIMENTAL FACTORS ON OVERALL EPIPHYTIC COMMUNITY STRUCTURES

In the PCoA ordination plots, samples in each dataset showed an apparent segregation by position and by sampling month, but not by treatment. For the 16S Cyanobacteria dataset, axes 1 and 2 of the PCoA plot explained 33.3% and 14.7% of the total variance, respectively. The grouping of samples by plot position was on the first axis (Fig. 6), and the grouping of samples by month was on the second axis (Fig. S5). For the rbcL dataset, axes 1 and 2 of the PCoA plot explained 31.8% and 21.6% of the total variance, respectively. The grouping of samples by plot position was on the first axis (Fig. 7), and the grouping of samples by month was on the second axis (Fig. S6). For the 16S Universal dataset, axes 1 and 2 of the PCoA plot explained 9.3% and

6.1% of the total variance, respectively. The grouping of samples by month was on the first axis (Fig. S7), and the grouping of samples by plot position was on the second axis (Fig. 8).

The three-way PERMANOVA tests found that there was a significant effect of sampling month on community structure for all three gene marker datasets (Table S16). For each dataset, there was no significant three-way interaction between month, treatment, and position, and no significant two-way interaction between month and treatment (Table S16). There was no significant month X position interaction for the rbcL or 16S Universal datasets (Table S16), while there was a significant month X position interaction for the 16S Cyanobacteria dataset (Table S16).

For the 16S Cyanobacteria dataset, two-way PERMANOVA tests (separately run on the data from each sampling month) of the effects of treatment, position, and their interaction found that the interaction effect was insignificant in each month (Table S17). When the interaction term was removed, the two-way PERMANOVA tests showed that there was a significant effect of position in each month ($p<0.05$), and no significant effect of treatment in any month (Table 3).

For the rbcL dataset, the two-way PERMANOVA test of the effects of treatment, position, and their interaction found that the treatment X position interaction effect was not significant (Table S17). When the interaction term was removed, the two-way PERMANOVA test showed that there was a significant effect of position ($p<0.05$) on overall community structure, but no significant effect of treatment (Table 3).

For the 16S Universal dataset, the two-way PERMANOVA test of the effects of treatment, position, and their interaction found that the treatment X position interaction effect was not significant (Table S17). When the interaction term was removed, the two-way

PERMANOVA test showed that there was a significant effect of position ($p<0.05$) on overall community structure, but no significant effect of treatment (Table 3).

TAXONOMIC COMPOSITION OF EPIPHYTIC COMMUNITIES

Cyanobacteria

Of the 917 ASVs in the 16S Cyanobacteria dataset, 393 were shared between interior and edge samples, and 489 were shared between control and nitrogen samples (Fig. 9). ASVs assigned to the genera *Foliisarcina*, *Hyella*, *Nodosilinea*, *Nunduva*, *Prochlorococcus*, *Salileptolyngbya*, *Symploca*, and *Thainema* were among the most abundant ASVs across the entire dataset (Fig. 12). When classified at the genus level, the most abundant ASVs showed similar proportional abundances between nitrogen and control plots, while some differences between edge and interior plots were apparent, with *Symploca* and *Salileptolyngbya* ASVs showing greater proportional abundances in interior plots in all months (Fig. 12).

Among the ten orders most abundant across the entire dataset, the proportional abundances of each were similar between control and nitrogen plots in all sampling months while the proportional abundances of orders Chroococcidiopsidales, Coleofasciculales, Synechococcales showed consistent differences between edge and interior plots (Fig. 13). Taxonomic assignment at the genus level was lacking for ASVs in Chroococcidiopsidales, all of which were assigned to the family Chroococcidiopsidaceae, but the relative abundance of this order was higher in edge plots in all months (Fig. 13). The relative abundance of Coleofasciculales was similar between edge and interior plots in the July dataset, but was higher in interior plots in both April and September (Fig. 13). ASVs assigned to the genus *Symploca* accounted for the majority of Coleofasciculales reads in both positions and in all sampling months, with the exception of edge plots in July, which contained a large proportion of reads not

assigned taxonomy at the genus level (Fig. S8). The relative abundance of Synechococcales was higher in edge plots than interior plots in all months (Fig. 13). The proportional abundances of genera within this order were mostly similar between edge and interior plots, and the genera *Prochlorococcus*, *Cyanobium*, and *Anathece* were abundant (Fig. S9).

Diatoms

Of the 1,317 ASVs in the rbcL dataset, 755 were shared between interior and edge samples, and 905 were shared between control and nitrogen samples (Fig. 10).

ASVs assigned to class Bacillariophyceae accounted for the majority of all reads across the entire dataset (Fig. 14). Proportional abundances of each class were similar between control and treatment plots in each month, while the proportional abundance of Mediophyceae was higher in edge plots than in interior plots in all months (Fig. 14). *Terpsinoe* was among the most abundant genera in Mediophyceae and was almost exclusively found in edge plots (Fig. S10). *Minutocellus*, also among the most abundant genera in Mediophyceae, was similarly abundant in both plot positions across months, but did show a marked increase in abundance in the September dataset compared to the April and July datasets (Fig. S10).

Bacillariales and Naviculales were among the ten most abundant orders across the entire dataset, and were the two most abundant orders in both plot positions and both treatment groups in each month (Fig. 15). Among the ten genera most abundant across the entire dataset, the proportional abundances of each were mostly similar between edge and interior plots and between nitrogen and control plots, though several genera showed apparent differences in abundance among the different months (Fig. 16). *Bacillaria* was largely restricted to the September dataset, *Diploneis* was more abundant in April than in July or September, and *Halamphora* was more abundant in July than in April or September (Fig. 16).

Prokaryotes

Of the 3,729 ASVs in the 16S Universal dataset, 981 were shared between interior and edge samples, and 1,045 were shared between control and nitrogen samples (Fig. 11).

Proteobacteria, Planctomycetota, and Bacteroidota were among the ten most abundant phyla across the entire dataset (Fig. 17). For the ten most abundant phyla, the proportional abundances of each were similar between both treatment groups and between both plot position groups in all sampling months, with the exception of Halobacterota, an archaeal phylum that was present only in the September dataset and was more abundant in interior plots than in edge plots (Fig. 17). Archaeal ASVs as a whole accounted for only a small portion of reads across the entire dataset, and were almost exclusively found in only the September dataset (Fig. 18). The proportional abundance of reads accounted for by archaeal ASVs was higher in interior plots than in edge plots, and was slightly higher in control plots than in nitrogen plots (Fig. 18). ASVs assigned to the genus *Halogranum* accounted for a large proportion of all archaeal reads in both plot position groups and in both treatment groups (Fig. S11).

DISCUSSION

SEQUENCING DEPTH AND PERFORMANCE OF TAXONOMIC REFERENCE DATABASES

In terms of the number of reads obtained for each gene marker, the rbcL dataset dominated the Illumina MiSeq sequencing data (Table S6), compared to the other gene markers (Table S4; Table S5; Table S7). Despite their lower total read counts, the rarefaction curves generated for the 16S Cyanobacteria (Fig S1) and 16S Universal (Fig S2) datasets indicated that sufficient sequencing depth was attained for all samples in these datasets. Though the UPA gene marker dataset contained a greater total number of sequencing reads (Table S7) than the 16S Universal dataset (Table S5), the rarefaction curves generated for the samples in this dataset (Fig S4)

indicated that sequencing depth was insufficient for most of the samples collected in April. Quantifying DNA concentrations in each amplicon PCR product from each sample, and diluting each to an equal concentration prior to pooling them by sample, may have helped to prevent the uneven distribution of sequencing reads among gene marker datasets, as well as among samples within the UPA dataset. Ideally, the different gene markers would have been separately sequenced in individual MiSeq runs in order to maximize sequencing depth, but this was not a financially feasible option.

Though sequencing depth was lower than optimal for the 16S Cyanobacteria and 16S Universal datasets, the strong performance of the taxonomic reference databases used for these datasets (Lefler et al., 2022; Callahan et al., 2016; Quast et al., 2013) enabled the taxonomic compositions of samples from both datasets to be meaningfully analyzed. In the UPA dataset, however, only 54% of the ASVs were classified at the level of order, and 20% of all ASVs remained unclassified even at the level of class (Table S11), which was particularly problematic, given that a taxonomically wide variety of eukaryotic algae and cyanobacteria should have been represented in this dataset. An improved taxonomic reference database for the UPA gene marker may be required in order to maximize this marker's usefulness in metabarcoding studies of algal diversity in *S. alterniflora* epiphytic assemblages.

While the availability of taxa-specific amplicon primers and corresponding curated taxonomic reference databases makes metabarcoding a powerful tool for analyzing microbial communities (Bailet et al., 2020), a significant drawback of employing this methodology is that the associated sequencing costs can constrain the number of target taxa (e.g., specifically diatoms, or specifically cyanobacteria) that can be assessed within diverse microbial assemblages. In the future, target taxa should be carefully selected based on the specific goals of

each research project, and on a thorough assessment of the literature concerning the performance of various prospective taxa-specific barcoding regions and their associated reference databases.

EFFECTS OF EXPERIMENTAL FACTORS ON EPIPHYTIC DIATOM, CYANOBACTERIAL, AND PROKARYOTIC COMMUNITIES

In aquatic ecosystems in general (freshwater, coastal, and marine), anthropogenic eutrophication is typically associated with the proliferation and dominance of a small number of opportunistic algal species (i.e., lower alpha diversity), which are able to out-compete other species in the community when nutrients are elevated (Le Moal et al., 2019). Given the lack of research assessing the effects of nitrogen enrichment on epiphytic communities on emergent salt marsh macrophytes, no specific predictions were made at the outset of the present study regarding whether or not any significant effects of nitrogen enrichment would be observed. However, in the event that any significant effects of nitrogen enrichment on diatom or cyanobacterial alpha diversity were detected, nitrogen treated plots were expected to be characterized by lower alpha diversity, based on what is known about aquatic algal communities more broadly. Additionally, epiphytic communities in edge plots were expected to respond less strongly to nitrogen treatment than epiphytic communities in interior plots, given that epiphytic communities closer to the creek bank may already be exposed to relatively higher nitrogen concentrations as a result of more frequent tidal inundation (Tobias & Neubauer, 2019; Sullivan & Currin, 2002).

Nitrogen enrichment had a significant effect on Simpson diversity in the cyanobacterial communities, with lower diversity in nitrogen-treated plots, though there was no significant interaction between treatment and plot position (Table 2; Fig. 3), indicating that the effect of nitrogen treatment did not vary based on plot position as expected. Nitrogen enrichment was found to have no significant effect on the alpha diversity of diatom communities, however (Fig.

4; Table 1; Table 2), and the effect of plot position on alpha diversity metrics also differed between diatom and cyanobacterial communities. Plot position had no significant effect on either diversity metric for cyanobacterial communities (Table 1; Table 2), but had a significant effect on both diversity metrics for diatom communities (Fig. 4; Table 1; Table 2). Neither nitrogen enrichment nor plot position had a significant effect on the alpha diversity metrics of the epiphytic prokaryotic (16S Universal dataset) communities (Fig. 5; Table 1; Table 2).

Previous studies of the effects of nitrogen enrichment on seagrass epiphytic algal communities have found that responses to nitrogen enrichment varied among the algal taxa present (Armitage et al., 2006; Coleman & Burkholder, 1995). Phytoplankton community structures are also influenced by differences in the ratios of limiting nutrients (e.g., nitrogen, phosphorus, silica), in terms of which algal groups (e.g., diatoms, cyanobacteria, green algae) dominate the communities (Tilman et al., 1982). Thus, the finding that nitrogen enrichment had different effects on the alpha diversity of the two microalgal communities studied here (diatoms and cyanobacteria) was not entirely surprising. One factor that may have contributed to this observed difference is the fact that a wide variety of cyanobacteria, including *S. alterniflora* epiphytes, are capable of fixing atmospheric nitrogen (Moisander et al., 2005), unlike diatoms. Nitrogen input may play an important role in shaping the structures of diazotrophic (nitrogen-fixing) epiphytic communities (Moisander et al., 2005), and thus the epiphytic cyanobacterial community structures may have been more strongly affected by the experimental nitrogen enrichment than the diatom community structures.

Whereas nitrogen treatment and plot position had differing effects on the alpha diversity of the three epiphytic communities, the effects of these factors on beta diversity were similar in nature across the three communities. In all three cases, overall epiphytic community structures in

the creek edge zone of the study site differed significantly from those in the interior zone, whereas community structures in the nitrogen treatment group and in the control group were not significantly different from each other (Table 3). No significant interactions between plot position and treatment group were observed (Table S17). The difference in community structures between the edge and interior zones was apparent in the PCoA ordination plots, particularly for the diatom (Fig. 7) and cyanobacterial (Fig. 6) communities. Variation in community structure within each position group was also evident, however, and the two groups were not completely separated from each other in any of the three epiphytic communities examined. Differences in the relative abundances of certain taxa between edge plots and interior plots were also observed in the epiphytic communities. In the cyanobacterial communities, ASVs in the orders Chroococcidiopsidales and Synechococcales were more abundant in edge plots, while ASVs in the order Coleofasciculales were more abundant in interior plots (Fig. 13). In the diatom communities, edge plots contained a greater relative abundance of ASVs in the class Mediophyceae (Fig. 14). In the prokaryotic communities, the relative abundance of Archaeal ASVs was slightly higher in interior plots than in edge plots (Fig. 18).

Several factors could have contributed to the observed differences in epiphytic community structures between the creek edge and marsh interior zones. One possible factor is differences in the relative contributions of both the underlying marsh sediments and flooding tidal waters to the epiphytic assemblages on *S. alterniflora*. Marsh sediments, and their associated benthic diatom communities, have been proposed as the primary source of epiphytic diatoms on *S. alterniflora* (Sullivan & Currin, 2002), but planktonic communities in tidal waters have also been hypothesized to contribute to observed epiphytic assemblages on other salt marsh plants (Sullivan, 1977). Biraphid diatoms are generally the most abundant diatoms in salt marsh

sediments (Sullivan & Currin, 2002), while centric diatoms occur less frequently, and their presence in the sediments has been attributed to the settling of planktonic forms from the water column (Stowe, 1972). The greater relative abundance of centric diatoms in the class Mediophyceae (e.g., *Terpsinoe*, *Thalassiosira;* Fig. S10) in the edge plots suggests that the observed difference in diatom community structures between the edge and interior zones could be in part due to planktonic populations contributing more to the epiphytic communities in the more-frequently inundated edge zone. The greater relative abundance of planktonic cyanobacteria in the order Synechococcales (e.g., *Prochloroccus*, *Anathece*; Fig. S9) observed in the edge plots suggests that this may also be true of the epiphytic cyanobacterial communities.

While epiphytic community members derived from the plankton of flooding tidal waters could be considered only secondarily, or transiently, epiphytic, the observed differences in community structures between the edge and interior zones may also reflect differences in environmental conditions that shape the primarily epiphytic (or benthic) members of the community. In addition to experiencing more frequent and prolonged tidal inundation, marsh areas closest to tidal creek banks are also often characterized by taller *S. alterniflora* growth forms (Drake et al., 2008; Fox et al., 2012). Both the overlying water column (during tidal inundation) and the *Spartina* canopy can reduce the photosynthetically active radiation (PAR) available to epiphytic algae (Jackson et al., 2009). Thus, microalgal species adapted to lower PAR availability may be more abundant in epiphytic communities near the creek edge, while those adapted to withstand higher ultraviolet irradiance may be more abundant in communities in the marsh interior. Desiccation has also been proposed as an important factor responsible for maintaining the *S. alterniflora* epiphytic community structure (Currin et al., 1998), so epiphytic

species with a greater tolerance for desiccation may be more abundant in the less-frequently inundated interior zone.

Given that marsh sediments have been proposed to represent the primary source of epiphytic diatoms on *S. alterniflora* (Sullivan & Currin, 2002), it is interesting that Clark et al. (2020) found that nitrogen enrichment led to changes in the overall community structures of estuarine benthic diatoms, as detected by a DNA metabarcoding assessment, whereas the present study found no significant differences in epiphytic diatom community structure between treatment groups. The nitrogen enrichment experiment conducted by Clark et al. (2020) was located in two unvegetated tidal flats, however, so differences in benthic diatom assemblages between these two habitat types (unvegetated tidal flat vs. vegetated salt marsh) could, in part, explain the different experimental findings. The present study's findings are also in contrast to those of Craig et al. (2021), which found that nitrogen enrichment led to differences in the overall community structures of sediment bacteria in experimental mesocosms set up with sediments obtained from the same GTMNERR field site that the present study's *S. alterniflora* samples were collected from. Similar to diatoms, epiphytic bacteria on *S. alterniflora* stems in salt marsh habitats are also likely derived largely from populations in the underlying marsh sediments (Moisander et al., 2005). Thus, the difference in findings between the present study and Craig et al. (2021) is particularly interesting, given that the bacterial communities analyzed in both studies might be expected to be highly similar in composition, and consequently they might also be expected to exhibit similar responses to nitrogen enrichment. The data obtained by Craig et al. (2021) suggests, however, that these two communities are less similar to each other than might be expected. Though the phyla Proteobacteria and Bacteroidota were abundant in both data sets, Planctomycetota was much more abundant in the present study's dataset (Fig. 18),

and Epsilonbacteraeota, which was not detected in the present study, was abundant in the data from Craig et al. (2021). Thus, one potential explanation for why the observed effects of nitrogen enrichment differed between this study and the study conducted by Craig et al. (2021) is that the compositions of the bacterial assemblages examined were actually quite distinct from each other. This could be due to stable differences between the epiphytic and sediment bacterial communities maintained by selective pressures unique to each microhabitat. However, the observed differences in bacterial community composition could also be an artifact introduced by differences in methodology. For instance, different marker regions of the 16S rRNA gene were used in each study, and Craig et al. (2021) also noted that conditions in the experimental mesocosms may have created a suboptimal environmental for certain bacterial taxa.

Sampling month, like plot position, had a significant effect on the overall community structures of the epiphytic cyanobacterial, diatom, and prokaryotic communities (Table S16), as well as a significant effect on cyanobacterial and diatom alpha diversity metrics (Table S12; Table S13; Table S14). Differences in overall community structures among the three sampling months were also apparent in the PCoA ordination plots for all three epiphytic communities examined (Fig. S5; Fig S6; Fig. S7), and marked differences in the relative abundances of certain taxa within the diatom and prokaryotic communities were also observed. Seasonal variability in the biomass of *S. alterniflora* epiphytic microalgae was observed by Jackson et al. (2006) and Verhulst (2013), and the latter study also found that sampling month had a significant effect on microalgal diversity (Shannon diversity index) and the relative abundances of different algal groups over the course of a two-year study period. Stowe (1972) also observed seasonal changes in the abundances of particular diatom genera on *S. alterniflora* stems. Seasonal growth patterns of the host plant species (*S. alterniflora)* have been proposed as a potential factor influencing

epiphytic microalgal communities (Verhulst, 2013; Stowe, 1972; Jackson et al., 2006), as have seasonal differences in tidal creek water temperature and nutrient concentrations (Jackson et al., 2009). Though conclusions regarding broader seasonal changes in the epiphytic communities cannot be extrapolated from the data collected for the present study, the findings of this study are consistent with those of other authors in that they indicate that the *S. alterniflora* epiphytic communities exhibit significant temporal variability.

While numerous studies have assessed the effects of nutrient enrichment on epiphytic microalgal communities on seagrasses (e.g., Twilley et al., 1985, Armitage et al., 2006, Coleman & Burkholder, 1995; Prado et al., 2008; Bryars et al., 2011; Wear et al., 1999; Nelson, 2017), only the present study and the study conducted by Verhulst (2013) have examined the responses of *S. alterniflora* epiphytes to nutrient enrichment. Verhulst (2013) found that nitrogen enrichment had no significant effect on epiphytic community alpha diversity, epiphytic biomass, or the relative abundances (as a percentage of total cells) of different algal divisions (e.g., diatoms, cyanobacteria, green algae) within the epiphytic communities. Whereas the present study employed DNA metabarcoding to separately analyze two microalgal communities (diatoms and cyanobacteria) in terms of both alpha diversity and beta diversity, Verhulst (2013) employed light microscopy to identity algal taxa and analyzed the alpha diversity of the entire algal community together, and did not analyze beta diversity. Thus, while only limited comparisons can be made between the findings of these two studies, taken together, they suggest that *S. alterniflora* epiphytic microalgal communities are not greatly impacted by elevated nitrogen inputs.

CONCLUSIONS

The present study found that nitrogen enrichment did not have a significant effect on epiphytic beta diversity, suggesting that, at a site-wide scale, environmental factors other than sediment nitrogen concentrations are largely responsible for shaping and maintaining the overall community structures of epiphytic diatoms, cyanobacteria, and prokaryotes on *S. alterniflora* stems. However, a significant difference in cyanobacterial alpha diversity between nitrogen-treated and control plots was found, which suggests that elevated nitrogen input does have the potential to alter these communities at smaller spatial scales. It is possible that significant effects of nitrogen enrichment on overall cyanobacterial community structures at a site-wide scale may also begin to manifest after a longer duration of time, which this study's five-month sampling period was not sufficient to detect, and a longer-term study of the effects of nitrogen enrichment on these communities should therefore be conducted in the future. Additionally, future metabarcoding-based studies should consider employing amplicon PCR primers designed to amplify a diazotroph-specific gene marker (Gaby et al., 2018) in order to specifically target diazotrophic epiphytic communities, as nitrogen input likely plays a large role in shaping their community structures (Moisander et al., 2005).

This study also found that the overall community structures of epiphytic diatoms, cyanobacteria, and prokaryotes on *S. alterniflora* stems are significantly different between the creek edge and marsh interior zones of the study site. Certain epiphytic taxa were also found to be largely concentrated in a particular zone, indicating habitat specificity. These findings suggest that, despite their close proximity to each other, the creek edge and marsh interior zones represent two distinct reservoirs of microbial biodiversity within the marsh, which may help to inform future management practices and research priorities in GTMNERR and other estuarine

habitat reserves. For instance, the distribution patterns of macroscopic flora and fauna may not indicate that these two zones represent such distinct habitats, each of which hosts a unique community of organisms, including a number of species that may be localized habitat specialists. An awareness of this complex yet "invisible" landscape of microbial biodiversity within the marsh may prompt reserve managers to prioritize additional microbial ecology and diversity research, in an effort to identify other potentially unique microbial habitats, and to gain a greater understanding of the amount of biodiversity contained within estuarine ecosystems.

REFERENCES

Armitage, A. R., Frankovich, T. A., & Fourqurean, J. W. (2006). Variable responses within epiphytic and benthic microalgal communities to nutrient enrichment. *Hydrobiologia*, 569: 423–435. https://doi.org/10.1007/s10750-006-0146-8

Bailet, B., Apothéloz-Perret-Gentil, L., Baričević, A., Chonova, T., Franc, A., Frigerio, J.-M., Kelly, M., Mora, D., Pfannkuchen, M., Proft, S., Ramon, M., Vasselon, V., Zimmermann, J., & Kahlert, M. (2020). Diatom DNA metabarcoding for ecological assessment: comparison among bioinformatics pipelines used in six European countries reveals the need for standardization. *Science of The Total Environment*, 745: 140948. https://doi.org/10.1016/j.scitotenv.2020.140948

Bell, K.L., Burgess, K.S., Botsch, J.C., Dobbs, E.K., Read, T.D., & Brosi, B.J. (2018). Quantitative and qualitative assessment of pollen DNA metabarcoding using constructed species mixtures. *Molecular Ecology*, 28(2): 431–455. https://doi.org/10.1111/mec.14840

Borrego-Ramos, M., Bécares, E., García, P., Nistal, A., & Blanco, S. (2021). Epiphytic diatom-based biomonitoring in Mediterranean ponds: Traditional microscopy versus metabarcoding approaches. *Water*, 13(10): 1351. http://dx.doi.org/10.3390/w13101351

Bricker, S. B., Longstaff, B., Dennison, W., Jones, A., Boicourt, K., Wicks, C., & Woerner, J. (2008). Effects of nutrient enrichment in the nation's estuaries: A decade of change. *Harmful Algae*, 8: 21–32. https://doi.org/10.1016/j.hal.2008.08.028

Bryars, S., Collings, G., & Miller, D. (2011). Nutrient exposure causes epiphytic changes and coincident declines in two temperate Australian seagrasses. *Marine Ecology Progress Series*, 441: 89-103. DOI: 10.3354/meps09384

Burford, M. A., Carey, C. C., Hamilton, D. P., Huisman, J., Paerl, H. W., Wood, S. A., & Wulff, A. (2020). Perspective: Advancing the research agenda for improving understanding of cyanobacteria in a future of Global Change. *Harmful Algae*, 91: 101601. https://doi.org/10.1016/j.hal.2019.04.004

Callahan, B.J., McMurdie, P.J., Rosen, M.J., Han, A.W., Johnson, A.J.A., & Holmes, S.P. (2016). DADA2: High-resolution sample inference from Illumina amplicon data. *Nature Methods*, 13: 581-583. doi: 10.1038/nmeth.3869

Chapman, S. K., Feller, I. C., Canas, G., Hayes, M.A., Dix, N., Hester, M., Morris, J., & Langley, J.A. (2021). Mangrove growth response to experimental warming is greatest near the range limit in northeast Florida. *Ecology*, 102(6): e03320. https://doi.org/10.1002/ecy.3320

Cheung, M.Y., Liang, S. & Lee, J. (2013). Toxin-producing cyanobacteria in freshwater: A review of the problems, impact on drinking water safety, and efforts for protecting public health. *Journal of Microbiology*, 51: 1–10 https://doi.org/10.1007/s12275-013-2549-3

Clark, D. E., Pilditch, C. A., Pearman, J. K., Ellis, J. I., & Zaiko, A. (2020). Environmental DNA metabarcoding reveals estuarine benthic community response to nutrient enrichment – evidence from an in-situ experiment. *Environmental Pollution*, 267: 115472. https://doi.org/10.1016/j.envpol.2020.115472

Coleman, V.L., & Burkholder, J.M. (1995). Response of microalgal epiphyte communities to nitrate enrichment in an eelgrass (*Zostera marina*) meadow. *Journal of Phycology*, 31: 36-45.

Craig, H., Antwis, R., Cordero, I., Ashworth, D., Robinson, C., Osborne, T., Bardgett, R., Rowntree, J., & Simpson, L. (2021). Nitrogen addition alters composition, diversity, and

functioning of microbial communities in mangrove soils: An incubation experiment. *Soil Biology and Biochemistry*, 153: 108076. DOI: 10.1016/j.soilbio.2020.108076.

Currin, C.A. & Paerl, H.W. (1998). Epiphytic nitrogen fixation associated with standing dead shoots of smooth cordgrass, *Spartina alterniflora*. *Estuaries*, 21(1): 106-117. https://doi.org/10.2307/1352550

Currin, C.A., Newell, S.Y., & Paerl, H.W. (1995). The role of standing dead *Spartina alterniflora* and benthic microalgae in salt marsh food webs: considerations based on multiple stable isotope analysis. *Marine Ecology Progress Serie*s, 121: 99-116.

Djemiel, C., Plassard, D., Terrat, S., Crouzet, O., SauzE, J., Mondy, S., Nowak, V., Wingate, L., Ogée, J., & Maron, P. (2019). µgreen-db (1.1) [Data set]. Zenodo. https://doi.org/10.5281/zenodo.3695186

Drake, D.C., Peterson, B.J., Deegan, L.A., Harris, L.A., Miller, E.E., & Warren, R.S. (2008). Plant nitrogen dynamics in fertilized and natural New England salt marshes: a paired ^{15}N tracer study. *Marine Ecology Progress Series*, 354: 35-46.

Escobar-Zepeda, A., Vera-Ponce de León, A., & Sanchez-Flores, A. (2015). The road to metagenomics: from microbiology to DNA sequencing technologies and bioinformatics. *Frontiers in Genetics,* 6: 348. doi: 10.3389/fgene.2015.00348

Fox, L., Valiela, I. & Kinney, E.L. (2012). Vegetation cover and elevation in long-term experimental nutrient-enrichment plots in Great Sippewissett Salt Marsh, Cape Cod, Massachusetts: implications for eutrophication and sea level rise. *Estuaries and Coasts*, 35: 445–458. https://doi.org/10.1007/s12237-012-9479-x

Frazel, D. (2009). Site Profile of the Guana Tolomato Matanzas National Estuarine Research Reserve. Ponte Vedra, FL.

Gaby, J. C., Rishishwar, L., Valderrama-Aguirre, L. C., Green, S. J., Valderrama-Aguirre, A., Jordan, I. K., & Kostka, J. E. (2018). Diazotroph community characterization via a high-throughput *nifH* amplicon sequencing and analysis pipeline. *Applied and Environmental Microbiology*, 84(4): e01512-17. https://doi.org/10.1128/AEM.01512-17

Gleason, D.F. & Zimmerman, R.J. (1984). Herbivory potential of postlarval brown shrimp associated with salt marshes. *Journal of Experimental Marine Biology and Ecology*, 84(3): 235-246. https://doi.org/10.1016/0022-0981(84)90183-7

Guiry, M.D. & Guiry, G.M. (2023). AlgaeBase. National University of Ireland, Galway. https://www.algaebase.org

Hallegraeff, G.M. (1993). A review of harmful algal blooms and their apparent global increase. *Phycologia*, 32(2): 79-99.

Jackson, G., Zingmark, R., Lewitus, A.J., Tymowski, R.G., & Stuckey, J. (2006). Spatial and temporal dynamics of epiphytic microalgae on the cordgrass *Spartina alterniflora* in North Inlet Estuary, South Carolina. *Estuaries and Coasts*, 29: 1212–1221. https://doi.org/10.1007/BF02781821

Jackson, G., Zingmark, R.G., & Lewitus, A.J. (2009). Modeling epiphytic community production. *Marine Ecology Progress Series,* 387: 61-70. doi: 10.3354/meps08101

Kandlikar, G.S., Gold, Z.J., Cowen, M.C., Meyer, R.S., Freise, A.C., Kraft, N.J.B., Moberg-Parker, J., Sprague, J., Kushner, D.J., & Curd, E.E. (2018). ranacapa: An R package and Shiny web app to explore environmental DNA data with exploratory statistics and interactive visualizations. *F1000 Research*, 7: 1734. https://doi.org/10.12688/f1000research.16680.1

Khan, F.A. & Ansari, A.A. (2005). Eutrophication: an ecological vision. *The Botanical Review*, 71: 449–482.

Lapointe, B. E., Herren, L. W., Brewton, R. A., & Alderman, P. K. (2020). Nutrient over-enrichment and light limitation of seagrass communities in the Indian River Lagoon, an urbanized subtropical estuary. *Science of The Total Environment*, 699: 134068. https://doi.org/10.1016/j.scitotenv.2019.134068

Le Moal, M., Gascuel-Odoux, C., Ménesguen, A., Souchon, Y., Étrillard, C., Levain, A., Moatar, F., Pannard, A., Souchu, P., Lefebvre, A., & Pinay, G. (2019). Eutrophication: A new wine in an old bottle? *Science of The Total Environment*, 651: 1–11. https://doi.org/10.1016/j.scitotenv.2018.09.139

Lefler, F., Berthold, D., & Laughinghouse, H. D. (2022). CyanoSeq v1.1.1. Zenodo. https://doi.org/10.5281/zenodo.7110927

Lemley, D. A., Adams, J. B., & Bate, G. C. (2016). A review of microalgae as indicators in South African estuaries. *South African Journal of Botany*, 107: 12–20. https://doi.org/10.1016/j.sajb.2016.04.008

Martin, M. (2011). Cutadapt removes adapter sequences from high-throughput sequencing reads. *EMBnet.journal,* 17(1): 10-12. doi:https://doi.org/10.14806/ej.17.1.200

McMurdie, P. J., & Holmes, S. (2013). phyloseq: an R package for reproducible interactive analysis and graphics of microbiome census data. *PLoS ONE,* 8(4): e61217. https://doi.org/10.1371/journal.pone.0061217

Moisander, P.H., Piehler, M.F., & Paerl, H.W. (2005). Diversity and activity of epiphytic nitrogen-fixers on standing dead stems of the salt marsh grass *Spartina alterniflora*. *Aquatic Microbial Ecology*, 39: 271-279.

Nelson W. G. (2017). Development of an epiphyte indicator of nutrient enrichment: a critical evaluation of observational and experimental studies. *Ecological Indicators,* 79: 207–227. https://doi.org/10.1016/j.ecolind.2017.04.034

Nelson, W.G. (2017). Development of an epiphyte indicator of nutrient enrichment: A critical evaluation of observational and experimental studies. *Ecological Indicators*, 79: 207-227. https://doi.org/10.1016/j.ecolind.2017.04.034

Nübel, U., Garcia-Pichel, F., & Muyzer, G. 1997. PCR primers to amplify 16S rRNA genes from cyanobacteria. *Applied and Environmental Microbiology,* 63(8): 3327–3332.

Oksanen, J., Blanchet, F. G., Kindt, R., Legendre, P., Minchin, P. R., O'hara, R. B., Simpson, G. L., et al. (2013). "vegan": community ecology package. R package version 2.4-6. https://cran.r-project.org/web/packages/vegan/index.html

Pascal, P. & Fleeger, J.W. (2013). Diverse dietary responses by saltmarsh consumers to chronic nutrient enrichment. *Estuaries and Coasts*, 36: 1115-1124. DOI: 10.1007/s12237-013-9624-1

Prado, P., Alcoverro, T., & Romero, J. (2008). Seasonal responses of *Posidonia oceanica* epiphytic assemblages to nutrient increase. *Marine Ecology Progress Series*, 359: 89-98. DOI: 10.3354/meps07438

Quast, C., Pruesse, E., Yilmaz, P., Gerken, J., Schweer, T., Yarza, P., Peplies, J., & Glöckner, F. O. (2013). The SILVA ribosomal RNA gene database project: improved data processing and web-based tools. *Nucleic Acids Research*, 41(Database issue): D590–D596. https://doi.org/10.1093/nar/gks1219

Quiñones-Rivera, Z.J. & Fleeger, J.W. (2005). The grazing effects of grass shrimp, Palaemonetes pugio, on epiphytic microalgae associated with Spartina alterniflora. *Estuaries*, 28(2): 274-285. https://doi.org/10.1007/BF02732861

Rimet, F., Gusev, E., Kahlert, M., Kelly, M.G., Kulikovskiy, M., Maltsev, Y., Mann, D.G., Pfannkuchen, M., Trobajo, R., Vasselon, V., Zimmermann, J., & Bouchez, A. (2019). Diat.barcode, an open-access curated barcode library for diatoms. *Nature Scientific Reports*, 9: 15116. https://doi.org/10.1038/s41598-019-51500-6

Sherwood, A., Presting, G. 2007. Universal primers amplify a 23s rDNA plastid marker in eukaryotic algae and cyanobacteria. *Journal of Phycology* 43(3): 605-608.

Smith, V.H. & Schindler, D.W. (2009). Eutrophication science: where do we go from here? *Trends in Ecology & Evolution*, 24(4): 201-207. DOI: 10.1016/j.tree.2008.11.009

Stowe, W.C. (1972). Community structure and production of the epiphytic algae in the Barataria Bay area of Louisiana. LSU Historical Dissertations and Theses, 2315. https://repository.lsu.edu/gradschool_disstheses/2315

Sullivan, M.J. (1977). Structural characteristics of a diatom community epiphytic on *Ruppia maritima*. *Hydrobiologia*, 53: 81–86. https://doi.org/10.1007/BF00021236

Sullivan, M.J., & Currin, C.A. (2002). Community structure and functional dynamics of benthic microalgae in salt marshes. *In*: Weinstein, M.P., & Kreeger, D.A. (eds), Concepts and Controversies in Tidal Marsh Ecology. Springer, Dordrecht. https://doi.org/10.1007/0-306-47534-0_6

Tilman, D., Kilham, S.S., & Kilham, P. (1982). Phytoplankton community ecology: The role of limiting nutrients. *Annual Review of Ecology and Systematics*, 13: 349–372. doi:10.1146/annurev.es.13.110182.002025

Tobias, C. & Neubauer, S.C. (2019). Salt marsh biogeochemistry—an overview. *In*: Perillo, G.M.E., Wolanksi, E., Cahoon, D.R., & Hopkinson, C.S. (Eds.), Coastal Wetlands, 2nd ed. Elsevier, Masachusetts, pp. 539-596.

Twilley, R.R., Kemp, W.M., Staver, K.W., Stevenson, J.C., & Boynton, W.R. (1985) Nutrient enrichment of estuarine submersed vascular plant communities. 1. Algal growth and effects on production of plants and associated communities. *Marine Ecology Progress Series*, 23: 179-191. DOI: 10.3354/meps023179

Van Dolah, F.M., Roelke, D., & Greene, R.M. (2001). Health and ecological impacts of harmful algal blooms: risk assessment needs. *Human and Ecological Risk Assessment: An International Journal*, 7(5): 1329-1345, DOI: 10.1080/20018091095032

Vasselon, V., Rimet, F., Tapolczai, K., & Bouchez, A. (2017). Assessing ecological status with diatoms DNA metabarcoding: Scaling-up on a WFD monitoring network (Mayotte Island, France). *Ecological Indicators*, 82: 1–12. https://doi.org/10.1016/j.ecolind.2017.06.024

Verhulst, S. (2013). Response of the epiphytic algal communities to experimentally elevated nutrient levels in intertidal salt marsh habitats. UNF Graduate Theses and Dissertations, 435. https://digitalcommons.unf.edu/etd/435

Wear, D.J., Sullivan, M.J., Moore, A.D., & Millie, D.F. (1999). Effects of water-column enrichment on the production dynamics of three seagrass species and their epiphytic algae. *Marine Ecology Progress Series*, 179: 201-213.

Wijewardene, L., Wu, N., Fohrer, N., & Riis, T. (2022). Epiphytic biofilms in freshwater and interactions with macrophytes: Current understanding and future directions. *Aquatic Botany*, 176: 103467. https://doi.org/10.1016/j.aquabot.2021.103467

CHAPTER 2: CULTURE-DEPENDENT CHARACTERIZATION OF BENTHIC CYANOBACTERIA ISOLATED FROM THE GUANA TOLOMATO MATANZAS NATIONAL ESTUARINE RESEARCH RESERVE, A SUB-TROPICAL ESTUARINE ECOSYSTEM

ABSTRACT

Cyanobacteria often dominate benthic algal assemblages in intertidal ecosystems, which are characterized by harsh environmental conditions including high levels of ultraviolet irradiation and periodic desiccation. In these environments, cyanobacteria provide a number of important ecosystem services, including sediment stabilization and atmospheric nitrogen fixation. Despite the significance of these organisms, relatively little effort has been made to characterize benthic cyanobacterial diversity in sub-tropical estuarine ecosystems, such as the Guana Tolomato Matanzas National Estuarine Research Reserve (GTMNERR), located in northeastern Florida (USA). In this work, sixteen strains of benthic cyanobacteria from the GTMNERR were isolated and characterized using a polyphasic approach. Based on the combined results of morphological, molecular, and ecological analyses of the isolated strains, two novel species were described in the present work. Six novel species, as well as two novel genera, were also tentatively identified, indicating that intertidal habitats such as the one studied here represent an untapped wealth of novel cyanobacterial diversity.

INTRODUCTION

The Cyanobacteria constitute a remarkably ecologically and morphologically diverse group of oxygenic photoautotrophic bacteria. Putative evidence of this ancient lineage appears in the fossil record as far back as 3.5 BYA, in the form of fossilized layered microbial mats, called stromatolites (Knoll, 2008). Extant cyanobacteria now colonize myriad terrestrial and aquatic habitats from tropical to polar regions, and their morphology ranges from solitary cells less than one micron wide, to structurally complex filamentous forms capable of producing terminally differentiated cell types (Muro-Pastor & Hess, 2012). Over the course of their billions of years in existence, cyanobacteria have profoundly influenced the development of life on Earth. The oxygenation of Earth's atmosphere was ultimately enabled by the evolution of oxygenic photosynthesis in cyanobacteria (Garcia-Pichel, 2009), and the derivation of the plastid from a cyanobacterial endosymbiont subsequently allowed this photosynthetic capacity to propagate throughout the eukaryotic domain (Rockwell et al., 2014). Cyanobacteria currently maintain a significant role in the global carbon cycle, contributing up to 50% of the total primary productivity of the open oceans (Garcia-Pichel, 2009), and in the nitrogen cycle, with many taxa capable of biological nitrogen fixation (Knoll, 2008).

In estuarine tidal flats and salt marshes, benthic (i.e., substrate-associated) cyanobacteria are of particular importance. Cyanobacteria often dominate harsh environments such as tidal flats (Vogt et al., 2019), which experience high levels of ultraviolet irradiation, periodic desiccation, and strong fluctuations in temperature and salinity (Bolhuis et al., 2014). The exudation of extracellular polymeric substances (EPS) by cyanobacteria promotes sediment stability and increases resistance to erosion (Serôdio & Paterson, 2021), and, as a source of organic matter,

helps to form the foundation of microbial food webs (Bolhuis et al., 2014). In this way, cyanobacteria pioneer the development of intertidal microbial mats, and the structural and chemical conditions created by these mats in turn enables colonization of the sediment by more "complex" organisms, ultimately facilitating the formation of coastal ecosystems such as salt marshes (Bolhuis et al., 2014). In salt marshes, primary production by benthic cyanobacteria and other microalgae is of particular importance during parts of the year when vascular plants (e.g., Spartina alterniflora) are dormant (Sullivan & Currin, 2002). Nitrogen fixation by benthic cyanobacteria may also constitute a significant component of the nitrogen cycle in certain salt marshes (Sullivan & Currin, 2002), particularly in young or restored marshes (Tobias & Neubauer, 2019). Benthic cyanobacteria are thus crucial to not only the initial development of estuarine ecosystems, but also to their sustained health.

Despite the prevalence and ecological importance of benthic cyanobacteria in estuarine ecosystems, their biodiversity in these habitats remains relatively poorly studied. Compared to their aquatic (e.g., planktonic) counterparts, benthic and terrestrial cyanobacterial assemblages have been less thoroughly investigated (Nabout et al., 2013; Gama et al., 2014; Lopes et al., 2012). In tropical and sub-tropical estuarine ecosystems, this limited understanding of benthic cyanobacterial diversity is compounded by the fact that efforts to study cyanobacterial diversity in general have historically been concentrated in temperate regions (Gama et al., 2014; Dvořák et al., 2015a; Komárek, 1995). Exacerbating this issue even further is the taxonomic confusion plaguing the relatively under-studied coccoid cyanobacteria (Gama et al., 2014; Komárek, 1995; Shalygin et al., 2019; Mareš et al., 2019), which often constitute the dominant cyanobacterial taxa in benthic intertidal habitats (Vogt et al., 2019), thus obscuring the true extent of cyanobacterial diversity in these environments.

In an effort to ameliorate these issues, the objective of the present study was to characterize the biodiversity of benthic cyanobacteria within the Guana Tolomato Matanzas National Estuarine Research Reserve (GTMNERR), a sub-tropical estuary in northeastern Florida (USA). Sixteen strains of cyanobacteria were isolated from three sites within GTMNERR, and were characterized using a polyphasic, or total evidence, approach. The polyphasic approach to characterization considers morphological, ecological, and molecular data (Komárek et al., 2014), the latter of which typically includes phylogenies based on 16S rRNA gene sequence data, as well as predicted RNA secondary structures for semi-conserved regions of the 16S-23S internal transcribed spacer (ITS) region (Mareš et al., 2019). The polyphasic analysis thus conducted revealed considerable morphological and phylogenetic diversity among the cyanobacterial strains isolated, many of which will require the description of novel species, and in some cases genera, to accommodate them. Two novel species are formally described in the present work, and an additional six novel species, as well as two novel genera, are tentatively identified. These findings suggest that benthic habitats within tropical to sub-tropical estuarine ecosystems, such as GTMNERR, represent rich sources of cyanobacterial taxa that have yet to be discovered and formally described.

METHODS

SAMPLING SITES AND SAMPLE COLLECTION

Samples for isolation and cultivation of cyanobacterial strains were collected from the Guana Tolomato Matanzas National Estuarine Research Reserve (GTMNERR) in northeast Florida, USA (Fig. 1A). Samples of sediment/substrate material were collected from three sites within the GTMNERR (Wet Feet Middle, Guana Dam South, and Shell Bluff; Fig. 1A), all of which are tidally influenced and experience periodic submersion. The Wet Feet Middle (WFM) site (Fig.

1B) is located in an estuarine tidal marsh habitat within the GTMNERR's southern portion. Vegetation at the WFM site, predominantly *Spartina alterniflora*, as well as *Batis maritima* and *Avicennia germinans,* provides partial shade to the underlying substrate. The Guana Dam South (GDS) and Shell Bluff (SB) sites (Fig. 1C; Fig. 1D), located within the northern portion of the GTMNERR, lack vegetation or other shade-providing structures and are exposed to full sunlight.

Six samples of sediment/substrate material were collected in glass vials from each site on August 10th, 2021 (Table S1). Substrate material collected from the WFM site had a soft, muddy texture. Substrate samples collected from the GDS and SB sites were both characterized by a coarser texture: GDS substrate material was sandy, while SB substrate was composed primarily of small shell fragments.

CYANOBACTERIA ISOLATION AND CULTIVATION

Sediment/substrate material was spread on marine Z8 (Edvardsen et al., 2004) agar plates using sterile inoculating loops. Plates were incubated at ambient light and temperature and routinely monitored for cyanobacterial growth. Single cyanobacterial colonies and filaments were transferred to new agar plates using sterilized tweezers or inoculating loops. Colonies and/or or filaments were repeatedly transferred to new agar plates in this manner until microscopic inspection of cultured material confirmed the presence of only a single cyanobacterial strain on a given plate. Material from cultured isolates was then transferred onto triplicate marine Z8 agar slants for long-term maintenance and analysis. Cyanobacterial isolates were thereafter maintained in triplicate cultures at ambient light and temperature for the duration of this study. When necessary, cycloheximide was applied to cultures to control fungal growth.

MORPHOLOGICAL CHARACTERIZATION OF ISOLATES

Cyanobacterial isolates were examined and photographed via light microscopy using an Olympus BX-51 microscope, OMAX 18MP camera, and OMAX ToupView software. When possible, cultures of each isolate were observed and photographed at different ages in order to document morphological changes associated with growth stage. To determine cell length and width (or diameter, in the case of spherical cells), a minimum of twenty cells were measured for each isolated strain. Descriptions of each isolate's observed morphological details were compiled and compared to taxonomic descriptions in Komárek & Anagnostidis (2008a; 2008b).

MOLECULAR TECHNIQUES

16S rRNA and 16S-23S ITS region DNA sequences were amplified directly from cell lysate using primers CYA8F (Lane, 1991) and CYAB23S (Lepère et al., 2000). To obtain cell lysate from each culture, biomass was transferred via sterile inoculating loop from the agar slant to a microcentrifuge tube containing 250 µL of nuclease-free water. The cells were then briefly vortexed, placed in a -20°C freezer for 30 minutes, and centrifuged at high speed for 10 minutes. The resulting supernatant was then used as cell lysate in PCR reactions. Each PCR reaction mix consisted of 25 µL of DreamTaq™ Green PCR Master Mix (Thermo Fisher Scientific), 0.5 µL each of forward and reverse primers, and 24 µL of cell lysate, for a total reaction volume of 50 µL. Thermocycler parameters for amplification were as follows: initial denaturation at 95°C for 5 minutes, followed by 35 cycles of 95°C for 1 minute, 57°C for 45 seconds, and 72°C for 4 minutes, and final elongation at 72°C for 5 minutes. Direct PCR products were cleaned using the PureLink™ Quick PCR Purification Kit (Thermo Fisher Scientific), and 10 µL of cleaned PCR products were then analyzed using agarose gel electrophoresis to confirm the presence and expected size of amplicons. Purified PCR products yielding amplicons of the expected size were

sequenced by Eurofins Genomics (Louisville, KY, USA). Three sequencing reactions were prepared for each sample, each containing 8 μL of PCR product and 4 μL of one of the following primers: CYA8F, CYANO515F, or CYAB23S. Resulting nucleotide sequences were manually inspected and trimmed using SnapGene Viewer 6.1 (www.snapgene.com).

PHYLOGENETIC ANALYSIS

Forward and internal sequences from each sample, obtained using primers CYA8F and CYANO515F, respectively, were concatenated using DNA Subway (https://dnasubway.cyverse.org/). A BLASTn (https://blast.ncbi.nlm.nih.gov/Blast.cgi) search was performed for each concatenated sequence, excluding uncultured/environmental sequences from the search set. Based on the taxonomic affiliations revealed by the BLASTn searches, the GTMNERR strains were separated into four groups for the purposes of phylogenetic analysis, and separate 16S-based phylogenetic analyses were conducted for each group. For each analysis, the top ten BLAST matches with ≥90% query coverage for each GTMNERR strain in the analysis group were included in the 16S rRNA gene sequence dataset. Additional sequences from related taxa, including type strains, when available, were also included in the dataset. Two sequences of *Gloeobacter* (*G. violaceus* and *G. kilaueensis*) were used as an outgroup in all analyses. Nucleotide sequences included in the analyses were retrieved from GenBank and the Joint Genome Institute Integrated Microbial Genomes & Microbiomes portal (https://img.jgi.doe.gov/cgi-bin/m/main.cgi).

Sequences were aligned using MAFFT version 7 (Katoh & Standley, 2013) and alignments were viewed and manually trimmed in AliView version 1.28 (Larsson, 2014). The trimmed alignment spanned 1,284 positions for the analysis including GTMNERR strains 1, 4, 7, 2, and 3, 1,330 positions for the analysis including strains 5 and 6, 1,321 positions for the

analysis including strains 12 and 13, and 1,323 positions for the analysis including strains 10, 14, 15, 19, 20, 21, and 22. jModelTest 2 (Darriba et al., 2012) was used to select the best substitution model using the Akaike Information Criterion. GTR + I + G was selected as the best model and was applied in all analyses. Maximum likelihood analyses were carried out with 1,000 bootstrap pseudoreplicates using RAxML version 8.2.12 (Stamatakis, 2014). Bayesian analyses were done using MrBayes version 3.2.7 (Ronquist et al., 2012). The Bayesian analyses employed two runs of four Markov chains for at least three million generations, sampling every 100th generation, until the average standard deviation of split frequencies was less than 0.01. The first 25% of trees were discarded as burn-in. The CIPRES Science Gateway (Miller et al., 2010) was used for all sequence alignments, model selection, and phylogenetic tree reconstructions.

ITS SECONDARY STRUCTURE ANALYSIS

Reverse sequences from each sample, obtained using primer CYAB23S, were converted to their reverse-complements using SnapGene Viewer 6.1 (www.snapgene.com). For the analyses of strains GTM5 and GTM6, nucleotide sequences for the 16S-23S ITS regions of closely related strains were retrieved from GenBank and the Joint Genome Institute Integrated Microbial Genomes & Microbiomes portal (https://img.jgi.doe.gov/cgi-bin/m/main.cgi). Annotation of all D1-D1' and BoxB regions, as well as tRNA genes, was done manually in Microsoft Word. Hypothetical secondary structures of the D1-D1` and BoxB regions were folded using mFold RNA Folding Form version 2.3 (Zuker, 2003), with structure draw mode set to untangle with loop fix and default settings for all other parameters. Corrections were made to the D1-D1' structures of strains SKTU126, CCY 0110, and WH 8501 (not sequenced in this study) by employing folding constrains (as described by Mareš et al., 2019) in mFold. In all three cases, the first four bases were forced to pair. For strain CCY 0110, bases 127 through 135 were forced

to be single-stranded. For strain WH 8501, bases 55 through 65 and bases 82 through 88 were forced to be single-stranded. No folding constraints were employed for any BoxB structures. In cases where more than one possible D1-D1' or BoxB structure was generated, the structure with the lowest Gibbs free energy was selected for analysis.

RESULTS

OVERVIEW OF CYANOBACTERIAL STRAINS ISOLATED

A total of sixteen strains of cyanobacteria were isolated from the GTMNERR samples collected on August 10th, 2021. Ten strains were isolated from the Guana Dam South samples, one was isolated from the Shell Bluff samples, and five were isolated from the Wet Feet Middle samples (Table S1). The sixteen strains were found to belong to ten different morphotypes, of which four exhibited filamentous morphology and six exhibited coccoid morphology. Morphological traits of the filamentous and coccoid strains isolated are summarized in Table 1 and Table 2, respectively. Detailed morphological descriptions of all strains are also included in Appendix A.

The taxonomic classifications of all isolated strains, based on the conducted polyphasic analyses, are described in the following section. Taxonomic classifications of all isolated strains are summarized in Table 3.

CLASSIFICATION OF ISOLATED STRAINS BASED ON POLYPHASIC CHARACTERIZATION

Strain GTM2

Strain GTM2 (Fig. 2) was characterized by more or less solitary filaments, which were loosely and irregularly aggregated in culture, forming a fine, thin layer on the surface of the culture medium. Trichomes were narrow and enveloped by very thin, colorless sheaths, with longer-than-wide cells and rounded apical cells. Cell content was blue-green, without aerotopes, and solitary prominent granules were often present near cell crosswalls.

The BLAST search of GTM2's 16S rRNA gene sequence found that this strain had 100% 16S sequence similarity with *Baaleninema simplex* strain PCC 7105 (Table 4) and had sequences similarities >99% with several ambiguously named "*Geitlerinema* sp." strains. *B. simplex* PCC 7105 was previously also classified as "*Geitlerinema* sp," but was revised and reclassified by Samylina et al. (2021). The phylogenetic cluster formed by *B. simplex* PCC 7105 and its relatives had previously been referred to as the "marine *Geitlerinema*" group, as it is composed of strains isolated from marine habitats, whose 16S sequences were mainly deposited in GenBank under the name "*Geitlerinema* sp." (Samylina et al., 2021; Strunecký et al., 2017). This cluster was not considered to belong to the genus *Geitlerinema*, however, as it was previously found to be phylogenetically distant from the clade containing the reference strain for the type species of the genus (*G. splendidum* strain CCALA 1004), and its constituent strains also differ ecologically and morphologically from *Geitlerinema*, which has a freshwater distribution and is characterized by bent apical cells, which do not occur in the "marine *Geitlerinema*" strains (Samylina et al., 2021; Strunecký et al., 2017). Samylina et al. (2021) thus erected the genus *Baaleninema* to accommodate strains within one clade of the "marine *Geitlerinema*" group, and transferred "*Geitlerinema* sp." strain PCC 7105 to *Baaleninema simplex*, designating this strain as the type strain of the genus. The authors also determined that "*Geitlerinema* sp." strain Flo1 belongs to *B. simplex,* and that several other strains (e.g., CENA552) belong to another closely related species (Samylina et al., 2021), though these strains all currently retain the incorrect name "*Geitlerinema* sp." in GenBank. Additionally, Samylina et al. (2021) determined that a phylogenetically distinct cluster of several strains (e.g., BBD P2b-1) represented a clearly separate species within the genus *Baaleninema*, though the species could not be validly described, as the strains were not available in culture.

Strain GTM2, *B. simplex* PCC 7105, "*Geitlerinema* sp." strains Flo1 and H8DM, and "*Oscillatoria* sp." strain S8, had 100% 16S sequence similarity with one another (Table S2) and clustered together in a well-supported clade (Bayesian and Maximum Likelihood (ML) branch supports of 0.9468 and 85, respectively) in the 16S rRNA phylogenies (Fig. 12) This group, together with "*Geitlerinema* sp." strains CENA552 and CENA556, and strain A28DM, formed a strongly-supported group (Bayesian and ML branch supports of 1.00 and 98), separate from a smaller clade composed of "*Geitlerinema* sp." strains BBD HS223, BBD HS217, BBD P2b-1, and W-1. All of these strains together formed a strongly-supported clade (100% branch support in both methods), sister to which is the genus *Sodalinema*. Analysis of the 16S-23S ITS regions from GTM2 and closely related strains found that GTM2, Flo1, and PCC 7105 all had identical D1-D1' sequences (and thus identical secondary structures), which differed from the sequence and secondary structure of the D1-D1' region of CENA552 and CENA556 (Fig. 16). All five strains had identical BoxB sequences (Fig. 17). Sequence data for the 16S-23S ITS region was not available for strains S8, H8DM, A28DM, W-1, or the BBD strains.

The morphology and habitat type of GTM2 is consistent with that of the genus *Baaleninema*, as described by Samylina et al. (2021). Though the only available information regarding the habitat of the type strain (PCC 7105) is that the habitat is "marine" (Samylina et al., 2021), the GenBank records associated with strains CENA552, CENA556, and A28DM indicate that these strains were isolated from benthic marine or intertidal habitats, similar to GTM2.

Based on the combined results of the morphological, ecological, phylogenetic, and ITS secondary structure analyses, strain GTM2 is identified as belonging to the species *Baaleninema simplex*. The results of the phylogenetic and ITS secondary structure analyses also suggest that

strain Flo1 should be classified as *B. simplex*, and that strains CENA552 and CENA556 should be classified as a separate but closely related species of *Baaleninema,* as was proposed by Samylina et al. (2021).

Strain GTM5

Strain GTM5 (Fig. 3) was characterized by roughly spherical to rod-shaped cells, mostly irregularly aggregated in amorphous colonies, but sometimes arranged in a sheet-like single layer of cells. Colonial mucilage was present, but was usually diffluent, indistinct, and visible only with staining. Colonies initially formed bright blue-green to green spots and/or films on the surface of the culture medium, which later aggregated into larger, more or less dome-shaped, dark blue-green, gelatinous-looking masses.

The BLAST search of GTM5's 16S rRNA gene sequence found that this strain had 99.4% 16S sequence similarity with both *Zehria* sp. strain KO11DG and *Zehria* sp. strain SK40 (Table 4). These strains were originally identified as "*Gloethece* sp." by Ohki et al. (2008), but were transferred to the genus *Zehria* by Mareš et al. (2019). *Zehria* was erected by Mareš et al. (2019) to accommodate these strains, as well as several strains originally classified as "*Cyanothece* sp," as part of a larger effort to revise the taxonomy of several coccoid cyanobacterial genera, including *Cyanothece* and *Gloethece*, which numerous cyanobacterial strains had previously been incorrectly assigned to. *Z. floridana* strain WH8904, previously classified as "*Cyanothece* sp," was designated as the reference strain for the type species (*Z. floridana*) of the genus (Mareš et al., 2019).

GTM5 fell into a strongly-supported clade (Bayesian and ML branch supports of 0.9997 and 94, respectively) containing all other *Zehria* strains in the 16S phylogenies (Fig. 13). GTM5 and the *Zehria* sp. strains KO11DG, SK40, SKTU126, and KO68DGA, clustered together in a highly-

supported group (100% branch support in both methods) separate from the type species, *Z. floridana* (strain WH8904). The relationship of GTM5 to the *Zehria* sp. strains, however, was not well-resolved by the phylogenies. GTM5 and the *Zehria* sp. strains had between 97.3-97.7% 16S sequence similarity with *Z. floridana* WH8904, while 16S sequence similarity among GTM5 and the *Zehria* sp. strains was 98.9-99.7% (Table S3).

Analysis of the 16S-23S ITS regions from GTM5 and closely related strains found that the sequence and predicted RNA secondary structure of GTM5's D1-D1' region was distinct from that of all other *Zehria* sp. strains (Fig. 18), with GTM5 having the shortest D1-D1' sequence. The D1-D1' sequences of strains KO11DG and KO68DGA differed from each other by only a single nucleotide, and their corresponding secondary structures were highly similar to one another. SK40's D1-D1' sequence was only one nucleotide longer than that of KO68DGA, but its predicted RNA secondary structure was distinct from that of KO68DGA and KO11DG. Strain SKTU126 had the longest D1-D1' sequence, and its predicted RNA secondary structure was distinct from the structures predicted for all other *Zehria* sp. strains. Strains KO68DGA and KO11DG shared identical BoxB sequences, which differed from GTM5's BoxB's sequence at 5 nucleotide positions, and strains SK40 and SKTU126 shared identical BoxB sequences, which differed from GTM5's BoxB's sequence at 3 nucleotide positions. The predicted RNA secondary structures of the BoxB region were structurally identical among all the strains, however (Fig. 19). No sequence data for the 16S-23S ITS region was available for the type species, *Z. floridana* WH8904.

Strains SKTU126, SK40, KO11DG, and KO68DGA are described by Ohki et al. (2008) as having cells of a similar size and shape to those of GTM5. SK40, KO11DG, and KO68DGA are also described as dividing by binary fission in a single plane transverse to the long axis of the

cell, as is the case for GTM5, and as forming sheet-like aggregates similar to those formed by GTM5 (Ohki et al., 2008). However, the genus *Zehria* is described by Mareš et al. (2019) as not forming colonies and as lacking mucilage, which is inconsistent with the observed morphology of GTM5. The apparent difference in morphology between GTM5 and *Zehria*, as it is described, may stem from the fact that the observations of Mareš et al. (2019) were based exclusively on culture material of *Z. floridana* WH8904, as cultures of the strains classified as *Zehria* sp. were not available. Available data concerning the habitats from which other strains of *Zehria* were isolated indicate that the genus occurs in marine or intertidal habitats similar to that of GTM5. Strains SK40, KO11DG, and KO68DGA were all isolated from Singapore, from an intertidal zone beneath mangroves, the surface of sand, and the surface of seaweed, respectively (Ohki et al., 2008). SKTU126 was isolated from Japan, and is described only as having been isolated from coastal water (Ohki et al., 2008). *Z. floridana* WH8904 is described by Mareš et al. (2019) as having been isolated from mangroves in Florida in 1989.

Based on the strong phylogenetic support for GTM5 belonging to the genus *Zehria*, and based on this strain's phylogenetic separation from the only other validly described species in the genus, *Z. floridana*, the species *Z. dixii*, sp. nov., is here proposed to accommodate strain GTM5. Given the inconsistencies between the described morphology of the genus and the observed morphology of *Z. dixii* GTM5, an emended morphological description of the genus *Zehria* is also recommended.

TAXONOMIC DESCRIPTION OF *ZEHRIA DIXII*, SP. NOV.

Diagnosis: Separated from the only other named *Zehria* species, *Z. floridana,* based on phylogenetic separation.

Description: Coccoid. In culture, thallus initially forming bright blue-green to green spots and/or films on surface of agar, later aggregating into larger, more or less hemispherical, dark blue-green, gelatinous-looking masses. Cells aggregated in mostly amorphous colonies, occasionally somewhat lobate or clathrate. Cells in colonies somewhat densely to very densely aggregated, irregularly arranged or sometimes exhibiting an indistinct parallel row-like arrangement; in smaller colonies and near margins of larger colonies, cells are often closely and irregularly arranged in a sheet-like single layer. Cells sometimes loosely arranged in short chains, mostly evident only near colony borders or in very small colonies. Colonial mucilage colorless, usually indistinct (only visible with staining); large masses of cells occasionally with distinctly delimited, slightly widened common mucilage. Cells more or less spherical to oval or widely cylindrical with rounded ends, 1.9-3.5 μm wide by 2.7-4.7 μm long (dividing cells up to 5.3 μm long), without individual mucilaginous envelopes. Cell content blue-green, sometimes with one to a few solitary granules. Cells divide by binary fission in a single plane, transverse to long axis of the cell; cells sometimes in pairs following division.

Habitat: Intertidal, on coarse substrate composed of shell fragments.

Type locality: Guana Tolomato Matanzas National Estuarine Research Reserve, Florida, USA.

Reference strain: *Zehria dixii* GTM5.

Etymology: *dixii* = Named in honor of Nicole Dix, research director at the Guana Tolomato Matanzas National Estuarine Research Reserve, who facilitated the research project which led to the discovery of this species.

Taxonomic notes: While the predicted D1-D1` secondary structure of strain GTM5 is distinct from that of all *Zehria* sp. strains (SKTU126, SK40, KO11DG, and KO68DGA), there is also

variation in D1-D1` secondary structures among the *Zehria* sp. strains, and a clear phylogenetic separation between GTM5 and these strains was not resolved. In the absence of available cultures of any of these strains, however, the provisional placement of all these strains in *Zehria* sp. (Mareš et al., 2019) is retained here.

Strain GTM6

Strain GTM6 (Fig. 4) exhibited remarkably different morphological forms over the course of its growth cycle, but the most commonly-observed form consisted of oval to subspherical cells, mostly in groups of 2-8 cells, with colorless or yellowish-brown mucilaginous envelopes surrounding cells and groups of cells. Cells and small groups of cells were irregularly aggregated together, forming dark blue-green to nearly black masses on the surface of the culture medium.

The BLAST search of GTM6's 16S rRNA gene sequence found that this strain had between 99.3-99.4% 16S sequence similarity with *Crocosphaera* sp. 1 strains KO38CU6, KO30D1, and KO20B5 (Table 4). These strains were originally identified as "*Gloecapsa* sp." by Ohki et al. (2008), but were later transferred to the genus *Crocosphaera* by Mareš et al. (2019), along with a number of strains incorrectly classified as "*Cyanothece* sp." *Crocosphaera* was first validly described by Mareš et al. (2019), in the same work that included the description of the genus *Zehria*.

GTM6 fell into a strongly-supported clade (Bayesian and ML branch supports of 0.9973 and 93, respectively) containing all other *Crocosphaera* strains in the 16S phylogenies (Fig. 13). GTM6, *C. chwakensis* CCY 0110, *C. subtropica* ATCC 51142, a cluster of *Crocosphaera* sp. 1 strains, and a cluster of *Crocosphaera* sp. 2 strains, together formed a highly-supported phylogenetic group (Bayesian and ML branch supports of 1.00 and 98) separate from all sequences of the type species, *C. watsonii*. Within this group, the three *Crocosphaera* sp. 1

strains clustered together with strong support (Bayesian and ML branch supports of 1.00 and 95), as did the five *Crocosphaera* sp. 2 strains (100% branch support in both methods). *C. subtropica* ATCC 51142 was placed as the sister taxon to the *Crocosphaera* sp. 1 group, but with weak support. The relationship of GTM6 to *C. chwakensis* CCY 0110 was poorly resolved. Both strains formed separate, but very short, branches within this group. The similarity matrix based on an alignment of the 16S sequences of all strains in the genus found that *C. chwakensis* CCY 0110 had the highest 16S sequence similarity with GTM6 (Table S4).

Compared to all other *Crocosphaera* strains with 16S-23S ITS sequence data available, the D1-D1' sequence of *C. chwakensis* CCY 0110 was unusually long, while that of *C. subtropica* ATCC 51142 was unusually short. The D1-D1' sequences of all *C. watsonii* and *Crocosphaera* sp. 1 strains were 92 nucleotides in length, while GTM6's D1-D1' sequence was 90 nucleotides in length. The predicted RNA structure of the D1-D1' region of GTM6 (Fig. 20) also exhibited a unilateral bulge not present in the structures of any other strains in the genus. *C. watsonii* strains WH8502, WH0003, and WH0401 had identical D1-D1' sequences, and the D1-D1' sequence of *C. watsonii* strain WH8501 differed from the other *C. watsonii* strains at only a single nucleotide position. *Crocosphaera* sp. 1 strains KO38CU6, KO30D1, and KO20B5 had identical D1-D1' sequences. All *C. watsonii* strains had identical BoxB sequences, and all *Crocosphaera* sp. 1 strains had identical BoxB sequences. The BoxB sequence of the *C. watsonii* strains differed from that of GTM6 at seven nucleotide positions, but the predicted RNA structure (Fig. 21) was structurally identical to that of GTM6. The BoxB sequence of *C. subtropica* ATCC 51142 was one nucleotide shorter than that of all other strains (34 nucleotides vs 35 nucleotides), but its predicted RNA secondary structure was similar to that of GTM6 and the *C. watsonii* strains. *C. chwakensis* CCY 0110's BoxB sequence differed from that of GTM6

at three nucleotide positions, but its predicted RNA secondary structure was distinct from that of all other strains in the genus, including GTM6. The predicted RNA secondary structure for the BoxB region of the *Crocosphaera* sp. 1 strains was also distinct from all other strains in the genus. 16S-23S ITS sequence data was not available for any of the *Crocosphaera* sp. 2 strains.

Most strains within *Crocosphaera* are described as forming different types of colonies, or aggregations of cells, during different growth phases (Ohki et al., 2008; Mareš et al., 2019), as was observed in strain GTM6. *C. subtropica* and *C. chwakensis* are described as forming elongated cells during certain growth phases (Mareš et al., 2019), which was also observed in GTM6. However, the presence of yellowish-brown mucilaginous envelopes surrounding cells and groups of cells, observed in GTM6 during certain growth phases, is not mentioned in the description of the genus or any species therein (Mareš et al., 2019). Given the highly variable morphology observed in GTM6, it is possible that other *Crocosphaera* strains also produce similar mucilaginous envelopes during certain growth phases and/or under certain conditions, and that this trait was not previously observed. Strains within the genus Crocosphaera have been isolated from tropical and subtropical marine habitats, including several substrate-associated habitats, similar to GTM6. The three *Crocosphaera* sp. 1 strains were isolated from Singapore, from the surface of seaweed, the surface of mud in an intertidal zone, and from seawater (Ohki et al., 2008). *C. chwakensis* CCY 0110, *C. subtropica* ATCC 51142, the *Crocosphaera* sp. 2 strains, and the *C. watsonii* strains were isolated from marine sediments in Chwaka, Zanzibar, from an intertidal zone in Texas, from coastal waters near Korea, and from open waters in the tropical Atlantic Ocean, respectively (Mareš et al., 2019).

Based on the strong phylogenetic support for GTM6 belonging to the genus *Crocosphaera*, and based on its unique D1-D1' secondary structure compared to other species

within this genus, the species *C. variabilis,* sp. nov., is here proposed to accommodate strain GTM6.

TAXONOMIC DESCRIPTION OF *CROCOSPHAERA VARIABILIS*, SP. NOV.

Diagnosis: Separated from all other species in the genus based on unique 16S-23S ITS D1-D1' secondary structure.

Description: Coccoid. In culture, thallus forms very dark blue-green (nearly black) masses on surface of agar; masses irregularly hemispherical, with a warty or bumpy texture and irregular margins. Cells of markedly different shapes/sizes, and associated with somewhat different colony structures or other morphological characteristics, have been observed; these forms probably represent different phases of the growth cycle and/or are related to overall age and condition of the culture. The relationships between these various forms are presently unclear (e.g., which forms represent younger colony stages and which represent older colony stages), so the most commonly observed form is described first and in the most detail, and the less frequently observed forms are described briefly in separate paragraphs; the less frequent forms are described largely in terms of their morphological differences compared to the most frequently observed form.

Cells mostly in irregular, formless colonies, consisting of aggregations of cells or small 2-4-8-celled groups. Cells or small groups of cells surrounded by mucilaginous envelopes with clearly delimited margins; common mucilage surrounding groups of cells usually indistinctly to distinctly concentrically layered, with inner layers more or less following the cell outline; colorless or yellowish-brown, and in the latter case sometimes with a rough or bumpy-looking outer surface. Cells mostly oval to rounded-cylindrical, sometimes subspherical, 2.7-4.1 μm wide by 3.6-5.2 μm long. Cell content blue-green, often vividly so; sometimes with one to several

very prominent granules in cells surrounded by yellowish-brown envelopes. Cell division in multiple planes, either regular or irregular, likely sometimes in planes perpendicular to one another.

Observed in young cultures (8 days old) only: cells sometimes fairly loosely aggregated in formless colonies, with cells irregularly arranged in a sheet-like single layer; cells in these colonies are not in 2-4-8-celled groups, and sheet-like arrangement is mainly apparent only in small colonies or near margins of larger colonies. Small irregularly rounded colonies consisting of cells very tightly packed together were also observed in young cultures.

Cells sometimes markedly more elongate than usual (up to 7.7 μm long) and kidney-bean shaped, with more olive- to yellow-green cell content (not vivid blue-green). Cells of this shape are not in distinct groups of 2-4-8 cells, and are sometimes tightly packed together in small irregularly-shaped colonies, usually with scarcely discernible to indiscernible (or absent) mucilaginous envelopes around cells within these small colonies.

Cells sometimes more irregularly and variably shaped; hemispherical, somewhat pyriform, or irregular polygonal-rounded, with dividing cells sometimes gently tapered-pointed at the ends. Cells of this form are aggregated in small to large, irregular, formless colonies, consisting of cells or small packet-like groups of cells, but without cells in distinct groups of 2-4-8. Mucilaginous envelopes around cells or small packet-like groups of cells in these colonies are sometimes clearly discernible, otherwise indistinct (or absent), and are always colorless.

Habitat: Intertidal, on sandy substrate.

Type locality: Guana Tolomato Matanzas National Estuarine Research Reserve, Florida, USA.

Reference strain: *Crocosphaera variabilis* GTM6.

Etymology: *variabilis* = Adjective (Latin), variable. Named for the highly variable morphology observed in the reference strain.

Taxonomic notes: The current morphological description of the genus *Crocosphaera* does not reflect the observed morphology of *C. variabilis* strain GTM6, particularly with regards to the occurrence of pigmented (yellowish-brown) mucilaginous envelopes. An emended morphological description of the genus is recommended.

Strains GTM1, GTM4, and GTM7

Strains GTM1, GTM4, and GTM7 (Fig. 5) were all characterized by filaments in fascicle-like colonies, wide trichomes, often layered mucilaginous sheaths, discoid cells, and yellowish-brown cell color. These three strains were essentially morphologically indistinguishable, though the hormogonia formed by strain GTM1 often exhibited a characteristic morphology not seen in strains GTM4 or GTM7.

The BLAST searches identified the strain "*Hydrocoleum* sp." PMC 1116.19 as having the highest 16S sequence similarity with each of these strains (Table 4). This strain had 98.54% sequence similarity with GTM1, 98.69% with GTM4, and 98.82% with GTM7. Given the proposed species delimitation threshold of 98.7% (Dvořák et al., 2015), the BLAST search results indicated that "*Hydrocoleum* sp." PMC 1116.19 may belong to the same species as GTM1, GTM4, and GTM7.

Analysis of the 16S-23S ITS sequence data suggested that GTM1, GTM4, and GTM7 represent the same species, as all three strains had identical D1-D1' and BoxB sequences (Fig. S1). Sequences from GTM1, GTM4, and GTM7 also clustered together in the 16S phylogenies (Fig. 12), with high support (branch support=95) in the maximum likelihood phylogeny, but with

somewhat weaker support (branch support=0.89) in the Bayesian phylogeny. "*Hydrocoleum* sp." PMC 1116.19, together with two other "*Hydrocoleum* sp." PMC strains, formed a separate cluster closely related to the GTM strains. The GTM strains and PMC strains, along with one additional "*Hydrocoleum* sp." strain, comprised a strongly-supported clade (Bayesian and ML branch supports of 0.9993 and 89, respectively), which, together with *Hydrocoleum lyngbyaceum* HBC7, was resolved as a monophyletic group sister to the genus *Tenebriella* (family Microcoleacea).

The genus *Hydrocoleum* has been revised multiple times since its original description (Palińska et al., 2015), and has yet to be clearly delineated by phylogenetic evidence (Strunecký et al., 2023). Thus, the 16S phylogenies alone cannot discern whether the three GTM strains and their close relatives should be placed in this genus. Based on the morphological description of the genus, however, it is unlikely that these strains belong to *Hydrocoleum*. *Hydrocoleum* is described as having cells that are isodiametric, or slightly shorter or longer than wide, and is characterized by noticeably motile trichomes exhibiting gliding motility. In contrast, strains GTM1, GTM4, and GTM7 had cells that were much shorter than wide (discoid), and were either immotile or exhibited nearly indiscernible gliding motility.

In addition to their clear phylogenetic separation from *Tenebriella*, strains GTM1, GTM4, and GTM7 also differ from this genus in terms of morphology. The GTM strains were characterized by ensheathed trichomes arranged in fascicle-like bundles, with a common mucilaginous sheath often surrounding multiple filaments (filaments=individual trichomes with their own sheaths). In contrast, *Tenebriella* does not exhibit this fasciculated growth habit, and multiple trichomes are never contained within a single sheath (Hauerová et al., 2021). The GTM strains are also ecologically distinct from *Tenebriella*, which is found mainly in benthic

freshwater habitats, and does not occur in marine environments (Hauerová et al., 2021). Other strains closely related to GTM1, GTM4, and GTM7, were isolated from mangroves (Wang et al., 2023), subtidal stromatolite communities (Foster et al., 2009), and intertidal microbial mats (according to GenBank record for *Hydrocoleum* sp. MF1), and thus they are also ecologically distinct from *Tenebriella*. Unfortunately, little to no morphological information is available for the other strains related to GTM1, GTM4, and GTM7, though *Hydrocoleum lyngbyaceum* HBC7 is described as having either one or multiple trichomes in a sheath (Foster et al., 2009).

Morphological, ecological, and phylogenetic data all suggest that a new genus may need to be erected to accommodate GTM1, GTM4, and GTM7. Ecological and phylogenetic evidence also suggest that the "*Hydrocoleum*" strains belonging to the same phylogenetic group as the GTM strains should be transferred to this putative novel genus. However, given the present lack of morphological information available for these related strains, and the lack of 16S-23S ITS sequence data available for the "*Hydrocoleum* sp" PMC strains, the description and thorough taxonomic evaluation of this genus will be undertaken in a separate future work. Strains GTM1, GTM4, and GTM7 are thus provisionally classified as "Microcoleaceae cyanobacterium," pending a formal description of the novel genus that will be erected to accommodate them.

Strain GTM3

Strain GTM3 (Fig. 6) was characterized by trichomes of intermediate width, colorless sheaths, and rounded or conical-rounded apical cells, which were often yellowish-brown in color. Predicted RNA secondary structures for the BoxB and D1-D1' regions of the 16S-23S ITS region for strain GTM3 are shown in Figure S2.

The BLAST search identified the strain "*Symploca* sp." HBC5 as having the highest 16S sequence similarity with GTM3, with a percent identity value of 98.33% (Table 4). This value is

below the proposed species delimitation threshold of 98.7% sequence similarity (Dvořák et al., 2015), suggesting that strain GTM3 may represent a novel species.

GTM3 was found to belong to a strongly-supported phylogenetic group (Bayesian and ML branch supports of 1.00 and 91, respectively; Fig. 12) with genera in the order Coleofasciculales, including *Caldora*, *Moorena*, *Coleofasciculus*, *Symploca*, and *Anagnostidinema* (Strunecký et al., 2023). Within the Coleofasciculales clade, GTM3 occupied a phylogenetically distinct branch within a small group of "*Symploca* sp." strains, though phylogenetic support for this group (consisting of GTM3 and the "*Symploca* sp." strains) was not strong. This group was placed as the sister taxon to a strongly-supported clade (Bayesian and ML branch supports of 1.00 and 98) comprised of six strains, including *Symploca atlantica* PCC 8002, the reference strain for *Symploca* (Porta et al., 2003). The grouping of the *S. atlantica* PCC 8002 clade with the GTM3 clade was strongly supported (branch support=0.993) in only the Bayesian phylogenetic tree.

Based on the description of *S. atlantica* PCC 8002 given by Porta et al. (2003), this strain is highly morphologically similar to GTM3. Notably, the subterminal and terminal cells in trichomes of *S. atlantica* PCC 8002 are often less pigmented than other cells in the trichomes (Porta et al., 2003), an interesting characteristic also observed in GTM3. The only apparent morphological difference between GTM3 and *S. atlantica* PCC 8002 is the frequent occurrence of apical cells with a cap-like calyptra in the latter (Porta et al., 2003), and the lack of calyptrate apical cells in the former. Strains in both the *S. atlantica* PCC 8002 clade and the GTM3 clade were isolated from benthic coastal environments, including intertidal microbial mats (Porta et al., 2003), biofilms on sediments under mangroves (Wang et al., 2023), and salt marsh benthos (according to culture information for strain UTEX LB 2515, https://utex.org/).

16S sequence similarity between GTM3 and *S. atlantica* PCC 8002 was 96.22%, strongly suggesting that GTM3 belongs to a different species. Given that *S. atlantica* PCC 8002 is the reference strain for *Symploca*, the phylogenetic separation between the *S. atlantica* PCC 8002 clade and the GTM3 clade suggest that the latter may represent a distinct genus morphologically cryptic to *Symploca*. A more detailed analysis of morphological, ecological, and molecular (including 16S-23S ITS secondary structures) data will be required to resolve the taxonomy of this group, and will have to be undertaken in future work. Strain GTM3 is thus provisionally classified as cf. *Symploca* sp. (cf indicating uncertainty), pending further taxonomic assessment of the genus *Symploca* and a formal description of the species to which GTM3 belongs.

Strains GTM12 and GTM13

Strains GTM12 and GTM13 (Fig. 7) both exhibited narrow trichomes, thin, colorless sheaths, longer-than-wide cells, and apical cells that were often narrowed, elongated, and bent. Trichomes were motile, with bending/waving motility. These two strains were highly similar in morphology, though GTM13 exhibited more distinctly bent apical cells than GTM12.

The BLAST search identified the strain "*Jaaginema* sp." PMC 1073.18 as having the highest 16S sequence similarity with GTM12, with a percent identity value of 99.05% (Table 4). GTM13 had the highest sequence similarity with this same strain, with a percent identity value of 98.66%, though the query coverage was only 89% (Table 4). GTM12 and GTM13 fell into a strongly supported phylogenetic cluster (100% branch support in both methods) containing fifteen other strains, including eleven "*Jaaginema* sp." strains (Fig. 14). GTM12 and GTM13 were phylogenetically separated from one another within this clade, and they also differed in their 16S-23S ITS D1-D1' secondary structures (Fig. S3) suggesting that these strains may represent two morphologically cryptic species. The phylogenetic position of this clade relative to

other taxa was very poorly resolved (Fig. 14), however, and its taxonomic affiliations remain unclear even at the level of Order.

The phylogenetic group containing strains GTM12 and GTM13 is one of several clusters of ambiguously named "*Jaaginema* sp." strains distributed throughout the 16S phylogeny. Reliable sequence data for the type species of *Jaaginema* is lacking (Brito et al., 2017), and thus it is not clear which, if any, of these strains belong to the "true" *Jaaginema*. However, the genus *Jaaginema* is described as obligately immotile, and lacks the bent apical cells observed in strains GTM12 and GTM13, and thus morphological evidence indicates that these two strains should not be classified as *Jaaginema*. Morphological details (including trichome motility) are not available for many of the other strains within the "*Jaaginema*" clade containing GTM12 and GTM13, but at least one other strain has motile trichomes (Everroad et al., 2016), and at least two other strains have bent apical cells similar to GTM12 and GTM13 (Bravakos et al., 2016; Romeu et al., 2023).

A more thorough phylogenetic analysis will be required to determine GTM12's and GTM13's affiliations with known cyanobacterial orders and families, and a taxonomic treatment of the genus *Jaaginema* is required in order to determine whether or not these two strains and their close relatives should be retained in *Jaaginema*. Such work will have to be undertaken in a future research endeavor, and strains GTM12 and GTM13 are thus provisionally identified as "filamentous cyanobacterium."

Strain GTM19

Strain GTM19 (Fig. 8) was characterized by hemispherical to irregularly-shaped cells, mostly yellowish-brown in color, and exhibited complex colony morphology. Colonies were compound, consisting of very compact sub-colonies or distinct colony segments, and did not easily

dissociate into smaller sub-colonies. When viewed in cross-section, the segments (or sub-colonies) of compound colonies appeared to be radially arranged to some degree, and narrowed at their bases. Cells in each colony segment also appeared to be situated in radially arranged, irregular rows, such that colonies had an overall fan-like appearance when viewed in cross-section. Predicted RNA secondary structures for the BoxB and D1-D1' regions of the 16S-23S ITS region for strain GTM19 are shown in (Fig. S4).

The BLAST search identified *Foliisarcina bertiogensis* CENA333, which is the reference strain for the type species of *Foliisarcina,* as having the highest 16S sequence similarity with GTM19, with a percent identity value of 98.41% (Table 4). This value is below the proposed species delimitation threshold of 98.7% sequence similarity (Dvořák et al., 2015), suggesting that strain GTM19 may represent a novel species of *Foliisarcina*. In the 16S phylogenies (Fig. 15), GTM19 was positioned within a strongly-supported group (Bayesian and ML branch supports of 1.00 and 96, respectively) containing *F. bertiogensis* CENA333, *F. bertiogensis* strains CENA331, CENA346, and CENA337, and several ambiguously named strains (e.g., "*Pleurocapsa* sp.").

Given that *F. bertiogensis* strains CENA333 and CENA331 are both considered to be valid representatives of the genus *Foliisarcina* (Shalygin et al., 2019), phylogenetic evidence indicates that GTM19 belongs to this genus. However, the *Foliisarcina* clade was divided into two sub-groups, and *F. bertiogensis* CENA331 was placed in the smaller sub-group, phylogenetically separated from the other three *F. bertiogensis* strains, which were placed in the larger group. Within the larger sub-group, the other three *F. bertiogensis* strains formed a highly-supported cluster together (100% branch support in both methods). Strain CENA331's phylogenetic separation from the other three *F. bertiogensis* strains, including the reference

strain, suggest that CENA331 may represent a different species of *Foliisarcina*. Strain GTM19 occupied a distinct branch at the base of the larger sub-group of the *Foliisarcina* clade. Thus, if CENA331 should indeed be reclassified as a separate species of *Foliisarcina*, then GTM19 may represent a novel third species within this genus.

Given GTM19's fairly high 16S sequence similarity with the type strain of the genus, the described morphology of *Foliisarcina* (Oliveira Alvarenga et al., 2016) was surprisingly unlike the observed morphology of GTM19. While *Foliisarcina* is described as having cells of a similar size, shape, and color as GTM19, it is also described as forming only small colonies, which apparently do not exhibit the complex "fan-like" colony structure of GTM19 (Oliveira Alvarenga et al., 2016). It is possible that these apparent morphological differences are associated with differences in culture conditions (e.g., solid vs liquid growth media) or with different growth phases, and an *F. bertiogensis* culture, if available, should be studied in order to investigate these possibilities. Until the apparent morphological differences between *F. bertiogensis* and GTM19 are more clearly characterized, GTM19 is provisionally identified as *Foliisarcina* sp.

Strains GTM20, GTM21, and GTM22

Strains GTM20, GTM21, and GTM22 (Fig. 9) were morphologically indistinguishable from each other, and were characterized by hemispherical to irregularly-shaped cells, bright blue-green in color, and exhibited complex colony morphology. These strains formed compound colonies similar to those of GTM19, in that the colonies exhibited a similar overall fan-like appearance when viewed in cross-section. Unlike GTM19, however, the compound colonies of these strains easily dissociated into smaller sub-colonies, and their bright blue-green coloration was unlike the yellowish-brown color of GTM19.

"Pleurocapsales cyanobacterium" strain 319 was identified by the BLAST searches as the closest match to strains GTM20, GTM21, and GTM22, with a percent identity value of 95.61% in all three cases (Table 4). This value is well below the proposed species delimitation threshold of 98.7% sequence similarity (Dvořák et al., 2015), and is approaching the 94.5% genus delimitation value proposed for bacteria and archaea (Yarza et al., 2014; Shalygin et al., 2019). GTM20, GTM21, and GTM22 clustered together with 100% branch support in both the Bayesian and Maximum Likelihood phylogenies (Fig. 15), indicating that these three strains represent the same species. Additionally, the strains had identical D1-D1' and BoxB sequences (Fig. S5), further supporting the conclusion that they represent the same species. These strains formed a phylogenetically distinct branch near the base of the Pleurocapsaceae clade, suggesting they belong to this family, though branch support values were not strong near the base of Pleurocapsaceae (Fig. 15).

Based on the results of the 16S sequence data analyses, GTM20, GTM21, and GTM22 clearly represent a novel cyanobacterial species, and likely represent a novel genus. However, many cyanobacterial genera were described prior to the advent of gene sequencing technology and the widespread implementation of phylogenetic analyses in taxonomy, and these genera were established based only on morphological characteristics (Komárek et al., 2014). While GTM20, GTM21, and GTM22 were not found to conform to the described morphology of any coccoid cyanobacterial genera detailed in Komárek & Anagnostidis (2008), a more thorough review of morphologically described taxa, for which sequence data is lacking, is warranted before describing this potentially novel genus. These strains are thus provisionally identified as "Pleurocapsaceae cyanobacterium," and a novel taxon will likely be formally described in a future work in order to accommodate them.

Strains GTM14 and GTM15

Strains GTM14 and GTM15 (Fig. 10) were morphologically indistinguishable from each other, and were characterized by spherical cells of various sizes (up to 16.2 μm in diameter), often pale yellowish-grey in color, and frequent formation of baeocytes. Based on the formation of baeocytes observed in these strains, in addition to the high variability in cell size, strains GTM14 and GTM15 were identified as belonging to the family Pleurocapsaceae. The strains could not be identified at the genus level based on their morphology, as many genera within the Pleurocapsaceae exhibit complex and variable colony morphology, and morphological traits often overlap to some extent between taxa (Shalygin et al., 2019; Oliveira Alvarenga et al., 2016; Gama et al., 2014).

The BLAST searches identified "*Xenococcus* sp." PCC 7307 as the closest match to both GTM14 and GTM15, with percent identity values of 98.23% and 98.22%, respectively (Table 4). These values are below the proposed species delimitation threshold of 98.7% sequence similarity (Dvořák et al., 2015), suggesting that GTM14 and GTM15 may represent a novel cyanobacterial species. However, no morphological data was available for strain PCC 7307, so its morphological similarity to GTM14 and GTM15 could not be assessed.

The results of the phylogenetic analyses indicated that GTM14 and GTM15 represent the same species, as the strains clustered together with 100% branch support in both the Bayesian and Maximum Likelihood phylogenies (Fig. 15). Analysis of the strains' 16S-23S ITS sequence data supported this finding, as both strains had identical D1-D1' and BoxB sequences (Fig. S6). "*Xenococcus* sp." PCC 7307 was placed as the sister taxon to GTM14 and GTM15, with very high branch support (0.9999) in the Bayesian phylogenetic tree and weaker branch support (54) in the Maximum Likelihood tree. GTM14 and GTM15, together with "*Xenococcus* sp." PCC

7307, formed a sub-clade within Pleurocapsaceae, thus supporting the family level identification of GTM14 and GTM15 based on their morphology. The sub-clade containing GTM14, GTM15, and "*Xenococcus* sp." PCC 7307, was phylogenetically distant from "*Xenococcus* sp." PCC 7305, which Shalygin et al. (2019) recommended be considered a reference strain for the genus *Xenococcus*. The results of the phylogenetic analyses thus indicated that GTM14 and GTM15's sister taxon, "*Xenococcus* sp." PCC 7307, should not be classified as *Xenococcus.* The phylogenetic relationship of GTM14 and GTM15 to other genera within the Pleurocapsaceae was unclear, as most of the strains within this clade were ambiguously identified (e.g., "*Pleurocapsa* sp."), and few reference sequences for genera within this family were available.

While phylogenetic evidence indicated that GTM14 and GTM15 may represent a novel cyanobacterial species, and possibly a novel genus, further analyses of molecular (e.g., 16S-23S ITS secondary structures), ecological, and morphological data from phylogenetically closely related strains will greatly facilitate efforts to describe this likely novel taxon. GTM14 and GTM15 are thus provisionally identified as "Pleurocapsaceae cyanobacterium," pending further evaluation.

Strain GTM10

Strain GTM10 (Fig. 11) exhibited spherical cells, produced baeocytes, and formed more or less dome-shaped colonies that often exhibited distinctly different coloration in different areas of the colonies. Based on the formation of baeocytes observed in this strain, GTM10 was identified as belonging to the family Pleurocapsaceae. The strain could not be identified at the genus level based on its morphology, given the highly variable nature of the morphology of many genera within the Pleurocapsaceae (Shalygin et al., 2019; Oliveira Alvarenga et al., 2016; Gama et al.,

2014). Predicted RNA secondary structures for the BoxB and D1-D1' regions of the 16S-23S ITS region for strain GTM10 are shown in (Fig. S7).

The strain "Cyanobacteriota bacterium S5-8" was identified by the BLAST search as the closest match to GTM10, with a percent identity value of 98.58% (Table 4). In the 16S phylogenies (Fig. 15), GTM10 was placed in a strongly-supported group (Bayesian and ML branch supports of 1.00 and 96, respectively) containing "Cyanobacteriota bacterium" strains S5-8 and S5-13, "Xenococcus sp." S1-5, and "Xenococcaceae cyanobacterium" strains CENA315 and CENA345. This group was within a much larger clade, containing many strains ambiguously identified as genera in Pleurocapsaceae (e.g., "Xenococcus sp."), as well as reference strains of the genera *Foliisarcina*, *Pleurocapsa*, and *Stanieria*, which belong to Pleurocapsaceae (Strunecký et al., 2023). The results of the phylogenetic analyses thus supported GTM10's placement in the family Pleurocapsaceae, but did not enable identification at the genus level, as most genera are currently polyphyletic based on the classification of strains within the family. Unfortunately, no morphological information was available for any of the strains belonging to the same phylogenetic group as GTM10, so their morphological similarity to this strain could not be assessed.

GTM10's phylogenetic separation from other sequenced strains suggests that it may represent a novel species, though further analyses of molecular (e.g., 16S-23S ITS secondary structures), ecological, and morphological data from phylogenetically closely related strains will be required before this can be determined. Strain GTM10 is thus provisionally identified as "Pleurocapsaceae cyanobacterium," with the hope that the detailed morphological characterization of this strain (included in Appendix A) may aid in further resolving its taxonomic identity in the future.

DISCUSSION

Before molecular data could be leveraged to classify cyanobacteria, taxa were distinguished from one another on the basis of morphological characters. Given the high degree of morphological plasticity among cyanobacteria, and the prevalence of cryptic (i.e., morphologically indistinguishable) species, it is now known that this traditional system cannot adequately describe cyanobacterial biodiversity (Dvořák et al., 2015b). Indeed, phylogenetic analyses, based largely on 16S rRNA gene sequence data, have revealed the polyphyletic nature of many morphologically-defined genera (Komárek et al., 2014), prompting widespread taxonomic revisions. Cyanobacterial taxonomists continue to erect new genera in order to accommodate particular subsets of species within these morphologically-defined genera, thus dividing them into multiple, ideally monophyletic, genera (Mareš et al., 2019). Challenges to these taxonomic revisions arise, however, when sequence data is lacking for the type species of a genus, as in these cases there exists no phylogenetic point of reference for the species by which the genus, in its original sense, is defined (Shalygin et al., 2019). Consequently, when sequences (e.g., 16S rRNA gene sequences) are designated as belonging to such ambiguously-defined genera, there is no way to determine which, if any, of the sequenced strains truly represent the genus in question (Mühlsteinová et al., 2018). As a result, there exist many genera which are clearly polyphyletic, in the sense that sequences assigned to them are scattered widely throughout phylogenetic trees, and for which a significant amount of work will be required in order to resolve their taxonomy (Mühlsteinová et al., 2018; Shalygin et al., 2019).

The family Pleurocapsaceae is particularly replete with genera that have yet to be defined by molecular data (Komárek et al., 2014; Shalygin et al., 2019). Previously classified as a separate order, the Pleurocapsales (Komárek et al., 2014), this group of coccoid cyanobacteria

was recently subsumed into the order Chroococcales (Strunecký et al., 2023). Many members of the Pleurocapsaceae are characterized by high variability in cell size, shape, and type of division (Strunecký et al., 2023). Given the high degree of morphological variability that can occur within an individual taxon (genus, species, or strain), morphological traits often overlap between taxa, and identifying strains based on their morphological characteristics may prove extremely difficult (Shalygin et al., 2019; Oliveira Alvarenga et al., 2016; Gama et al., 2014). Seven of the strains isolated in this work were classified as members of the Pleurocapsaceae, based on their morphological characteristics and their positions in the 16S rRNA phylogenies. However, the lack of clearly established boundaries (either morphological or molecular in nature) between most genera within this family greatly complicated the task of identifying all but one of these strains at the genus level. These seven strains putatively represent novel taxa—one novel genus, two novel species of unclear generic identity, and one novel species of *Foliisarcina*—based on phylogenetic evidence (Fig. 15), and the formal descriptions of these taxa will have to be undertaken in a future work.

The seven Pleurocapsaceae strains were all isolated from samples collected at the Guana Dam South site, which consisted of coarse, sandy sediment. In a study of cyanobacterial diversity in tidal flats along a latitudinal gradient, Vogt et al. (2019) found that Pleurocapsaceae were frequently abundant in sites characterized by similar sediments, suggesting that members of this family may be prevalent components of benthic cyanobacterial assemblages in intertidal environments with coarse-grained sediments. Thus, the full extent of diversity of cyanobacteria in these coastal habitats may remain largely obscured until the current taxonomic confusion surrounding most genera within the Pleurocapsaceae is resolved.

In addition to the Pleurocapsaceae strains, all but one of the nine other strains isolated in this work were either formally described as novel taxa or were tentatively identified as novel taxa, pending formal descriptions, based on the combined results of morphological, ecological, and phylogenetic characterizations. *Zehria dixii*, sp. nov., and *Crocosphaera variabilis*, sp. nov., were described in this work, to accommodate strains GTM5 and GTM6, respectively. The ability to formally describe these novel coccoid cyanobacterial species in the present work was greatly facilitated by the taxonomic treatment of these and other coccoid genera, undertaken by Mareš et al. (2019), further underscoring the importance of continued efforts to improve the state of cyanobacterial taxonomy in illuminating the true biodiversity of cyanobacteria in intertidal environments.

Interestingly, many of the strains that were phylogenetically closely related to the GTMNERR strains were isolated during one of four surveys of cyanobacterial biodiversity in particular coastal and intertidal habitats. "*Symploca* sp." HBC5, "*Hydrocoleum lyngbyaceum"* HBC7, and "*Aphanocapsa* sp." HBC6, which were closely related to strains GTM3, GTM1/GTM4/GTM7, and GTM6, respectively, were all isolated by Foster et al. (2009), from subtidal stromatolite communities in Highborne Cay, Bahamas. Wang et al. (2023) isolated "*Symploca* sp." PMC 1123.19, "*Jaaginema* sp." PMC 1109.19, and "*Hydrocoleum* sp." PMC 1116.19, which were closely related to strains GTM3, GTM13, and GTM1/4/7, respectively, from benthic cyanobacterial assemblages in mangrove habitats on the Mayotte island of Grande-Terre. *Zehria* sp. strains SK40, KO11DG, and KO68DGA, which were closely related to strain GTM5, and *Crocosphaera* sp. 1 strains KO30D1, KO38CU6, and KO20B5, which were closely related to strain GTM6, were all isolated by Ohki et al. (2008), from various substrates (e.g., surfaces of sand and mud) in coastal habitats in Singapore. Lastly, "Xenococcaceae

cyanobacterium" CENA315, which was closely related to strain GTM10, and four strains of *Foliisarcina bertiogensis* (e.g., *F. bertiogensis* CENA333), which were closely related to strain GTM19, were all isolated by Oliveira Alvarenga et al. (2016), from the leaves of mangroves on the coast of Sao Paulo, Brazil. These findings suggest that similar cyanobacterial communities, composed of morphologically and phylogenetically diverse taxa, are present in many coastal habitats across tropical to subtropical latitudes. Thus, the descriptions of novel cyanobacterial taxa based on strains isolated from GTMNERR represents a significant contribution to the understanding of cyanobacterial biodiversity in subtropical to tropical coastal habitats more broadly.

In conclusion, the results of the present work indicate that the true diversity of benthic cyanobacteria in subtropical estuarine ecosystems is currently underestimated. While this may in part be due to the fact that these ecosystems have historically been underrepresented in studies of cyanobacterial biodiversity (Nabout et al., 2013; Gama et al., 2014; Lopes et al., 2012; Dvořák et al., 2015a; Komárek, 1995), the findings of this study showed that it is also a reflection of unresolved problems in the field of cyanobacterial taxonomy in general.

REFERENCES

Bolhuis, H., Cretoiu, M. S., & Stal, L. J. (2014). Molecular ecology of microbial mats. *FEMS Microbiology Ecology*, 90(2): 335–350. https://doi.org/10.1111/1574-6941.12408

Bravakos, P., Kotoulas, G., Skaraki, K., Pantazidou, A., & Economou-Amilli, A. (2016). A polyphasic taxonomic approach in isolated strains of Cyanobacteria from thermal springs of Greece. *Molecular Phylogenetics and Evolution*, 98: 147–160. https://doi.org/10.1016/j.ympev.2016.02.009

Brito, Â., Ramos, V., Mota, R., Lima, S., Santos, A., Vieira, J., Vieira, C. P., Kaštovský, J., Vasconcelos, V. M., & Tamagnini, P. (2017). Description of new genera and species of marine cyanobacteria from the Portuguese Atlantic coast. *Molecular Phylogenetics and Evolution*, 111: 18–34. https://doi.org/10.1016/j.ympev.2017.03.006

Clark, K., Karsch-Mizrachi, I., Lipman, D. J., Ostell, J., & Sayers, E. W. (2016). GenBank. *Nucleic acids research*, 44(D1): D67–D72. https://doi.org/10.1093/nar/gkv1276

Darriba, D., Taboada, G.L., Doallo, R., & Posada, D. (2012). jModelTest 2: more models, new heuristics and parallel computing. *Nature Methods* 9: 772.

Dvořák, P., Jahodářová, E., Hašler, P., Gusev, E., & Poulíčková, A. (2015)a. A new tropical cyanobacterium Pinocchia polymorpha gen. et sp. nov. derived from the genus Pseudanabaena. *Fottea*, 15(1): 113-120. DOI: 10.5507/fot.2015.010

Dvořák, P., Poulíčková, A., Hašler, P., Belli, M., Casamatta, D. A., & Papini, A. (2015)b. Species concepts and speciation factors in cyanobacteria, with connection to the problems of diversity and classification. *Biodiversity and Conservation*, 24(4): 739–757. https://doi.org/10.1007/s10531-015-0888-6

Edvardsen, B., Skulberg, R., & Skulberg, O.M. (2004). NIVA Culture Collection of Algae - microalgae for science and technology. *Nova Hedwigia*, 79: 99-114.

Everroad, R. C., Stuart, R. K., Bebout, B. M., Detweiler, A. M., Lee, J. Z., Woebken, D., Prufert-Bebout, L., & Pett-Ridge, J. (2016). Permanent draft genome of strain ESFC-1: ecological genomics of a newly discovered lineage of filamentous diazotrophic cyanobacteria. *Standards in Genomic Sciences*, 11(1): 53. https://doi.org/10.1186/s40793-016-0174-6

Foster, J. S., Green, S. J., Ahrendt, S. R., Golubic, S., Reid, R. P., Hetherington, K. L., & Bebout, L. (2009). Molecular and morphological characterization of cyanobacterial diversity in the stromatolites of Highborne Cay, Bahamas. *The ISME Journal*, 3(5): 573–587. https://doi.org/10.1038/ismej.2008.129

Gama, W.A., Laughinghouse, H.D., & Sant'Anna, C.L. (2014). How diverse are coccoid cyanobacteria? A case study of terrestrial habitats from the Atlantic Rainforest (São Paulo, Brazil). *Phytotaxa*, 178(2): 61-97. http://dx.doi.org/10.11646/phytotaxa.178.2.1

Garcia-Pichel, F. (2009). Cyanobacteria. *In*: Schaechter, M. (Ed.), Encyclopedia of Microbiology (3rd ed). Elsevier/Academic Press, Cambridge, MA, USA, pp. 107-124. https://doi.org/https://doi.org/10.1016/B978-012373944-5.00250-9

Hauerová, R., Hauer, T., Kaštovský, J., Komárek, J., Lepšová-Skácelová, O., & Mareš, J. (2021). Tenebriella gen. nov. - The dark twin of Oscillatoria. *Molecular Phylogenetics and Evolution*, 165: 107293. https://doi.org/10.1016/j.ympev.2021.107293

Katoh, K. & Standley, D. M. (2013). MAFFT multiple sequence alignment software version 7: improvements in performance and usability. *Molecular Biology and Evolution*. 30(4): 772–80.

Knoll, A. H. (2008). Cyanobacteria and Earth History. *In*: Herrero, A., & Flores, E. (Eds.), The Cyanobacteria: Molecular Biology, Genomics and Evolution. Caister Academic Press, Norfolk, UK, pp. 1-19. https://doi.org/https://doi.org/10.21775/9781913652531

Komárek, J. & Anagnostidis, K. (2008). Cyanoprokaryota-1. Teil/Part 1: Chroococcales. In H. Ettl, G. Gärtner, H. Heynig, & D. Mollenhauer (Eds.), *Süßwasserflora von Mitteleuropa* (Vol. 19/1). Heidelberg, Germany: Spektrum.

Komárek, J. & Anagnostidis, K. (2008)a. Cyanoprokaryota-1. Teil/Part 1: Chroococcales. In H. Ettl, G. Gärtner, H. Heynig, & D. Mollenhauer (Eds.), *Süßwasserflora von Mitteleuropa* (Vol. 19/1). Heidelberg, Germany: Spektrum.

Komárek, J. & Anagnostidis, K. (2008)b. Cyanoprokaryota-2. Teil/Part 2: Oscillatoriales. In B. Büdel, G. Gärtner, L. Krienitz, & M. Schagerl (Eds.), *Süßwasserflora von Mitteleuropa* (Vol. 19/2). Heidelberg, Germany: Spektrum.

Komárek, J., Kaštovský, J., Mareš, J., & Johansen, J. R. (2014). Taxonomic classification of cyanoprokaryotes (cyanobacterial genera) 2014, using a polyphasic approach. *Preslia*, 86(4): 295-335.

Komárek, J., Kaštovský, J., Mareš, J., & Johansen, J. R. (2014). Taxonomic classification of cyanoprokaryotes (cyanobacterial genera) 2014, using a polyphasic approach. *Preslia*, 86(4): 295-335.

Lane, D.J. (1991). 16S/23S rRNA Sequencing. *In*: Stackebrandt, E. & Goodfellow, M. (Eds.), Nucleic Acid Techniques in Bacterial Systematics. John Wiley and Sons, New York, pp. 115-175.

Larsson, A. (2014). AliView: a fast and lightweight alignment viewer and editor for large data sets. *Bioinformatics*, 30(22): 3276-3278. http://dx.doi.org/10.1093/bioinformatics/btu531

Lepère, C., Wilmotte, A., & Meyer, B. (2000). Molecular diversity of *Microcystis* strains (Cyanophyceae, Chroococcales) based on 16S rDNA sequences. *Systematics and Geography of Plants*, 70(2): 275–283. https://doi.org/10.2307/3668646

Lopes, V. R., Ramos, V., Martins, A., Sousa, M., Welker, M., Antunes, A., & Vasconcelos, V. M. (2012). Phylogenetic, chemical and morphological diversity of cyanobacteria from Portuguese temperate estuaries. *Marine Environmental Research*, 73: 7–16. https://doi.org/10.1016/j.marenvres.2011.10.005

Mareš, J., Johansen, J. R., Hauer, T., Zima, J., Jr, Ventura, S., Cuzman, O., Tiribilli, B., & Kaštovský, J. (2019). Taxonomic resolution of the genus *Cyanothece* (Chroococcales, Cyanobacteria), with a treatment on *Gloeothece* and three new genera, *Crocosphaera*, *Rippkaea*, and *Zehria*. *Journal of Phycology*, 55(3): 578–610. https://doi.org/10.1111/jpy.12853

Mareš, J., Johansen, J. R., Hauer, T., Zima, J., Jr, Ventura, S., Cuzman, O., Tiribilli, B., & Kaštovský, J. (2019). Taxonomic resolution of the genus *Cyanothece* (Chroococcales, Cyanobacteria), with a treatment on *Gloeothece* and three new genera, *Crocosphaera*, *Rippkaea*, and *Zehria*. *Journal of Phycology*, 55(3): 578–610. https://doi.org/10.1111/jpy.12853

Miller, M. A., Pfeiffer, W. & Schwartz, T. (2010). Creating the CIPRES Science Gateway for inference of large phylogenetic trees. *In*: Proceedings of the Gateway Computing Environments Workshop (GCE), New Orleans, LA, USA, pp. 1–8.

Mühlsteinová, R., Hauer, T., De Ley, P., & Pietrasiak, N. (2018). Seeking the true *Oscillatoria*: a quest for a reliable phylogenetic and taxonomic reference point. *Preslia*, 90: 151-169.

Muro-Pastor, A. M., & Hess, W. R. (2012). Heterocyst differentiation: from single mutants to global approaches. *Trends in Microbiology*, 20(11): 548–557. https://doi.org/10.1016/j.tim.2012.07.005

Nabout, J.C., da Silva Rocha, B., Carneiro, F.M., & Sant'Anna, C.L (2013) How many species of Cyanobacteria are there? Using a discovery curve to predict the species number. *Biodiversity and Conservation,* 22(12). DOI: 10.1007/s10531-013-0561-x

Ohki, K., Kamiya, M., Honda, D., Kumazawa, S., & Ho, K. K. (2008). Morphological and phylogenetic studies on unicellular diazotrophic cyanobacteria (cyanophytes) isolated from the coastal waters around Singapore. *Journal of Phycology*, 44(1): 142–151. https://doi.org/10.1111/j.1529-8817.2007.00428.x

Oliveira Alvarenga, D., Rigonato, J., Henrique Zanini Branco, L., Soares Melo, I., & Fatima Fiore, M. (2016). *Phyllonema aviceniicola* gen. nov., sp. nov. and *Foliisarcina bertiogensis* gen. nov., sp. nov., epiphyllic cyanobacteria associated with *Avicennia schaueriana* leaves. *International Journal of Systematic and Evolutionary Microbiology*, *66*(2): 689–700. https://doi.org/10.1099/ijsem.0.000774

Palińska, K.A., M. M. Abed, R., Charpy, L., Langlade, M., Beltrán-Magos, Y., & Golubic, S. (2015) Morphological, genetic and physiological characterization of Hydrocoleum, the most common benthic cyanobacterium in tropical oceans. *European Journal of Phycolog*y, 50(2): 139-154. DOI: 10.1080/09670262.2015.1010239

Porta, D., Hernández-Mariné, M., Herdman, M., & Rippka, R. (2003). Structural and ultrastructural characterization of *Symploca atlantica* Gomont, strain PCC 8002 (Oscillatoriales, Cyanophyta, Cyanobacteria). *Algological Studies*, 109: 509–524.

Rockwell, N.C., Lagarias, J.C., & Bhattacharya, D. (2014). Primary endosymbiosis and the evolution of light and oxygen sensing in photosynthetic eukaryotes. *Frontiers in Ecology and Evolution,* 2: 1-13.

Romeu, M. J., Morais, J., Gomes, L. C., Silva, R., Vasconcelos, V., & Mergulhão, F. J. M. (2023). Characterization and biofouling potential analysis of two cyanobacterial strains isolated from Cape Verde and Morocco. *FEMS Microbiology Ecology*, 99(3): fiad004. https://doi.org/10.1093/femsec/fiad004

Ronquist, F., Teslenko, M., van der Mark, P., Ayres, D. L., Darling, A., Hohna, S., Larget, B., Liu, L., Suchard, M. A., & Huelsenbeck, J. P. (2012). MrBayes 3.2: efficient Bayesian phylogenetic inference and model choice across a large model space. *Systematic Biology*, 61: 539–542.

Samylina, O. S., Sinetova, M. A., Kupriyanova, E. V., Starikov, A. Y., Sukhacheva, M. V., Dziuba, M. V., & Tourova, T. P. (2021). Ecology and biogeography of the 'marine *Geitlerinema*' cluster and a description of *Sodalinema orleanskyi* sp. nov., Sodalinema gerasimenkoae sp. nov., *Sodalinema stali* sp. nov. and *Baaleninema simplex* gen. et sp. nov. (Oscillatoriales, Cyanobacteria). *FEMS Microbiology Ecology*, 97(8), fiab104. https://doi.org/10.1093/femsec/fiab104

Serôdio, J. & Paterson, D.M. (2021). Role of microphytobenthos in the functioning of estuarine and coastal ecosystems. *In*: Leal Filho, W., Azul, A.M., Brandli, L., Lange Salvia, A., & Wall, T. (Eds.), Life Below Water. Encyclopedia of the UN Sustainable Development Goals. Springer, Cham. https://doi.org/10.1007/978-3-319-71064-8_11-1

Shalygin, S.S., Kavulic, K., Pietrasiak, N., Bohunická, M., Vaccarino, M.A., Chesarino, N.M., & Johansen, J.R. (2019). Neotypification of *Pleurocapsa fuliginosa* and epitypification of *P.*

minor (Pleurocapsales): resolving a polyphyletic cyanobacterial genus. *Phytotaxa*, 392(4). https://doi.org/10.11646/phytotaxa.392.4.1

Stamatakis, A. (2014). RAxML version 8: a tool for phylogenetic analysis and post-analysis of large phylogenies. *Bioinformatics*, 30(9): 1312-1313.

Strunecký, O., Bohunická, M., Johansen, J.R., Čapková, K., Raabová, L., Dvořák, P., & Komárek, J. (2017). A revision of the genus Geitlerinema and a description of the genus Anagnostidinema gen. nov. (Oscillatoriophycidae, Cyanobacteria). *Fottea*, 17(1): 114-126. doi: 10.5507/fot.2016.025

Strunecký, O., Ivanova, A.P. & Mareš, J. (2023). An updated classification of cyanobacterial orders and families based on phylogenomic and polyphasic analysis. *Journal of Phycology*, 59: 12-51. https://doi.org/10.1111/jpy.13304

Sullivan, M. J., & Currin, C. A. (2002). Community structure and functional dynamics of benthic microalgae in salt marshes. *In:* Weinstein, M.P. & Kreeger, D.A. (Eds.), *Concepts and Controversies in Tidal Marsh Ecology* (81–106). Springer, Germany. https://doi.org/10.1007/0-306-47534-0_6

Tobias, C. & Neubauer, S.C. (2019). *In*: Perillo, G.M.E., Wolanski, E., Cahoon, D.R., & Brinson, M.M. (Eds.), Coastal wetlands: an integrated ecological approach, Elsevier, Cambridge, MA, USA, pp. 445-492.

Vogt, J. C., Abed, R. M. M., Albach, D. C., & Palinska, K. A. (2019). Latitudinal gradient of cyanobacterial diversity in tidal flats. *PLoS ONE*, 14(11). https://doi.org/10.1371/journal.pone.0224444

Wang, H., Halary, S., Duval, C., Bernard, C., Troussellier, M., Beniddir, M., Brunel, J., Castaldi, A., Caudal, F., Golléty, C., Martin, C., Bourguet-Kondracki, M., & Duperron,

S. (2023). Diversity, metabolome profiling and bioactivities of benthic filamentous cyanobacteria isolated from coastal mangroves of Mayotte. *Frontiers in Marine Science*, 10. 10.3389/fmars.2023.1201594.

Yarza, P., Yilmaz, P., Pruesse, E., Glöckner, F. O., Ludwig, W., Schleifer, K. H., Whitman, W. B., Euzéby, J., Amann, R., & Rosselló-Móra, R. (2014). Uniting the classification of cultured and uncultured bacteria and archaea using 16S rRNA gene sequences. *Nature Reviews Microbiology*, 12(9): 635–645. https://doi.org/10.1038/nrmicro3330

Zuker, M. (2003). Mfold web server for nucleic acid folding and hybridization prediction. *Nucleic Acids Research,* 31(13): 3406-3415.

FIGURES AND TABLES: CHAPTER 1

FIGURES

Figure 1. Location of field experiment
A) Map of the southeastern United States, showing location of the Guana Tolomato Matanzas National Estuarine Research Reserve (GTMNERR) in northeastern Florida (inset), and location of the experimental field site within the southern component of GTMNERR. Map source: Google Maps. B) Image of field site, showing tidal creek.

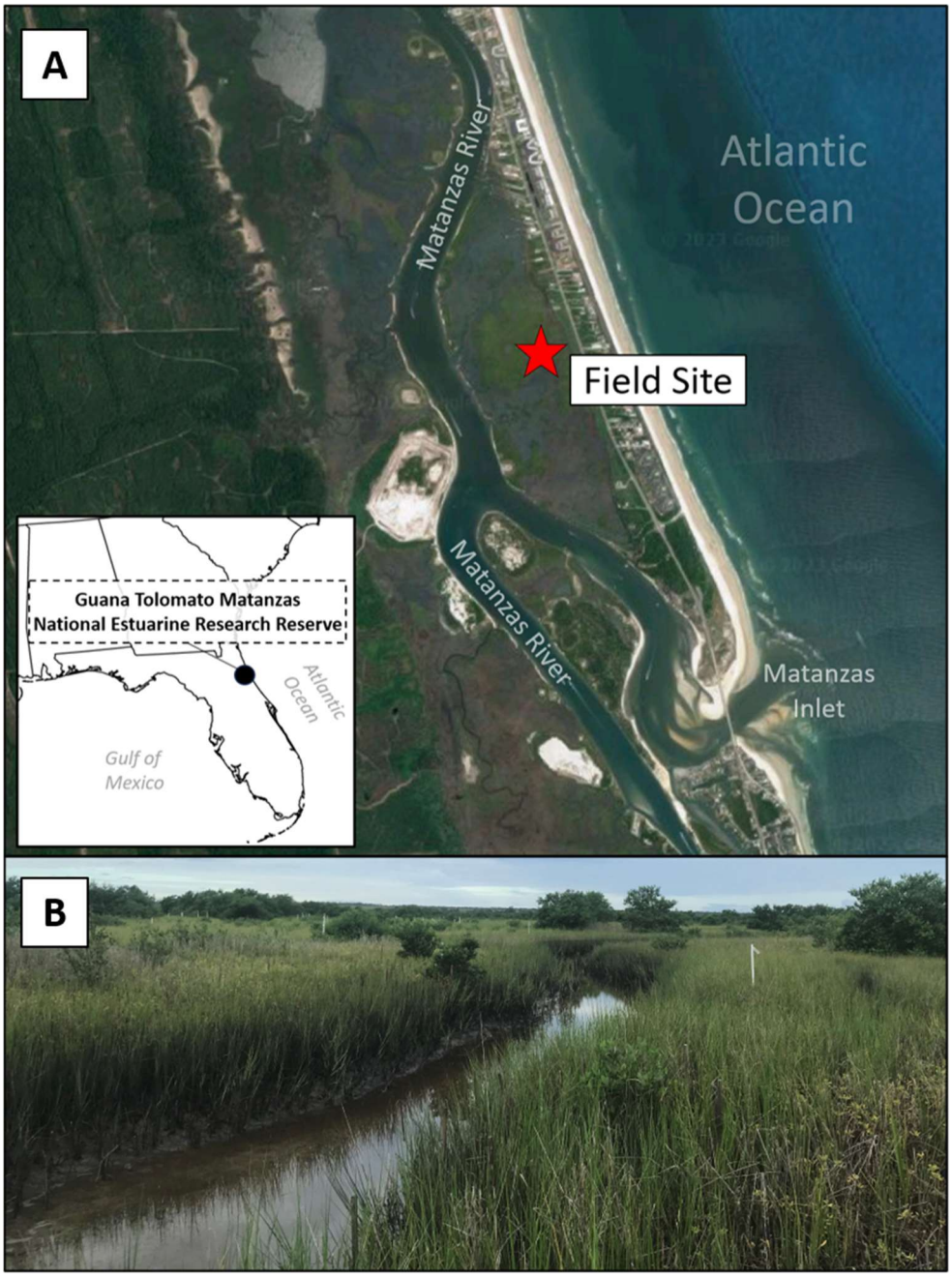

Figure 2. Schematic representation of experimental design

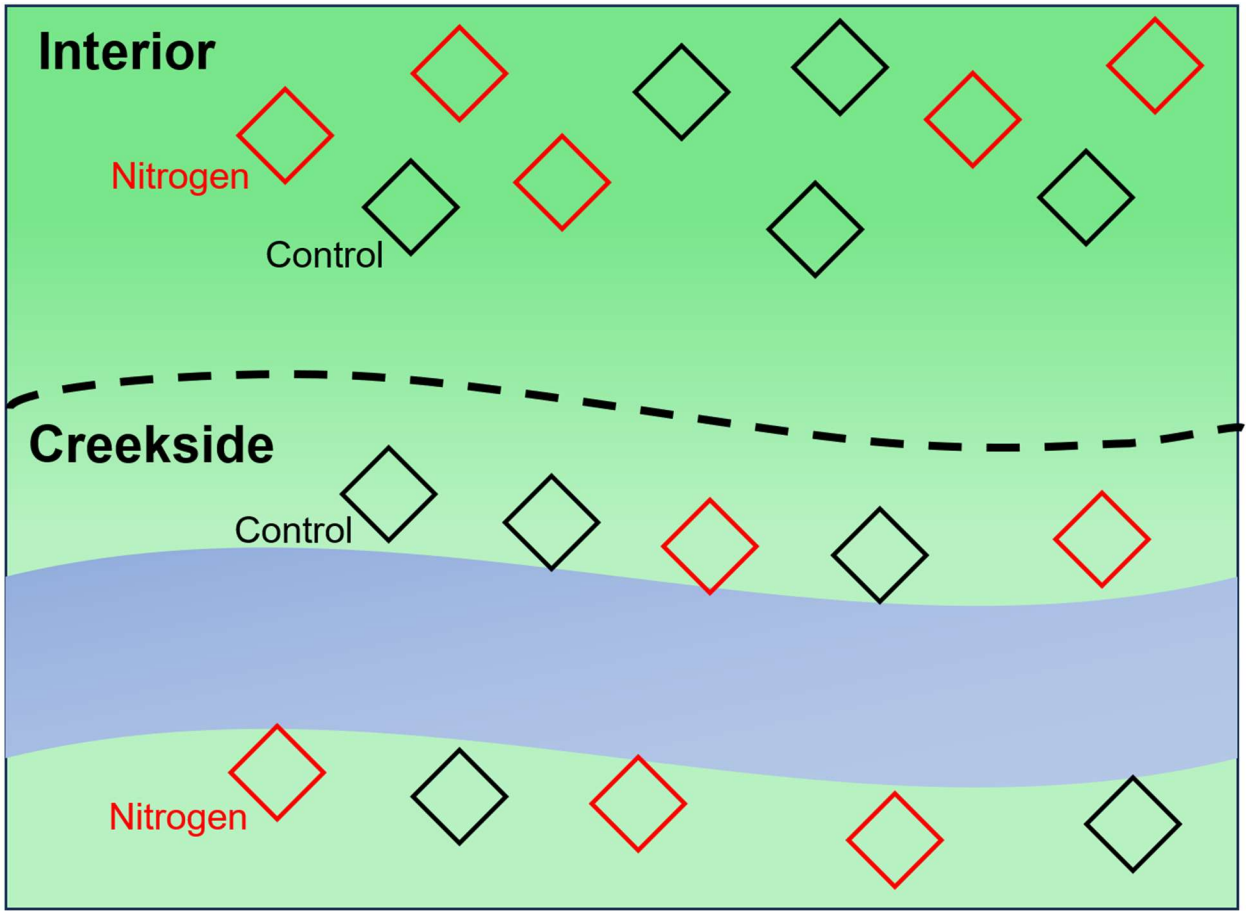

Figure 3. Boxplots of cyanobacterial community (16S Cyanobacteria) alpha diversity metrics.

Shannon (left) and Simpson (right) diversity indices for cyanobacterial communities in each treatment group within the creek edge and marsh interior zones.

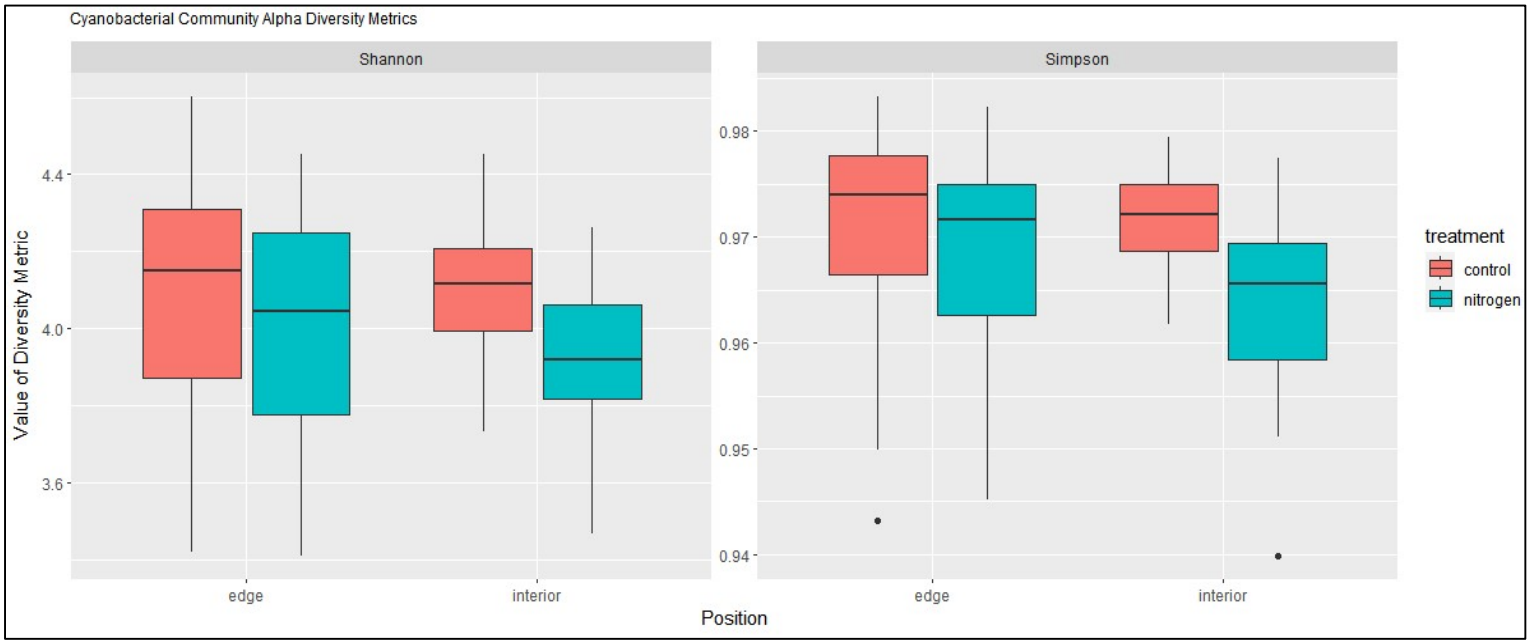

Figure 4. Boxplots of diatom community (rbcL) alpha diversity metrics.
Shannon (left) and Simpson (right) diversity indices for diatom communities in each treatment group within the creek edge and marsh interior zones.

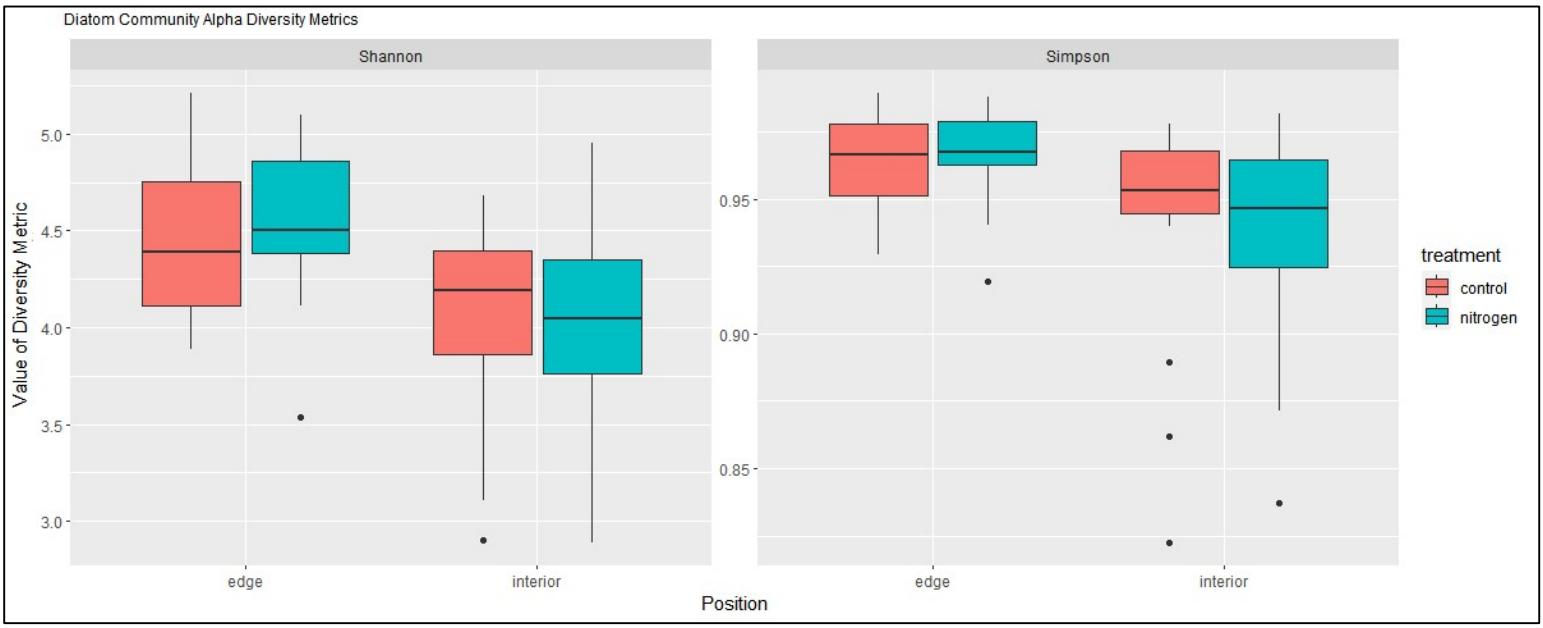

Figure 5. Boxplots of prokaryotic community (16S Universal) alpha diversity metrics. Shannon (left) and Simpson (right) diversity indices for prokaryotic communities in each treatment group within the creek edge and marsh interior zones.

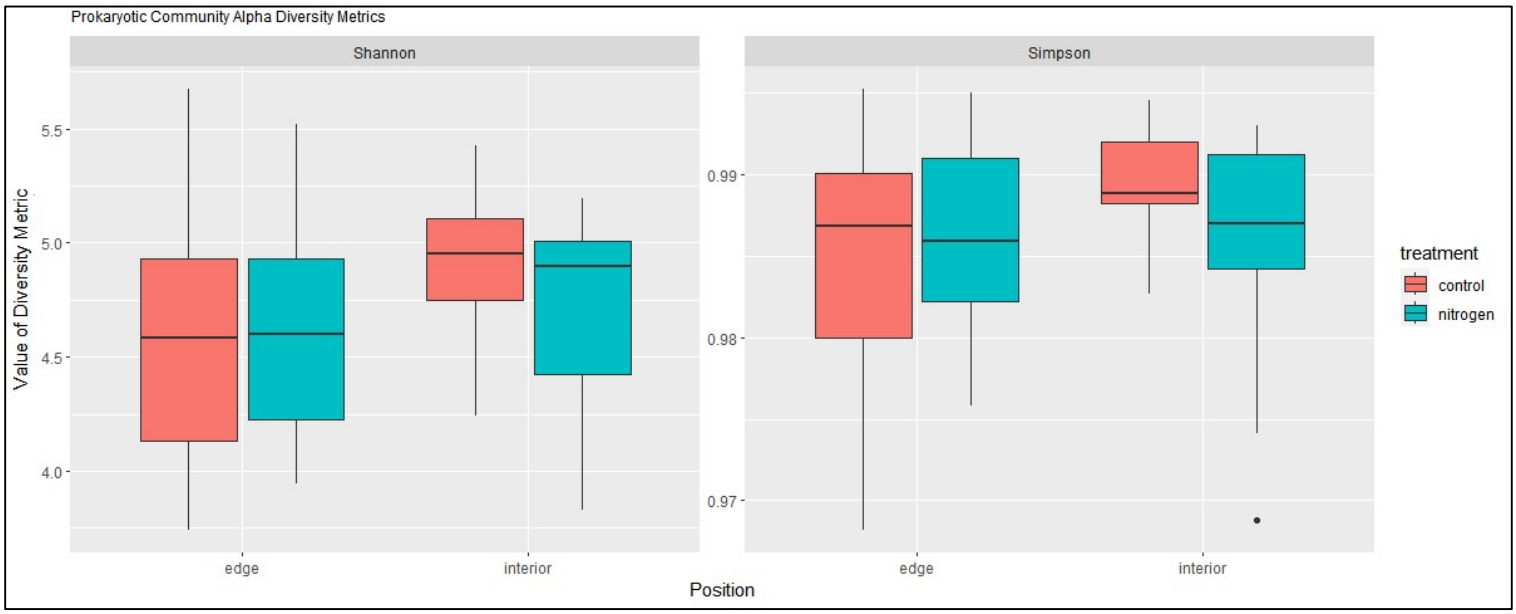

Figure 6. PCoA ordination plot of samples for cyanobacterial communities

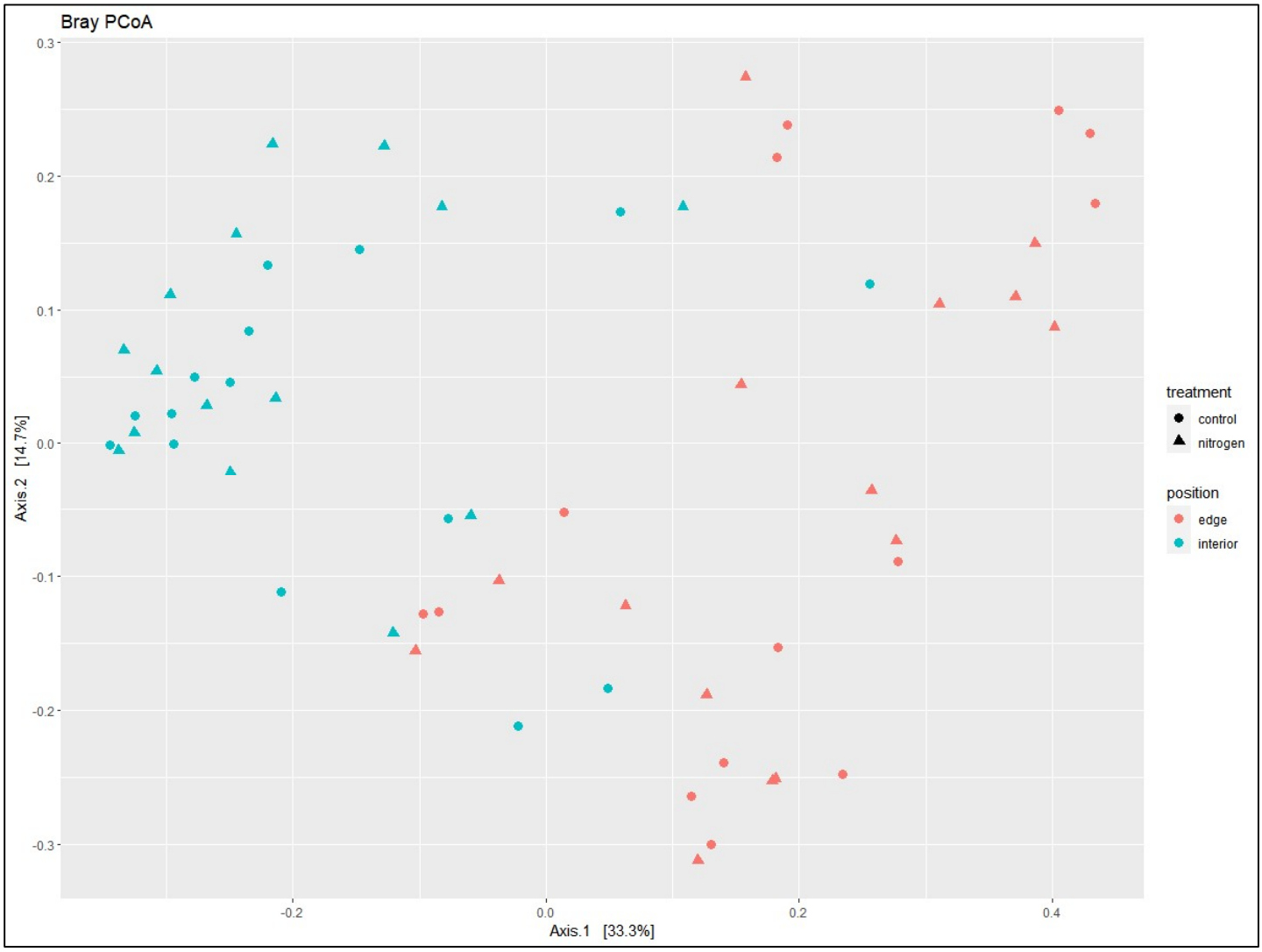

Figure 7. PCoA ordination plot of samples for diatom communities

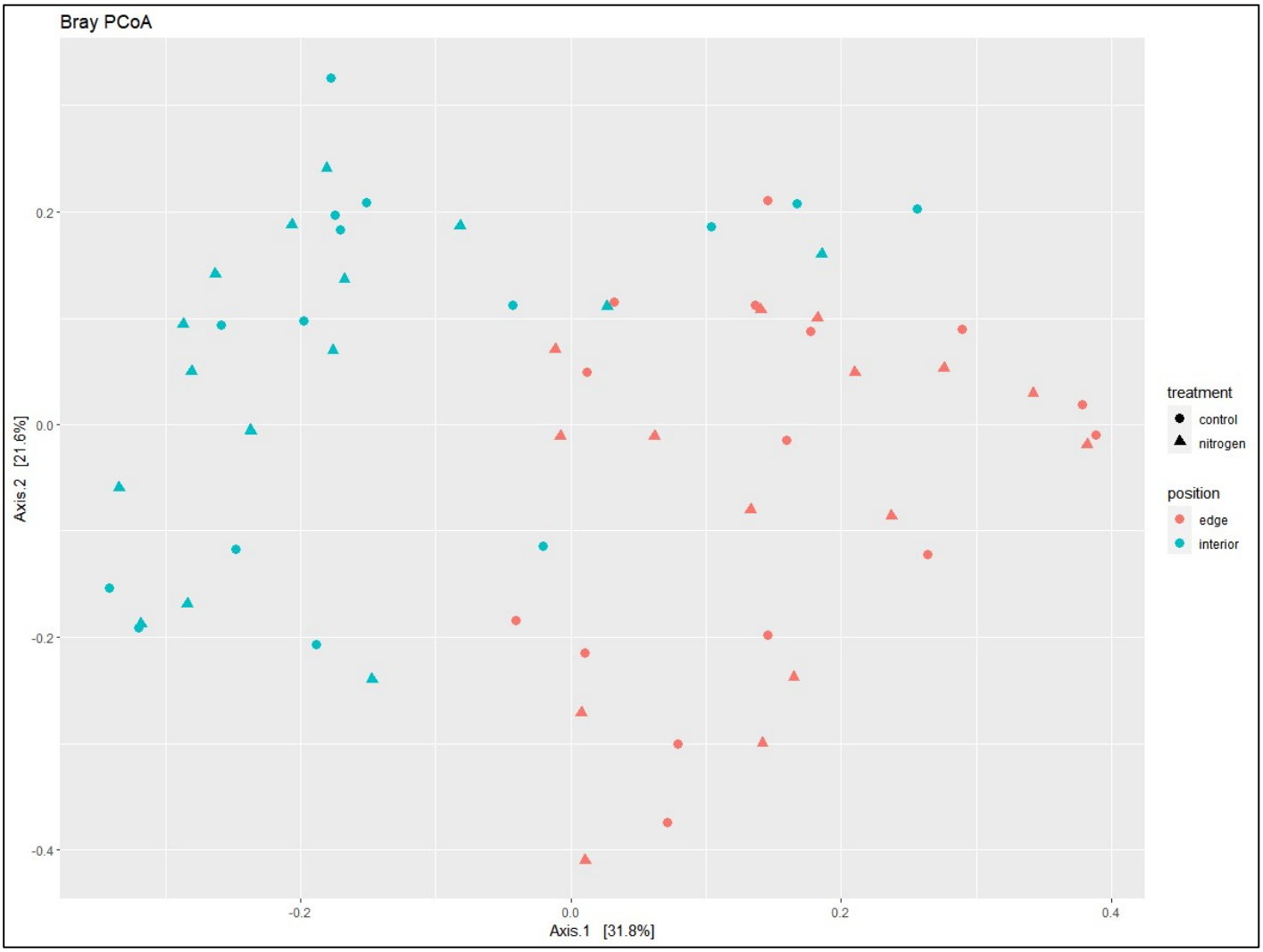

Figure 8. PCoA ordination plot of samples for prokaryotic communities

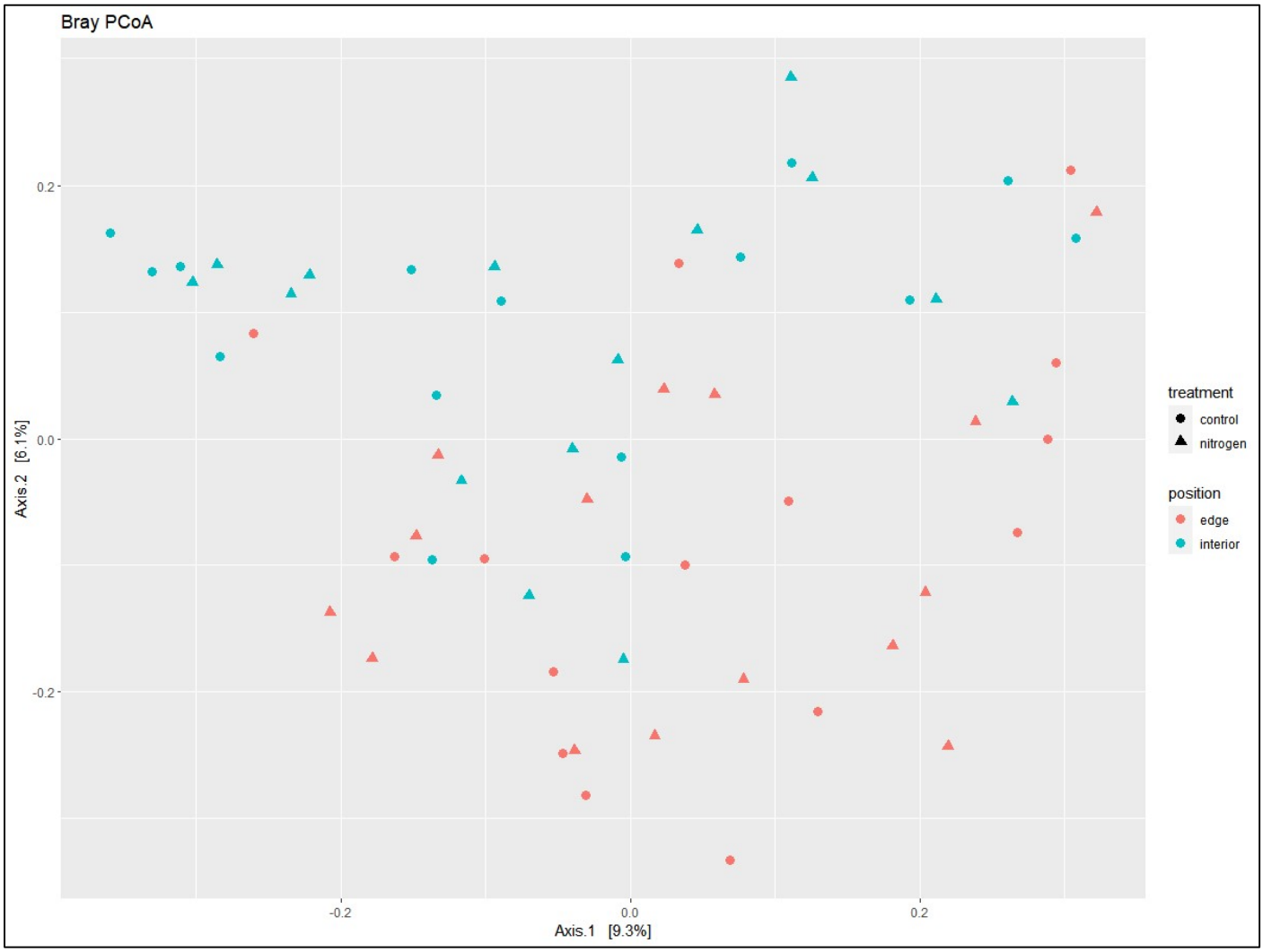

Figure 9. Venn diagrams showing the number of cyanobacteria ASVs unique and shared between and among experimental groups

A) number of cyanobacteria ASVs unique to, and shared between, treatment groups. B) number of cyanobacteria ASVs unique to, and shared between, position groups. C) number of cyanobacteria ASVs unique to, and shared between and among, sampling months.

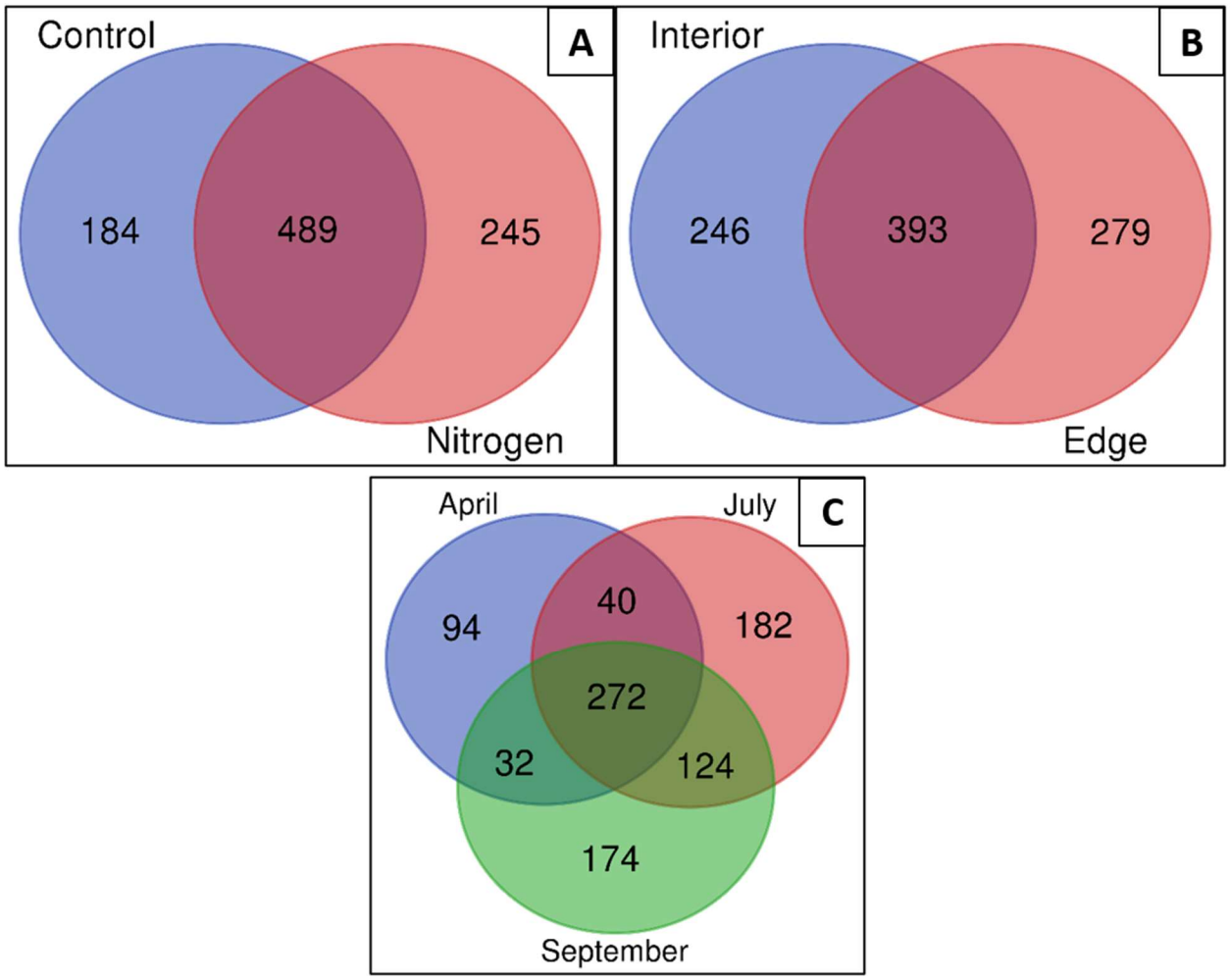

Figure 10. Venn diagrams showing the number of diatom ASVs unique and shared between and among experimental groups

A) number of diatom ASVs unique to, and shared between, treatment groups. B) number of diatom ASVs unique to, and shared between, position groups. C) number of diatom ASVs unique to, and shared between and among, sampling months.

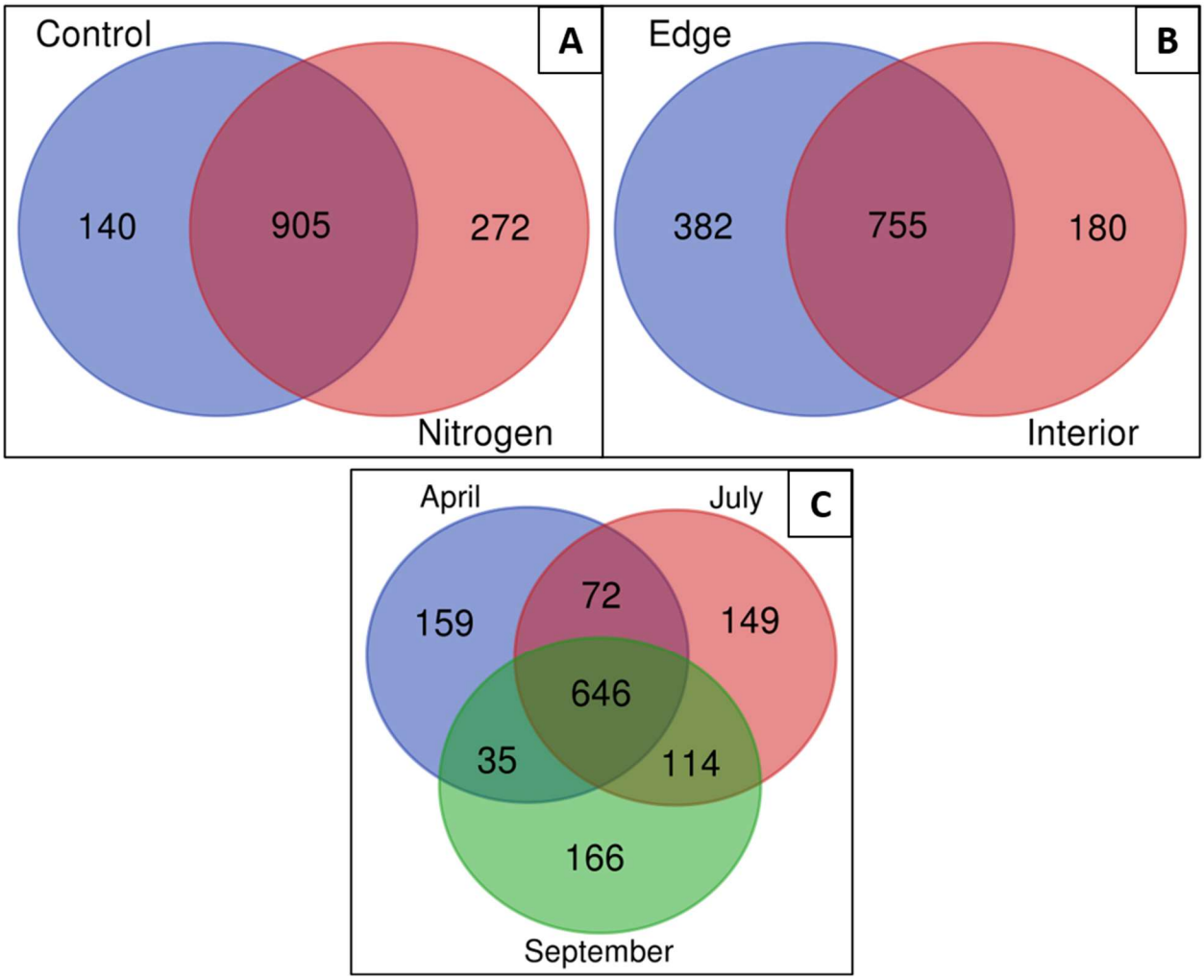

Figure 11. Venn diagrams showing the number of prokaryote ASVs unique and shared between and among experimental groups

A) number of prokaryote ASVs unique to, and shared between, treatment groups. B) number of prokaryote ASVs unique to, and shared between, position groups. C) number of prokaryote ASVs unique to, and shared between and among, sampling months.

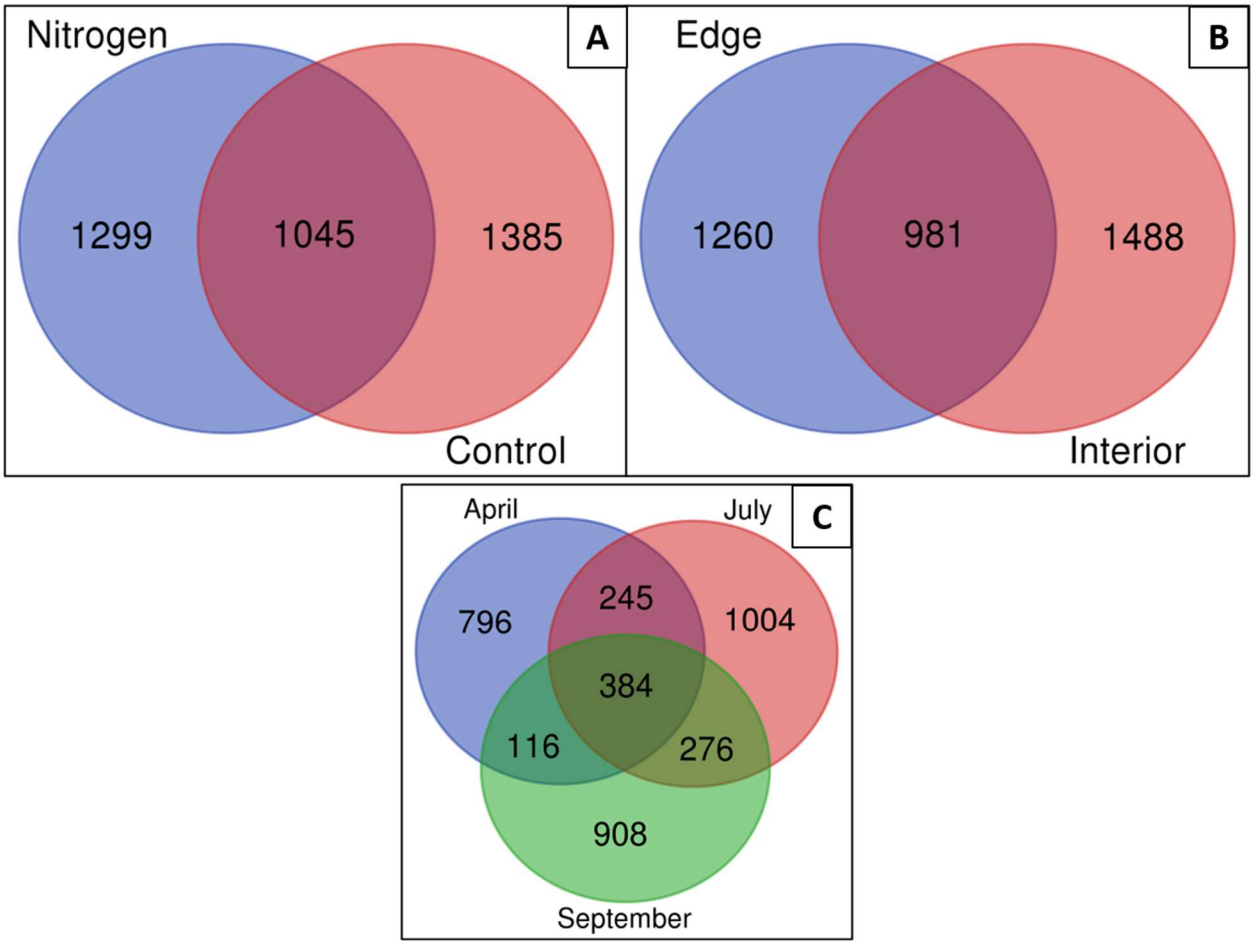

Figure 12. Top 30 cyanobacterial community ASVs

Proportional abundances of the 30 most abundant cyanobacterial ASVs across the entire dataset. Color indicates genus. Vertical columns in the figure represent (from left to right) April, July, and September sampling months. Horizontal rows in the figure represent creek edge (top row) and marsh interior (bottom row) groups. Within each month*position subsection of the figure, data are further grouped by treatment, with the control group on the left and the nitrogen treatment group on the right. The maximum value on the y-axis (5) is equivalent to 100% of all sequencing reads in each month*position*treatment group of 5 samples.

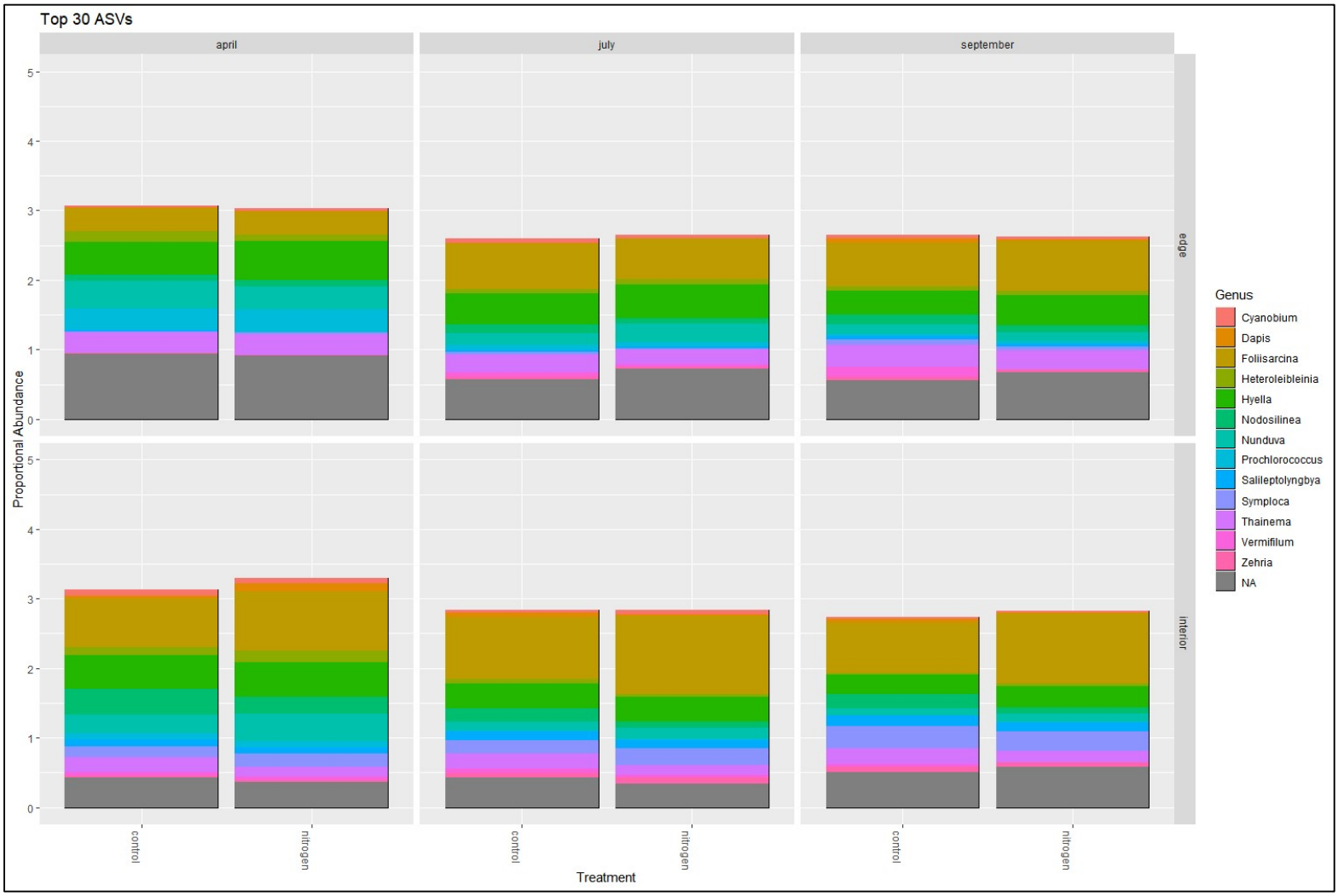

Figure 13. Top 10 cyanobacterial community orders

Proportional abundances of the 10 most abundant cyanobacterial orders across the entire dataset. Color indicates order. Vertical columns in the figure represent (from left to right) April, July, and September sampling months. Horizontal rows in the figure represent creek edge (top row) and marsh interior (bottom row) groups. Within each month*position subsection of the figure, data are further grouped by treatment, with the control group on the left and the nitrogen treatment group on the right. The maximum value on the y-axis (5) is equivalent to 100% of all sequencing reads in each month*position*treatment group of 5 samples.

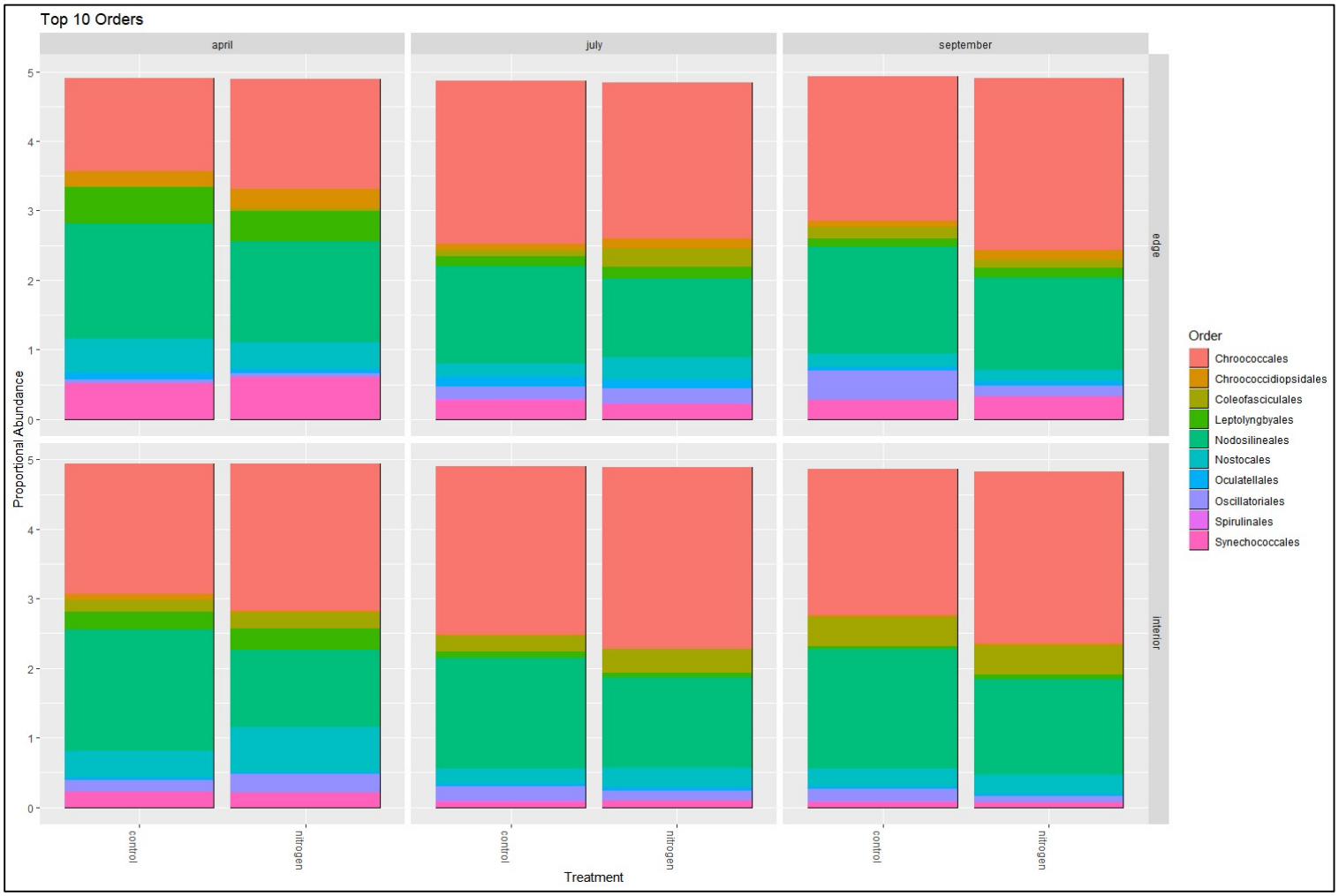

Figure 14. Proportional abundances of diatom classes

Proportional abundances of classes within the diatom communities. Color indicates class. Vertical columns in the figure represent (from left to right) April, July, and September sampling months. Horizontal rows in the figure represent creek edge (top row) and marsh interior (bottom row) groups. Within each month*position subsection of the figure, data are further grouped by treatment, with the control group on the left and the nitrogen treatment group on the right. The maximum value on the y-axis (5) is equivalent to 100% of all sequencing reads in each month*position*treatment group of 5 samples.

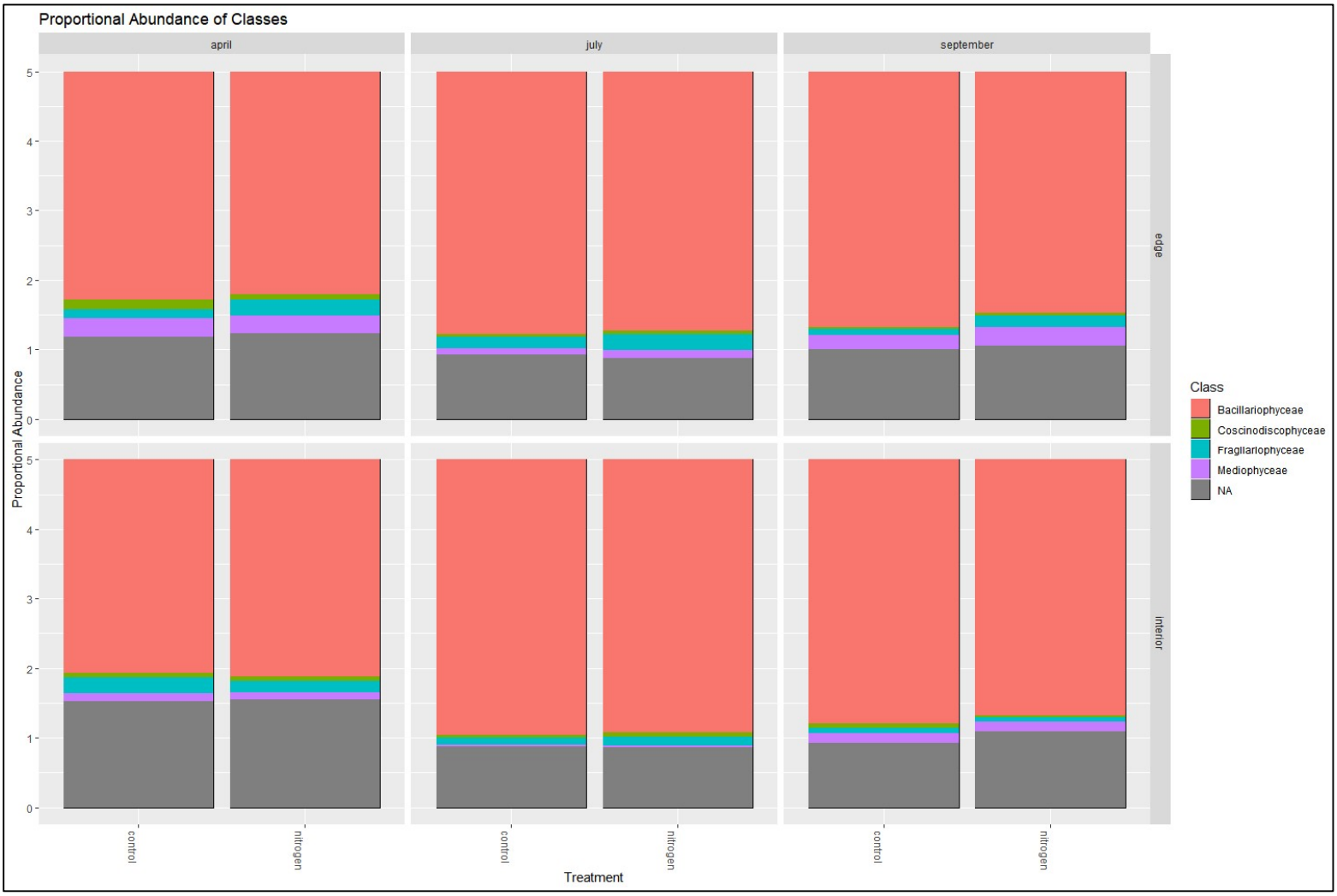

Figure 15. Top 10 diatom community orders

Proportional abundances of the 10 most abundant diatom orders across the entire dataset. Color indicates order. Vertical columns in the figure represent (from left to right) April, July, and September sampling months. Horizontal rows in the figure represent creek edge (top row) and marsh interior (bottom row) groups. Within each month*position subsection of the figure, data are further grouped by treatment, with the control group on the left and the nitrogen treatment group on the right. The maximum value on the y-axis (4) is equivalent to 80% of all sequencing reads in each month*position*treatment group of 5 samples.

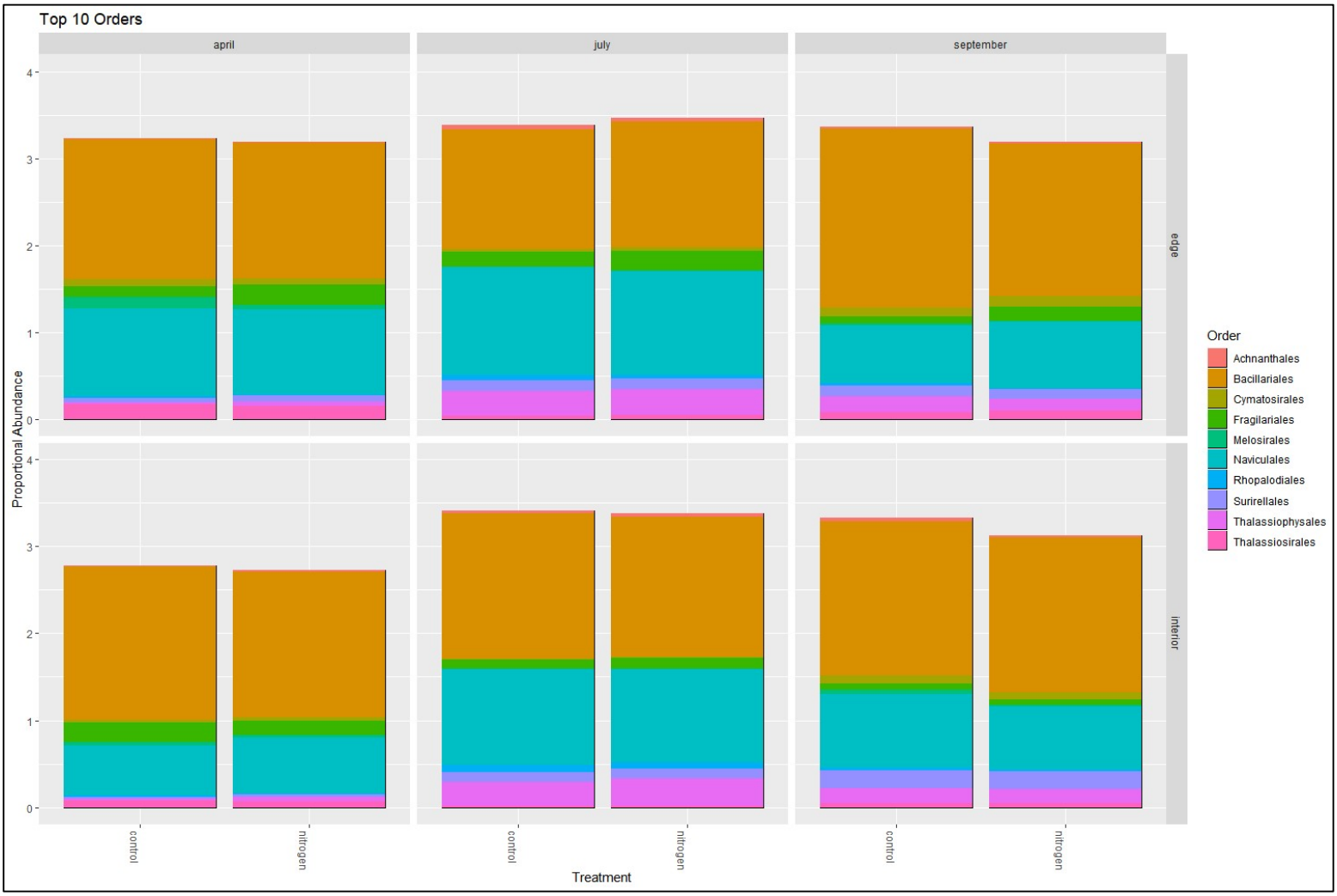

Figure 16. Top 10 diatom community genera

Proportional abundances of the 10 most abundant diatom genera across the entire dataset. Color indicates genus. Vertical columns in the figure represent (from left to right) April, July, and September sampling months. Horizontal rows in the figure represent creek edge (top row) and marsh interior (bottom row) groups. Within each month*position subsection of the figure, data are further grouped by treatment, with the control group on the left and the nitrogen treatment group on the right. The maximum value on the y-axis (2.5) is equivalent to 50% of all sequencing reads in each month*position*treatment group of 5 samples.

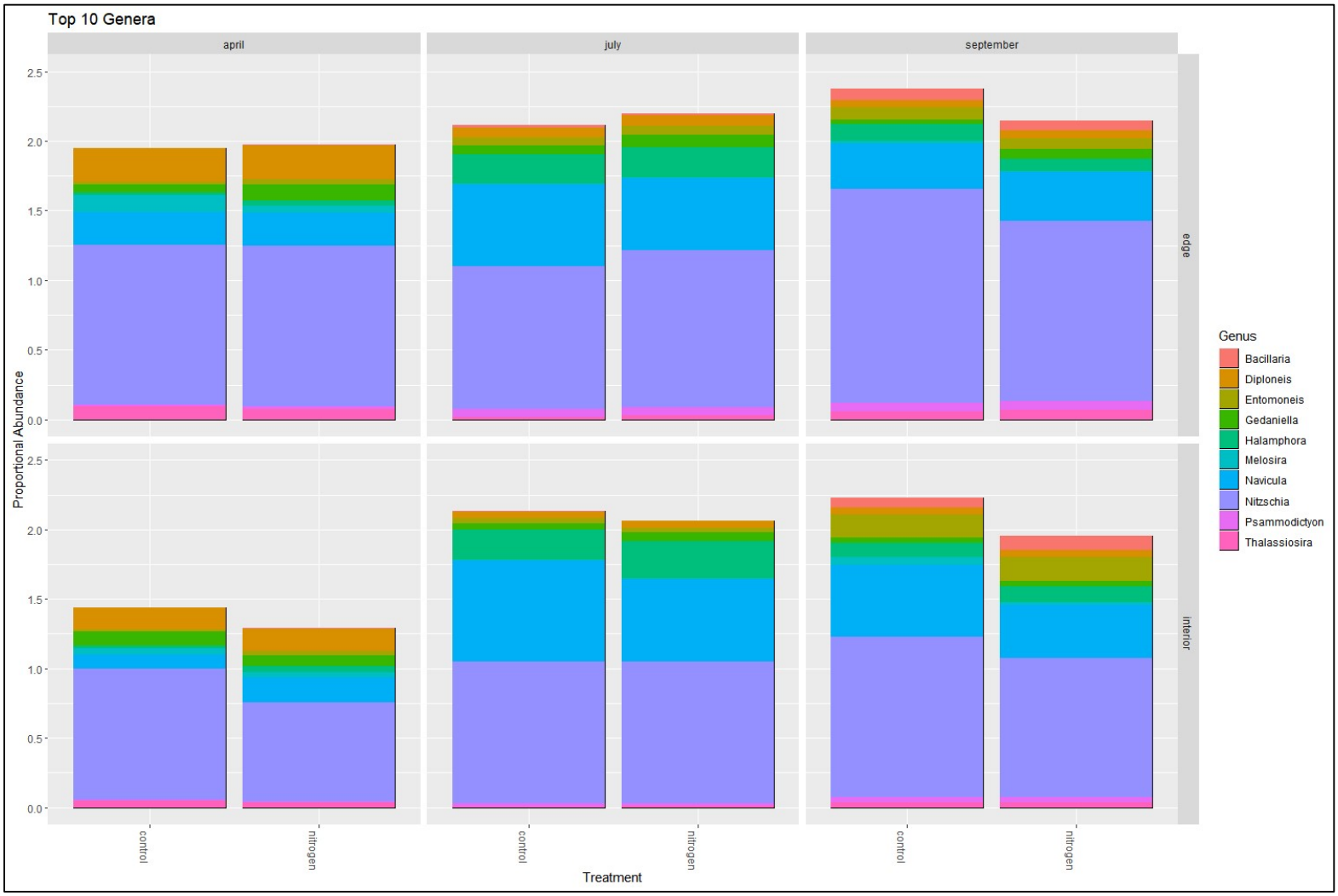

Figure 17. Top 10 prokaryotic community phyla

Proportional abundances of the 10 most abundant phyla within the prokaryotic communities across the entire dataset. Color indicates phylum. Vertical columns in the figure represent (from left to right) April, July, and September sampling months. Horizontal rows in the figure represent creek edge (top row) and marsh interior (bottom row) groups. Within each month*position subsection of the figure, data are further grouped by treatment, with the control group on the left and the nitrogen treatment group on the right. The maximum value on the y-axis (5) is equivalent to 100% of all sequencing reads in each month*position*treatment group of 5 samples.

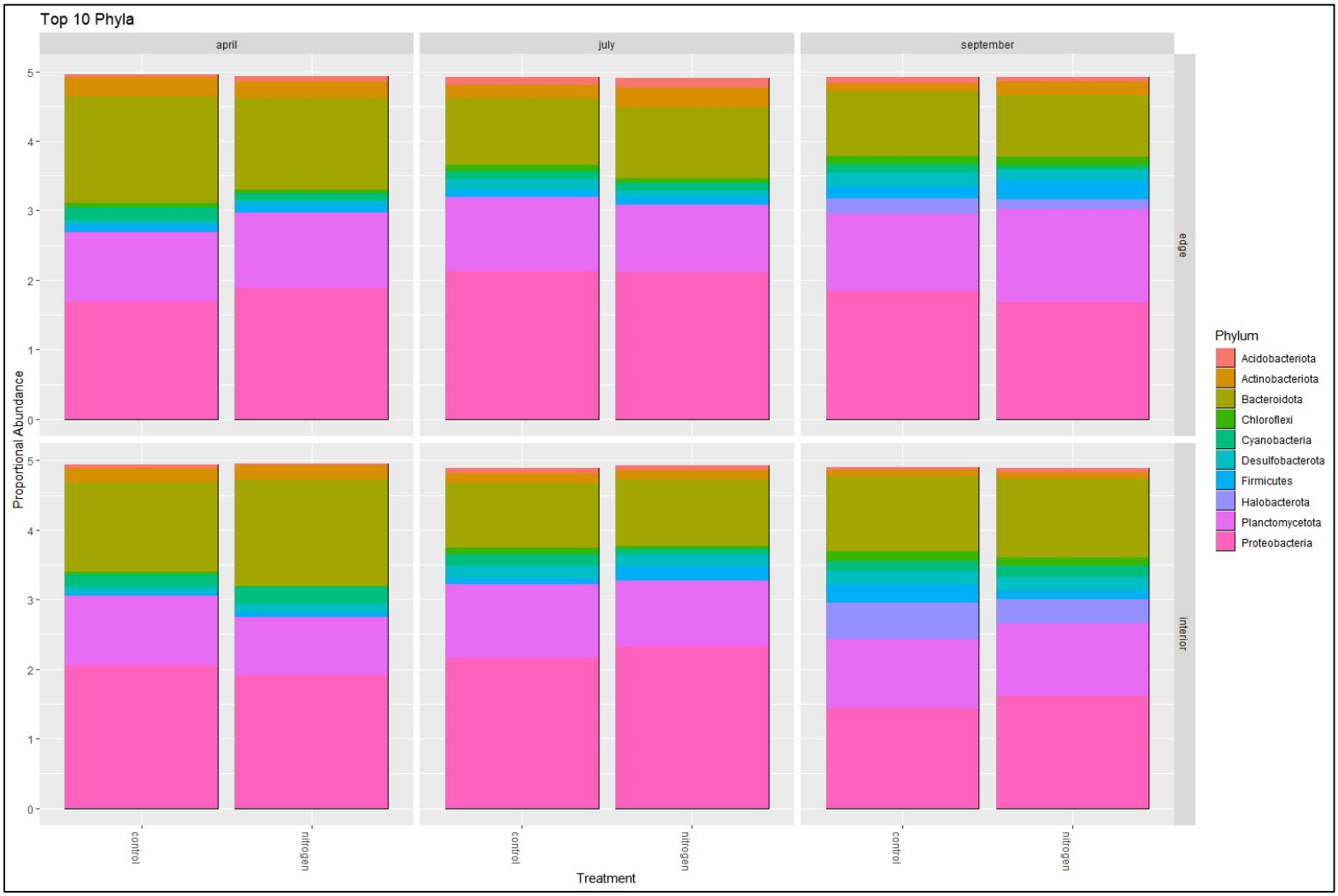

Figure 18. Proportional abundances of Bacteria and Archaea in prokaryotic communities
Proportional abundances of Bacteria and Archaea within the prokaryotic communities. Color indicates kingdom. Vertical columns in the figure represent (from left to right) April, July, and September sampling months. Horizontal rows in the figure represent creek edge (top row) and marsh interior (bottom row) groups. Within each month*position subsection of the figure, data are further grouped by treatment, with the control group on the left and the nitrogen treatment group on the right. The maximum value on the y-axis (5) is equivalent to 100% of all sequencing reads in each month*position*treatment group of 5 samples.

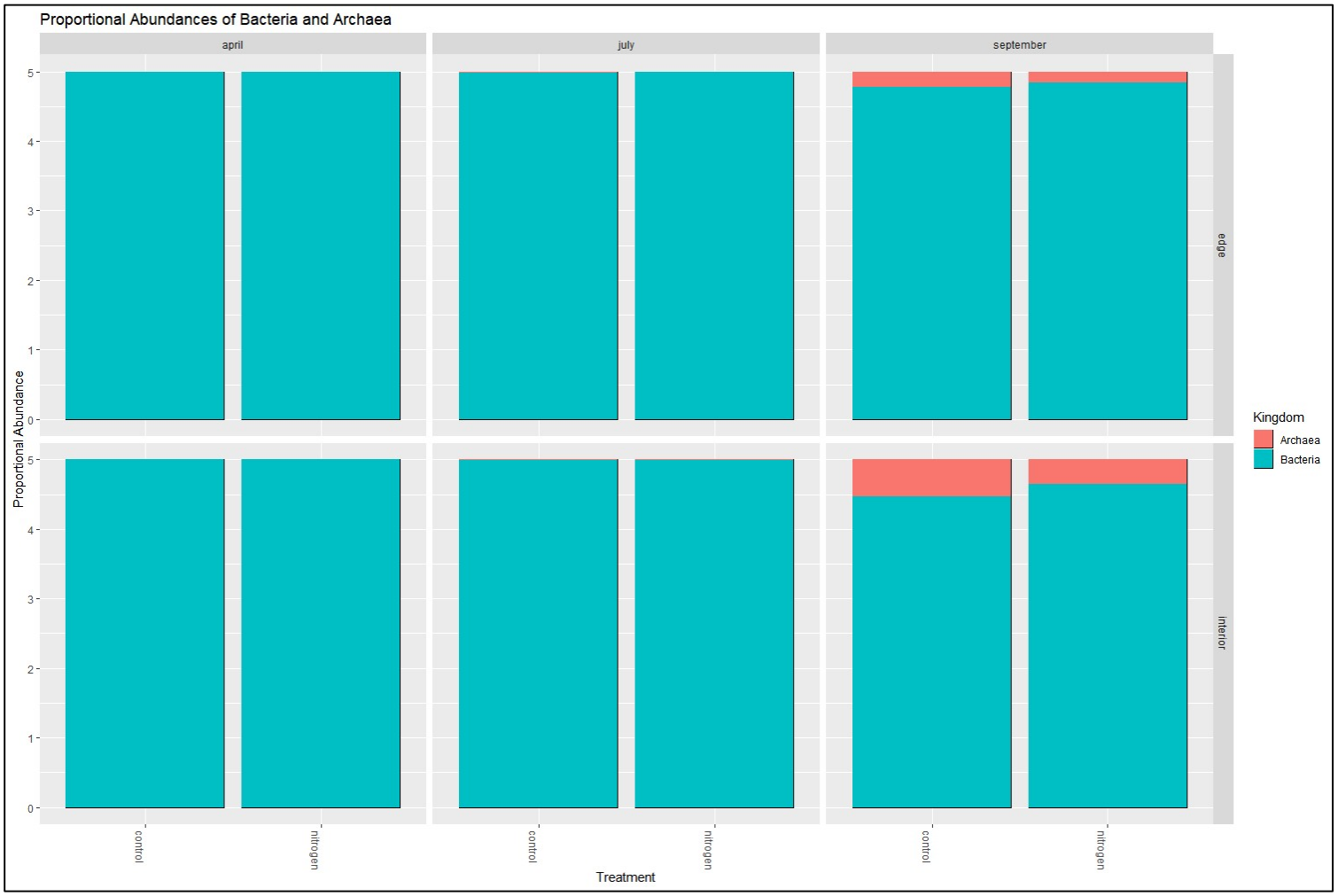

TABLES

Table 1. Effects of treatment and position on Shannon diversity, determined using two-way ANOVA tests

16S Cyanobacteria					
	Df	**Sum Sq**	**Mean Sq**	**F value**	**Pr(>F)**
Treatment	1	0.227	0.227	3.126	0.0824
Position	1	0.017	0.0166	0.23	0.634
Residuals	57	4.131	0.0725		
rbcL					
	Df	**Sum Sq**	**Mean Sq**	**F value**	**Pr(>F)**
Treatment	1	0.013	0.013	0.057	0.812
Position	1	3.664	3.664	15.922	0.000191
Residuals	57	13.117	0.23		
16S Universal					
	Df	**Sum Sq**	**Mean Sq**	**F value**	**Pr(>F)**
Treatment	1	0.141	0.141	0.704	0.405
Position	1	0.574	0.574	2.869	0.0957
Residuals	57	11.403	0.2		

Table 2. Scheirer-Ray-Hare tests of the effects of treatment, position, and their interaction on Simpson diversity

16S Cyanobacteria				
	Df	**Sum Sq**	**H**	**p.value**
Treatment	1	1.622E+03	5.319	0.0211
Position	1	3.456E+02	1.133	0.287
Treatment:position	1	1.473E+02	0.483	0.487
Residuals	56	1.588E+04		
rbcL				
	Df	**Sum Sq**	**H**	**p.value**
Treatment	1	1.644E-28	5.391E-31	1
Position	1	2.667E+03	8.743	0.00311
Treatment:position	1	2.017E+02	0.661	0.416
Residuals	56	1.513E+04		
16S Universal				
	Df	**Sum Sq**	**H**	**p.value**
Treatment	1	5.607E+01	0.184	0.668
Position	1	5.281E+02	1.731	0.188
Treatment:position	1	4.374E+02	1.434	0.231
Residuals	56	1.697E+04		

Table 3. Effects of treatment and position on overall community structure, determined using two-way PERMANOVA tests

16S Cyanobacteria					
April					
	Df	**Sum Of Sqs**	**R2**	**F**	**Pr(>F)**
Treatment	1	0.0586	0.0207	0.568	0.729
Position	1	1.020	0.360	9.889	0.0001
Residual	17	1.754	0.619		
Total	19	2.832	1.000		
July	**Df**	**Sum Of Sqs**	**R2**	**F**	**Pr(>F)**
Treatment	1	0.117	0.0404	1.000	0.367
Position	1	0.788	0.273	6.761	0.0001
Residual	17	1.982	0.687		
Total	19	2.887	1.000		
September	**Df**	**Sum Of Sqs**	**R2**	**F**	**Pr(>F)**
Treatment	1	0.123	0.0487	1.281	0.210
Position	1	0.768	0.304	8.003	0.0001
Residual	17	1.630	0.647		
Total	19	2.521	1.000		
rbcL					
	Df	**Sum Of Sqs**	**R2**	**F**	**Pr(>F)**
Treatment	1	0.103	0.0128	0.928	0.449
Position	1	1.601	0.199	14.378	0.0001
Residual	57	6.346	0.788		
Total	59	8.050	1.000		
16S Universal					
	Df	**Sum Of Sqs**	**R2**	**F**	**Pr(>F)**
Treatment	1	0.351	0.015996	0.965	0.524
Position	1	0.859	0.039143	2.361	0.0002
Residual	57	20.735	0.945		
Total	59	21.945	1.000		

SUPPLEMENTARY FIGURES

Figure S1. 16S Cyanobacteria rarefaction curves

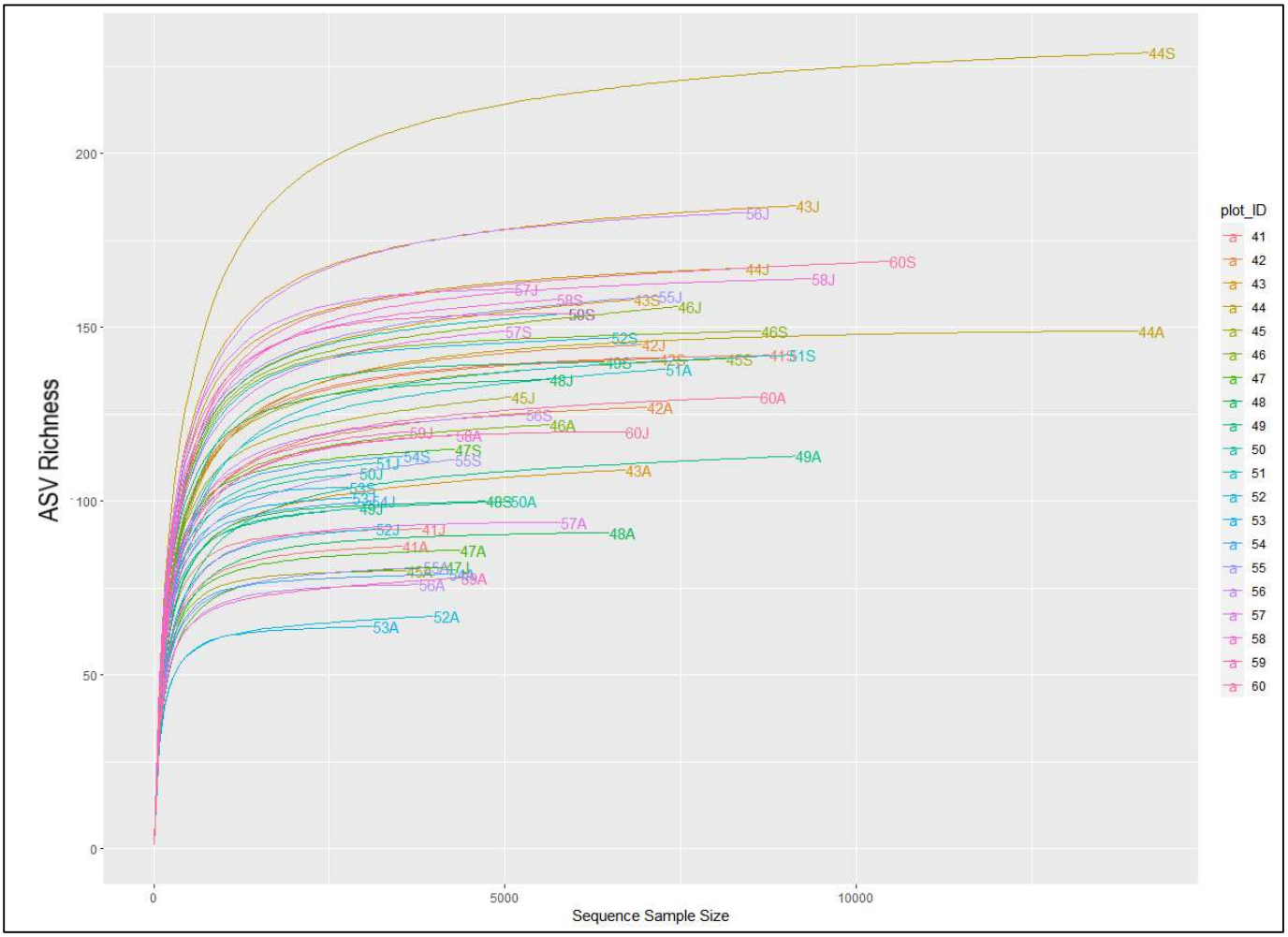

Figure S2. 16S Universal rarefaction curves

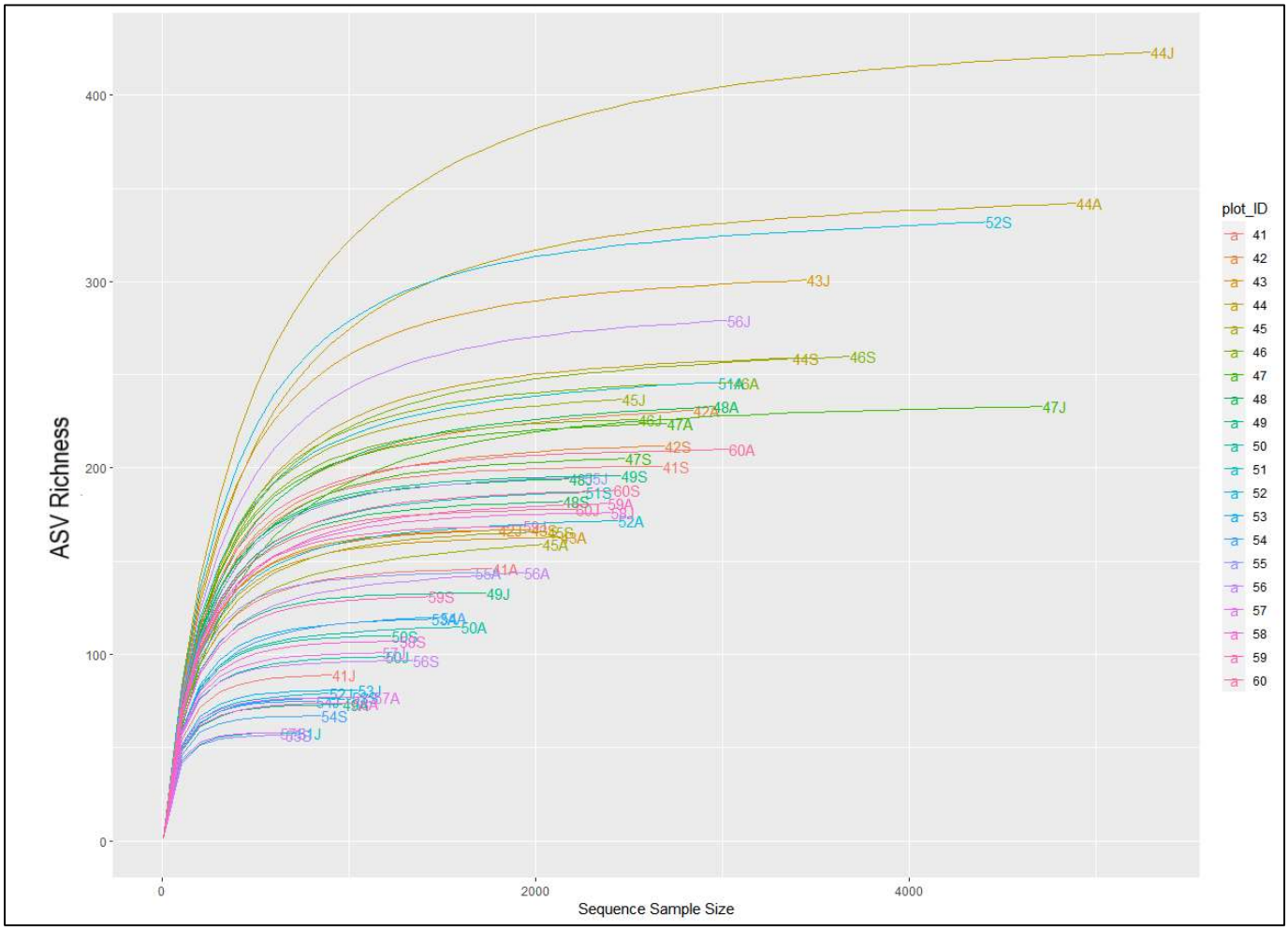

Figure S3. rbcL rarefaction curves

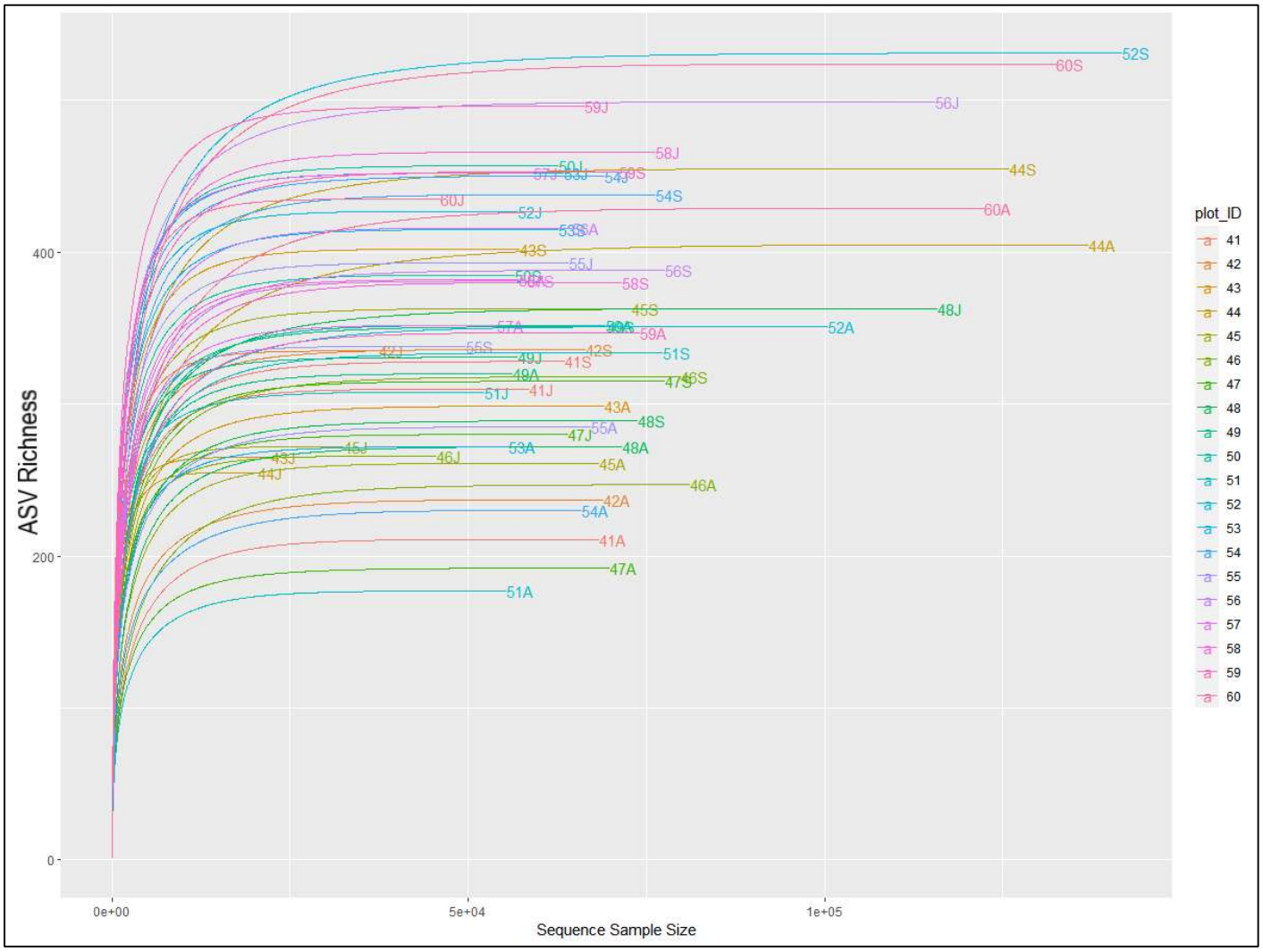

Figure S4. UPA rarefaction curves

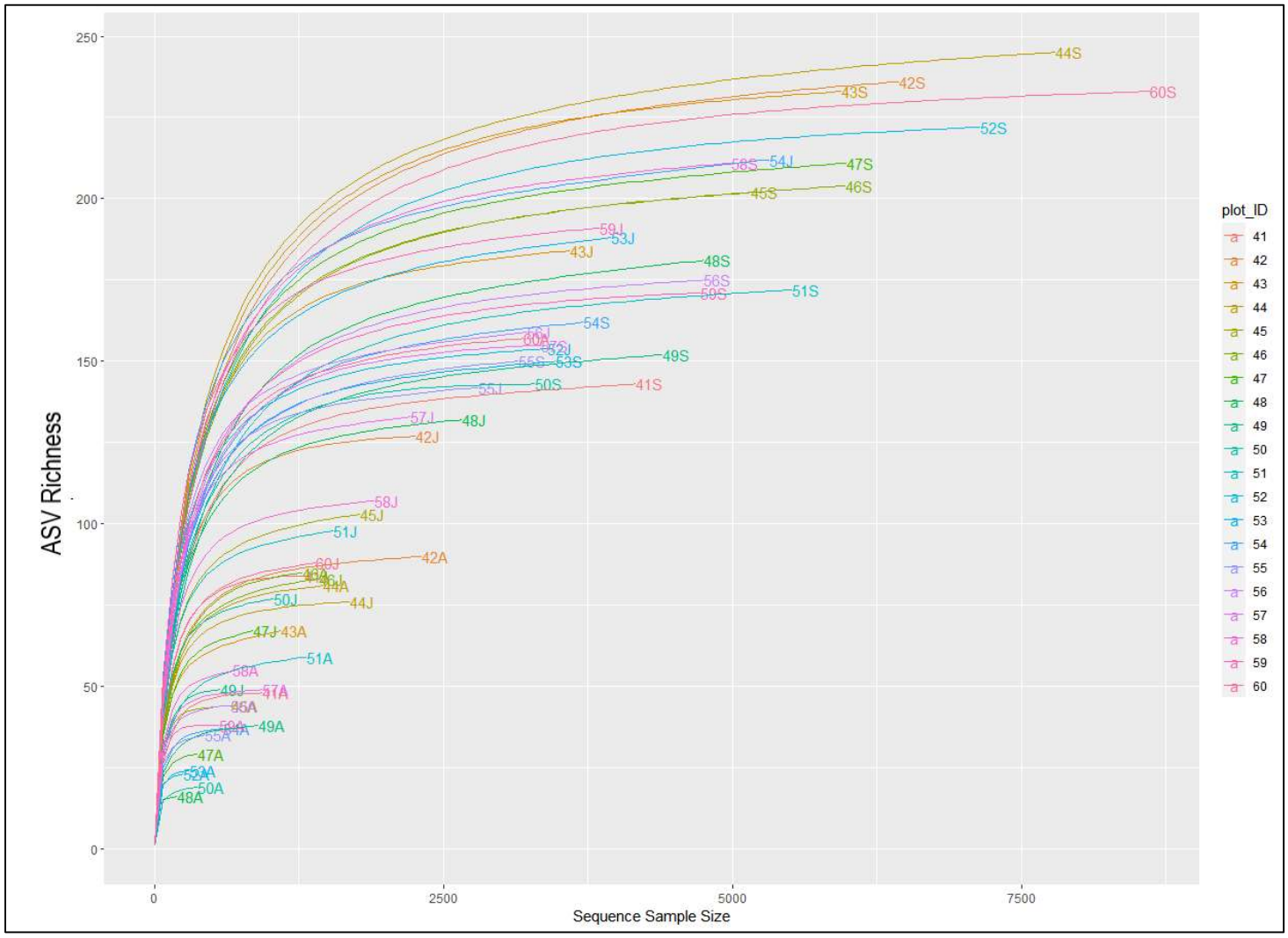

Figure S5. 16S Cyanobacteria PCoA ordination plot, with data points colored according to sampling month

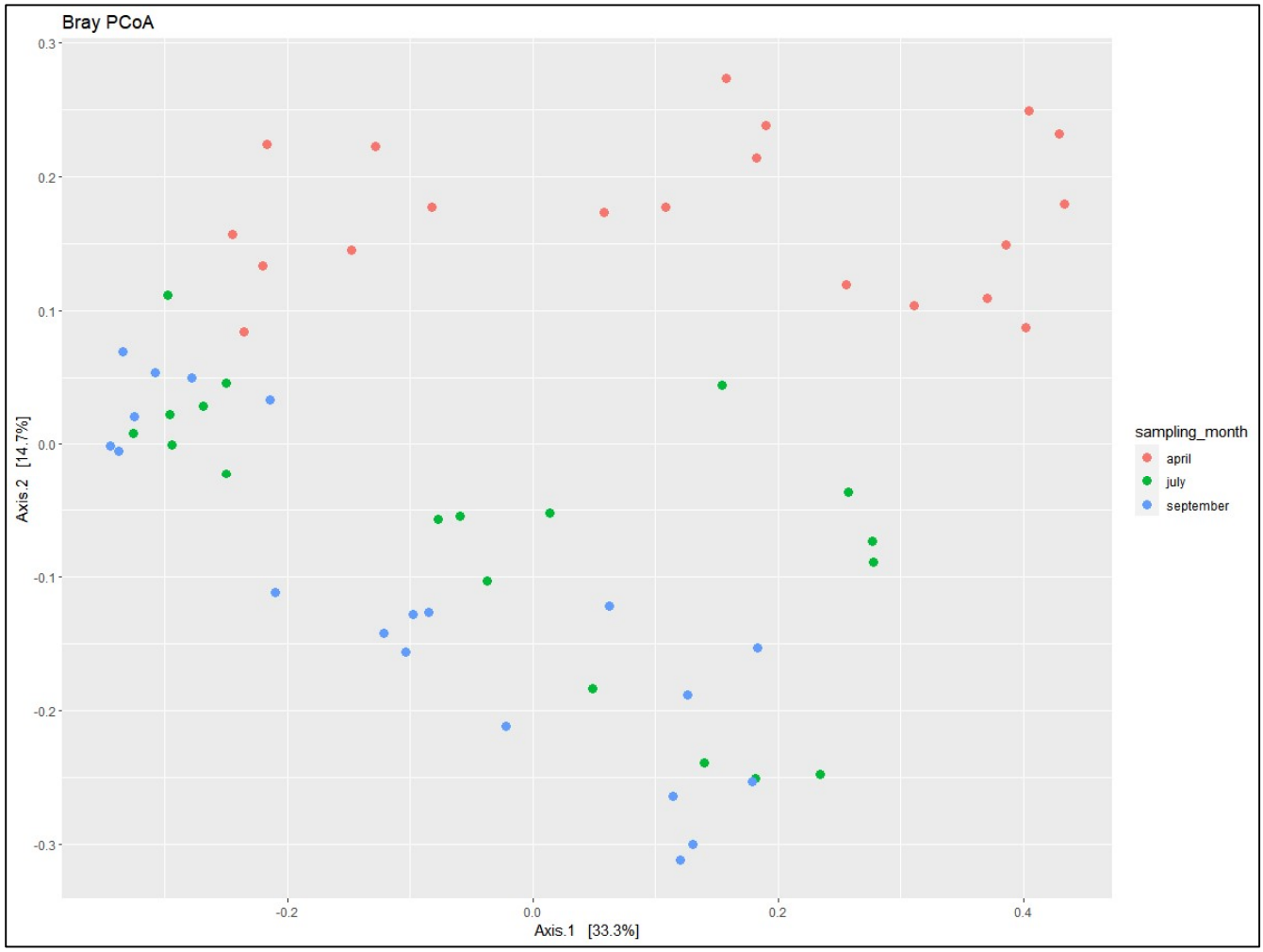

Figure S6. rbcL PCoA ordination plot, with data points colored according to sampling month

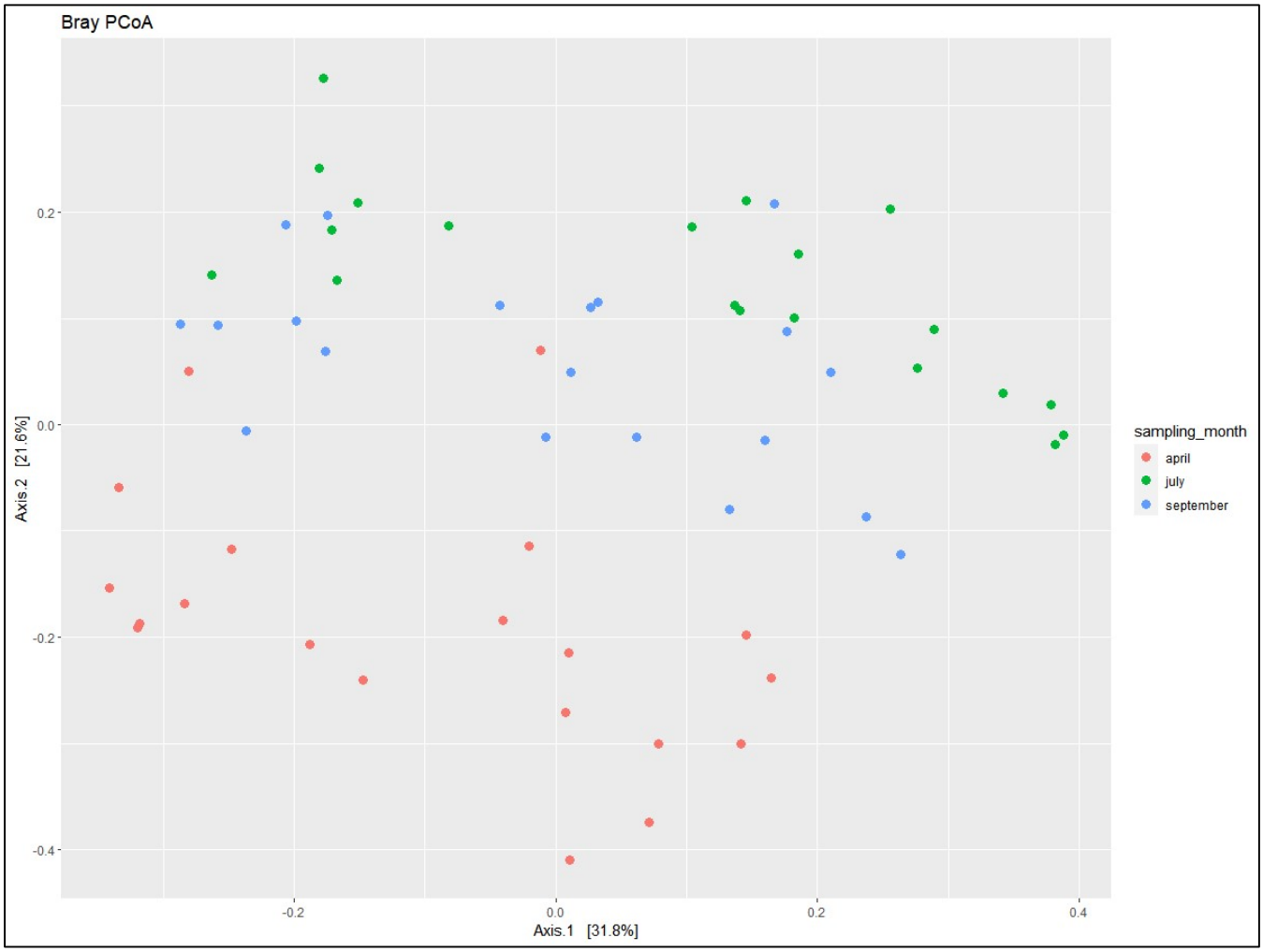

Figure S7. 16S Universal PCoA ordination plot, with data points colored according to sampling month

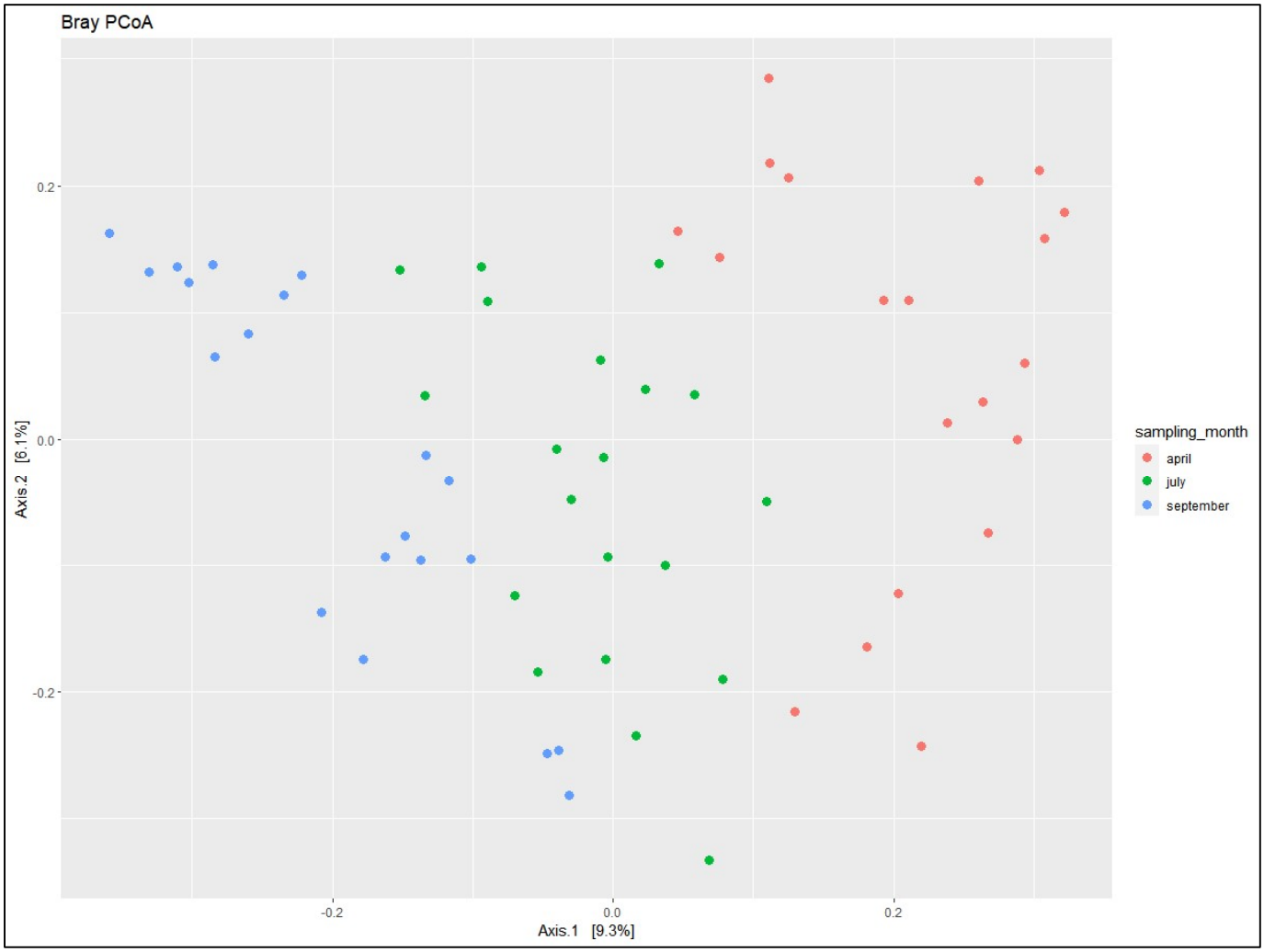

Figure S8. Coleofasciculales genera

Proportional abundances of genera with the order Coleofasciculales. Color indicates genus. Vertical columns in the figure represent (from left to right) April, July, and September sampling months. Horizontal rows in the figure represent creek edge (top row) and marsh interior (bottom row) groups. Within each month*position subsection of the figure, data are further grouped by treatment, with the control group on the left and the nitrogen treatment group on the right. The maximum value on the y-axis (0.5) is equivalent to 10% of all sequencing reads in each month*position*treatment group of 5 samples.

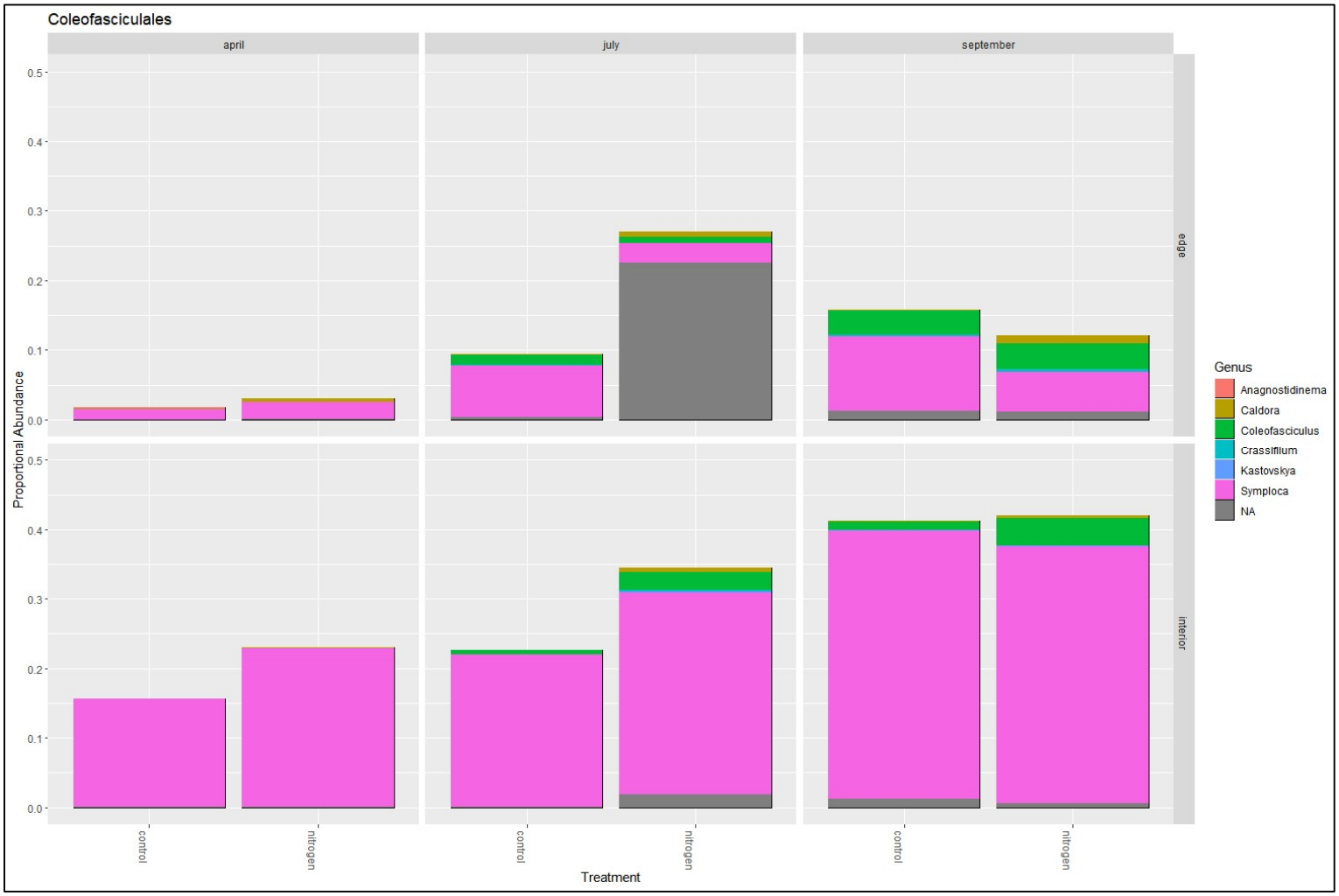

Figure S9. Synechococcales genera

Proportional abundances of genera with the order Synechococcales. Color indicates genus. Vertical columns in the figure represent (from left to right) April, July, and September sampling months. Horizontal rows in the figure represent creek edge (top row) and marsh interior (bottom row) groups. Within each month*position subsection of the figure, data are further grouped by treatment, with the control group on the left and the nitrogen treatment group on the right. The maximum value on the y-axis (0.75) is equivalent to 15% of all sequencing reads in each month*position*treatment group of 5 samples.

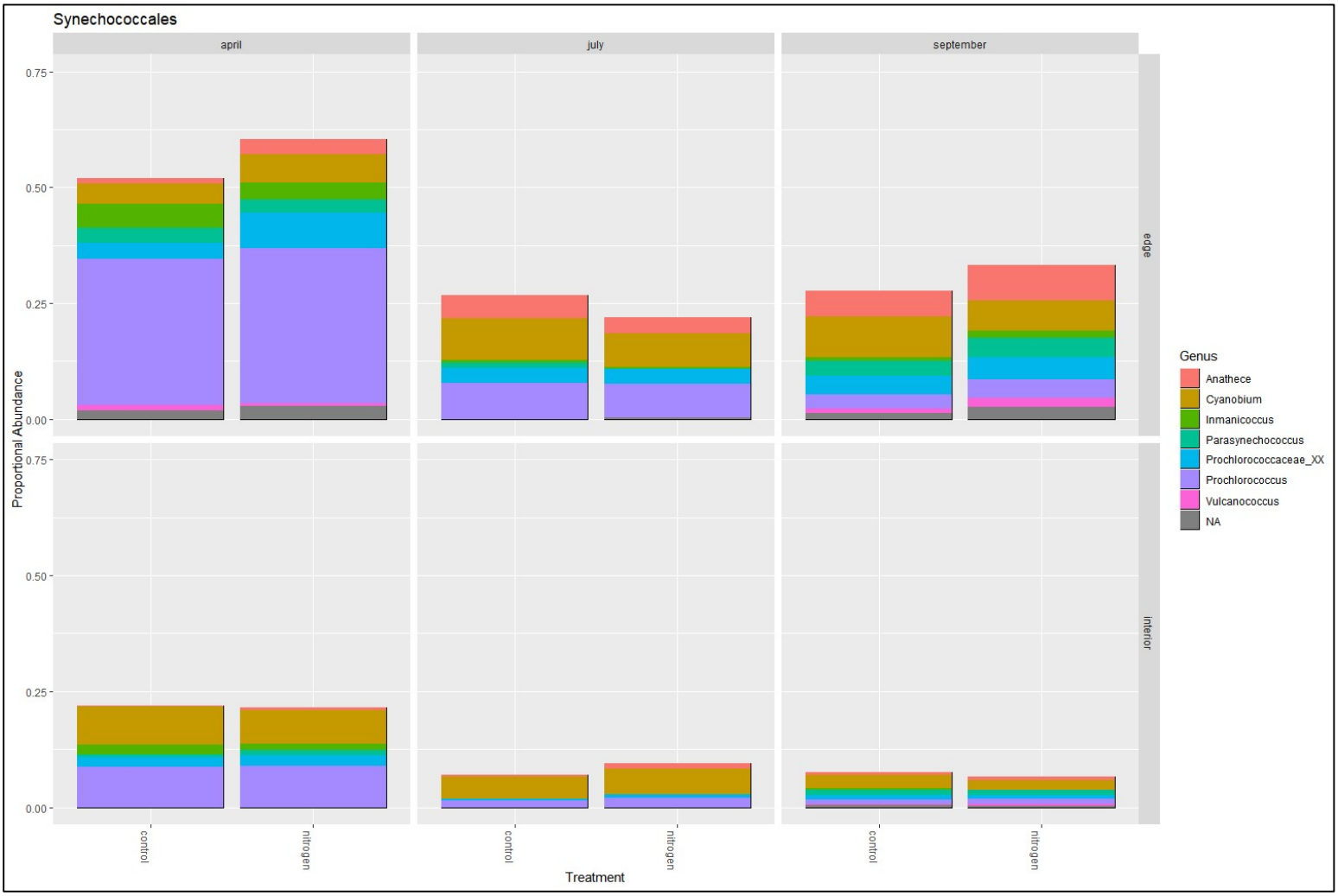

Figure S10. Top 10 Mediophyceae genera

Proportional abundances of the 10 most abundant genera within the class Mediophyceae across the entire dataset. Color indicates genus. Vertical columns in the figure represent (from left to right) April, July, and September sampling months. Horizontal rows in the figure represent creek edge (top row) and marsh interior (bottom row) groups. Within each month*position subsection of the figure, data are further grouped by treatment, with the control group on the left and the nitrogen treatment group on the right. The maximum value on the y-axis (0.25) is equivalent to 5% of all sequencing reads in each month*position*treatment group of 5 samples.

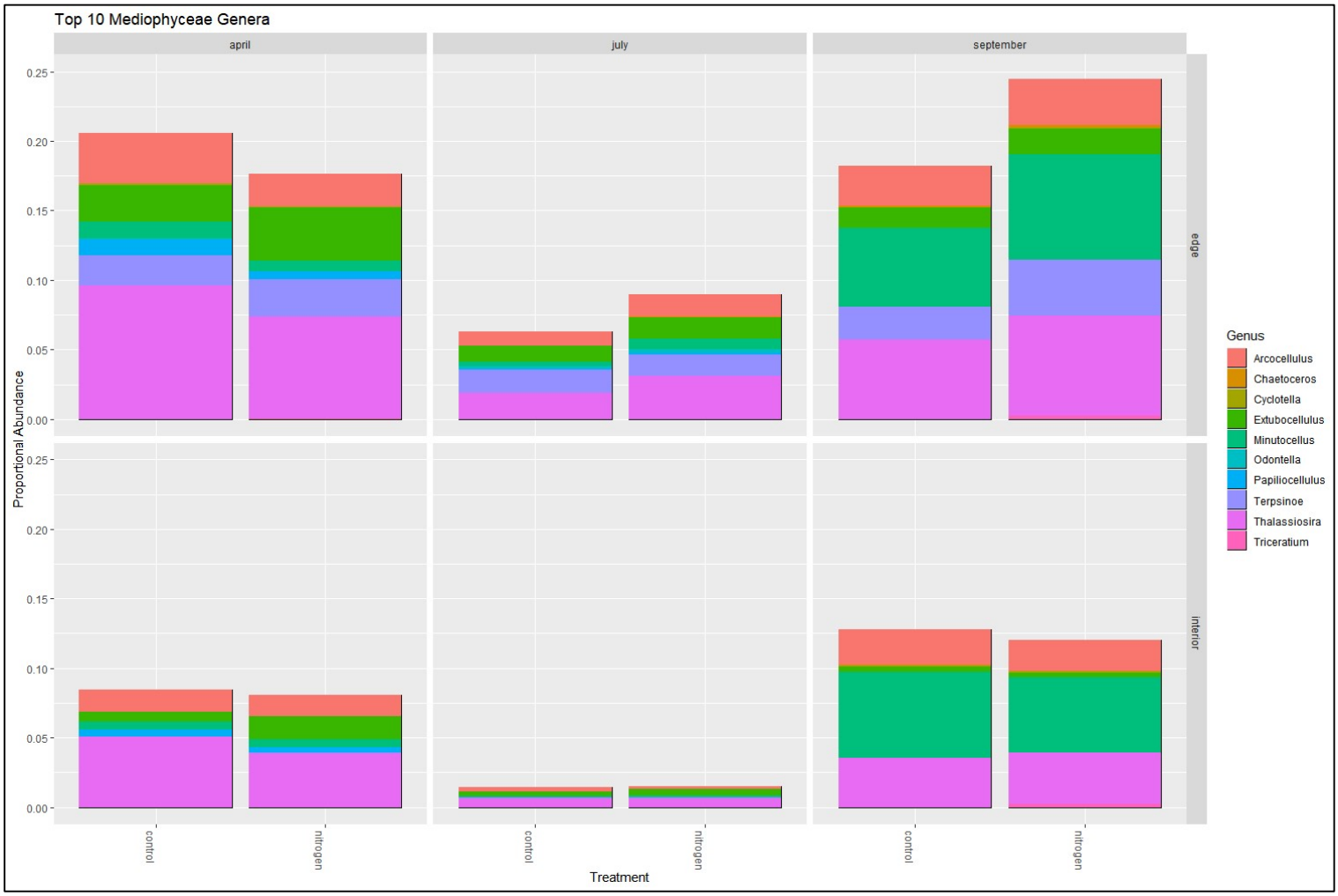

Figure S11. Archaeal genera

Proportional abundances of genera within the kingdom Archaea. Color indicates genus. Vertical columns in the figure represent (from left to right) April, July, and September sampling months. Horizontal rows in the figure represent creek edge (top row) and marsh interior (bottom row) groups. Within each month*position subsection of the figure, data are further grouped by treatment, with the control group on the left and the nitrogen treatment group on the right. The maximum value on the y-axis (0.75) is equivalent to 15% of all sequencing reads in each month*position*treatment group of 5 samples.

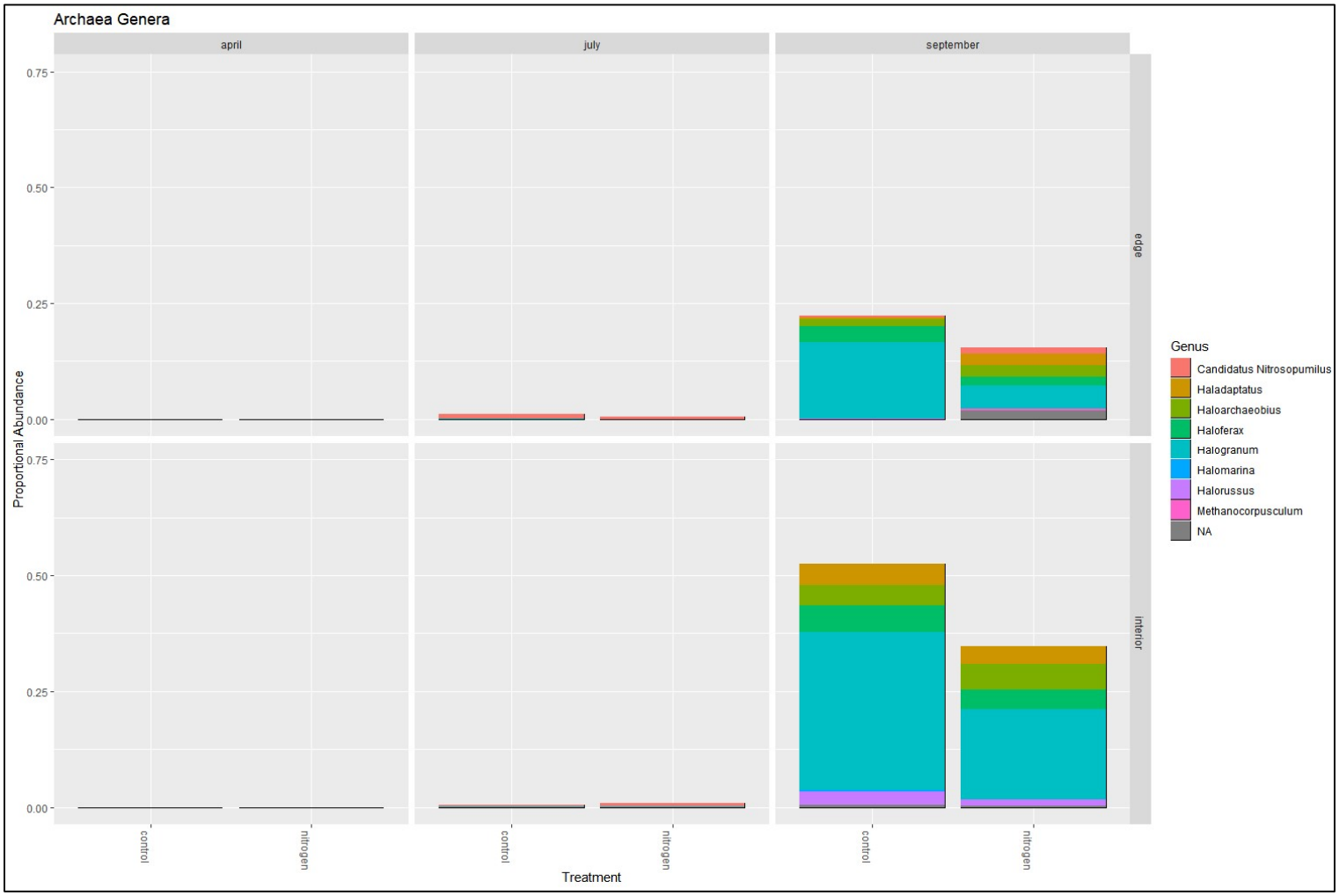

SUPPLEMENTARY TABLES

Table S1. Coordinates, position group, and treatment group of experimental plots.

Plot ID	Latitude	Longitude	Plot Position	Treatment
41	29°43.657 N	81°14.393 W	Interior	Control
42	29°43.648 N	81°14.419 W	Interior	Control
43	29°43.638 N	81°14.426 W	Interior	Control
44	29°43.629 N	81°14.423 W	Edge	Control
45	29°43.626 N	81°14.402 W	Interior	Control
46	29°43.635 N	81°14.398 W	Interior	Control
47	29°43.650 N	81°14.393 W	Interior	Nitrogen
48	29°43.639 N	81°14.394 W	Interior	Nitrogen
49	29°43.628 N	81°14.394 W	Interior	Nitrogen
50	29°43.636 N	81°14.421 W	Interior	Nitrogen
51	29°43.655 N	81°14.410 W	Interior	Nitrogen
52	29°43.635 N	81°14.428 W	Edge	Nitrogen
53	29°43.638 N	81°14.433 W	Edge	Control
54	29°43.650 N	81°14.430 W	Edge	Nitrogen
55	29°43.660 N	81°14.414 W	Edge	Control
56	29°43.666 N	81°14.387 W	Edge	Nitrogen
57	29°43.678 N	81°14.379 W	Edge	Control
58	29°43.672 N	81°14.390 W	Edge	Nitrogen
59	29°43.671 N	81°14.398 W	Edge	Control
60	29°43.671 N	81°14.404 W	Edge	Nitrogen

Table S2. Primers used to amplify selected gene markers

Microbial Community Targeted	Gene Marker	Primers	Primer Sequence (5'-3')
Cyanobacteria	16S rDNA (V3-V4 region)	CYA359F CYA781R	GGGGAATYTTCCGCAATGGG GACTACWGGGGTATCTAATCCCWTT
Prokaryotes (including cyanobacteria)	16S rDNA (V4-V5 region)	515F 926R	GTGCCAGCMGCCGCGGTAA CCGYCAATTYMTTTRAGTTT
Diatoms	*rbc*L	Equimolar mix of Diat_rbcL_708F_1 Diat_rbcL_708F_2 Diat_rbcL_708F_3	AGGTGAAGTAAAAGGTTCWTACTTAAA AGGTGAAGTTAAAGGTTCWTAYTTAAA AGGTGAAACTAAAGGTTCWTACTTAAA
		Equimolar mix of Diat_rbcL_R3_1 Diat_rbcL_R3_2	CCTTCTAATTTACCWACWACTG CCTTCTAATTTACCWACAACAG
Eukaryotic algae (including diatoms) and cyanobacteria	Universal Plastid Amplicon (23S rDNA)	p23SrV_f1 p23SrV_r1	GGACAGAAAGACCCTATGAA TCAGCCTGTTATCCCTAGAG
Illumina overhang adapter sequences appended to all primer sequences			Forward overhang: TCGTCGGCAGCGTCAGATGTGTATAAGAGACAG Reverse overhang: GTCTCGTGGGCTCGGAGATGTGTATAAGAGACAG

Table S3. Thermocycler settings for amplicon PCR

Gene marker(s)	Thermocycler settings for amplicon PCR	
16S rDNA (V3-V4 region) (16S Cyanobacteria) and 16S rDNA (V4-V5 region) (16S Universal)	Initial denaturing: 95°C for 5 minutes	
	35 cycles: Denaturing: 95°C for 30 s Annealing: 55°C for 30 s Extension: 72°C for 30 s	
	Final extension: 72°C for 5 minutes	
rbcL	Initial denaturing: 95°C for 15 minutes	
	40 cycles: Denaturing: 95°C for 45 s Annealing: 55°C for 45 s Extension: 72°C for 45 s	
	Final extension: 72°C for 5 minutes	
UPA (Touchdown PCR)	Initial denaturing: 95°C for 5 minutes	
	16 cycles: Denaturing: 94°C for 30 s Annealing: 66°C for 30 s (-0.5°C every cycle) Extension: 72°C for 30 s	19 cycles: Denaturing: 94°C for 30 s Annealing: 58°C for 30 s Extension: 72°C for 30 s
	Final extension: 72°C for 1 minute	

Table S4. 16S Cyanobacteria read counts tracked throughout DADA2 pipeline and phyloseq filtering steps.

	DADA2 pipeline steps						Filtering steps done using phyloseq	
	Input	filtered	denoisedF	denoisedR	merged	nonchim	Non-target ASV removal	Singleton and doubleton removal
Reads	1594630	1194165	1165749	1143250	952009	809490	358532	358223

Table S5. 16S Universal read counts tracked throughout DADA2 pipeline and phyloseq filtering steps.

	DADA2 pipeline steps						Filtering steps done using phyloseq	
	Input	filtered	denoisedF	denoisedR	merged	nonchim	Non-target ASV removal	Singleton and doubleton removal
Reads	359242	293194	233695	249122	165867	150411	129344	128386

Table S6. rbcL read counts tracked throughout DADA2 pipeline and phyloseq filtering steps.

	DADA2 pipeline steps						Filtering steps done using phyloseq		
	Input	filtered	denoisedF	denoisedR	merged	nonchim	Non-target ASV removal	Singleton and doubleton removal	Subtraction of reads from ASVs in negative controls
Reads	5742158	4899254	4843409	4855911	4532190	4322498	4307368	4307324	4293321

Table S7. UPA read counts tracked throughout DADA2 pipeline and phyloseq filtering steps.

	DADA2 pipeline steps						Filtering steps done using phyloseq		
	Input	filtered	denoisedF	denoisedR	merged	nonchim	Non-target ASV removal	Singleton and doubleton removal	Subtraction of reads from ASVs in negative controls
Reads	271589	232169	221678	226598	215588	191404	191140	190682	168813

Table S8. Number of ASVs assigned taxonomy in 16S Cyanobacteria dataset

Taxonomic Rank	Number of ASVs With Taxonomic Assignment	Percent of All ASVs in Dataset
Kingdom	917	100%
Phylum	917	100%
Class	917	100%
Order	882	96%
Family	840	92%
Genus	599	65%
Species	Ranking not included in reference database	N/A
Total ASVs	917	

Table S9. Number of ASVs assigned taxonomy in 16S Universal dataset

Taxonomic Rank	Number of ASVs With Taxonomic Assignment	Percent of All ASVs in Dataset
Kingdom	3729	100%
Phylum	3729	100%
Class	3729	100%
Order	3729	100%
Family	3729	100%
Genus	2396	64%
Species	Ranking not included in reference database	N/A
Total ASVs	3729	

Table S10. Number of ASVs assigned taxonomy in rbcL dataset

Taxonomic Rank	Number of ASVs With Taxonomic Assignment	Percent of All ASVs in Dataset
Kingdom	1317	100%
Phylum	1317	100%
Class	1181	90%
Order	951	72%
Family	Ranking not included in reference database	N/A
Genus	705	54%
Species	422	32%
Total ASVs	1317	

Table S11. Number of ASVs assigned taxonomy in UPA dataset

Taxonomic Rank	Number of ASVs With Taxonomic Assignment	Percent of All ASVs in Dataset
Kingdom	1118	93%
Phylum	1068	89%
Class	957	80%
Order	649	54%
Family	541	45%
Genus	504	42%
Species	446	37%
Total ASVs	1196	

Table S12. Effects of sampling month, position, treatment, and their interactions on Shannon diversity, determined using three-way ANOVA.

16S Cyanobacteria					
	Df	**Sum Sq**	**Mean Sq**	**F value**	**Pr(>F)**
sampling month	2	1.6398	0.8199	18.888	8.89E-07
position	1	0.0166	0.0166	0.383	0.5388
treatment	1	0.2265	0.2265	5.218	0.0268
sampling month:position	2	0.2321	0.116	2.673	0.0793
sampling month:treatment	2	0.1219	0.0609	1.404	0.2556
position:treatment	1	0.0317	0.0317	0.731	0.3967
sampling month:position:treatment	2	0.0218	0.0109	0.251	0.7791
Residuals	48	2.0836	0.0434		
rbcL					
	Df	**Sum Sq**	**Mean Sq**	**F value**	**Pr(>F)**
sampling month	2	7.916	3.958	40.849	4.36E-11
position	1	3.664	3.664	37.817	1.48E-07
treatment	1	0.013	0.013	0.136	0.714
sampling month:position	2	0.403	0.202	2.081	0.136
sampling month:treatment	2	0.099	0.05	0.513	0.602
position:treatment	1	0.023	0.023	0.233	0.632
sampling month:position:treatment	2	0.025	0.013	0.131	0.878
Residuals	48	4.651	0.097		
16S Universal					
	Df	**Sum Sq**	**Mean Sq**	**F value**	**Pr(>F)**
sampling month	2	0.077	0.0383	0.185	0.832
position	1	0.574	0.574	2.766	0.103
treatment	1	0.141	0.1409	0.679	0.414
sampling month:position	2	0.46	0.2299	1.108	0.339
sampling month:treatment	2	0.534	0.2669	1.286	0.286
position:treatment	1	0.255	0.2552	1.23	0.273
sampling month:position:treatment	2	0.117	0.0585	0.282	0.755
Residuals	48	9.96	0.2075		

Table S13. Scheirer-Ray-Hare tests of the effects of sampling month, position, and their interaction on Simpson diversity Simpson diversity

16S Cyanobacteria				
	Df	**Sum Sq**	**H**	**p.value**
sampling month	2	5.43E+03	1.78E+01	0.000136
position	1	3.46E+02	1.13E+00	0.287
sampling month:position	2	1.11E+03	3.63E+00	0.16
Residuals	54	1.11E+04		
rbcL				
	Df	**Sum Sq**	**H**	**p.value**
sampling month	2	8.48E+03	2.78E+01	9.15E-07
position	1	2.67E+03	8.74E+00	0.00311
sampling month:position	2	1.42E+01	4.67E-02	0.98
Residuals	54	6.83E+03		
16S Universal				
	Df	**Sum Sq**	**H**	**p.value**
sampling month	2	4.59E+02	1.50E+00	0.471
position	1	5.28E+02	1.73E+00	0.188
sampling month:position	2	4.97E+02	1.63E+00	0.44
Residuals	54	1.65E+04		

Table S14. Scheirer-Ray-Hare tests of the effects of sampling month, treatment, and their interaction on Simpson diversity Simpson diversity

16S Cyanobacteria				
	Df	**Sum Sq**	**H**	**p.value**
sampling month	2	5.43E+03	1.78E+01	0.000136
treatment	1	1.62E+03	5.32E+00	0.02
sampling month:treatment	2	5.06E+02	1.66E+00	0.44
Residuals	54	1.04E+04		
rbcL				
	Df	**Sum Sq**	**H**	**p.value**
sampling month	2	8.48E+03	2.78E+01	9.15E-07
treatment	1	1.26E-29	4.14E-32	1.00
sampling month:treatment	2	2.67E+02	8.76E-01	0.65
Residuals	54	9.25E+03		
16S Universal				
	Df	**Sum Sq**	**H**	**p.value**
sampling month	2	4.59E+02	1.50E+00	0.471
treatment	1	5.61E+01	1.84E-01	0.67
sampling month:treatment	2	1.17E+03	3.83E+00	0.15
Residuals	54	1.63E+04		

Table S15. Effects of treatment, position, and their interaction on Shannon diversity, determined using two-way ANOVA

16S Cyanobacteria					
	Df	**Sum Sq**	**Mean Sq**	**F value**	**Pr(>F)**
Treatment	1	0.227	0.22652	3.095	0.084
Position	1	0.017	0.01664	0.227	0.635
Treatment:Position	1	0.032	0.03175	0.434	0.513
Residuals	56	4.099	0.0732		
rbcL					
	Df	**Sum Sq**	**Mean Sq**	**F value**	**Pr(>F)**
treatment	1	0.013	0.013	0.056	0.813184
position	1	3.664	3.664	15.67	0.000215
treatment:position	1	0.023	0.023	0.096	0.757363
Residuals	56	13.094	0.234		
16S Universal					
	Df	**Sum Sq**	**Mean Sq**	**F value**	**Pr(>F)**
treatment	1	0.141	0.1409	0.708	0.404
position	1	0.574	0.574	2.884	0.095
treatment:position	1	0.255	0.2552	1.282	0.262
Residuals	56	11.147	0.1991		

Table S16. Effects of sampling month, position, treatment, and their interactions on overall community structure, determined using three-way PERMANOVA

16S Cyanobacteria					
	Df	**Sum Of Sqs**	**R2**	**F**	**Pf(>F)**
sampling month	2	1.742	0.17452	8.2794	0.0001
position	1	2.109	0.21129	20.0476	0.0001
treatment	1	0.1728	0.01731	1.6429	0.1038
sampling month:position	2	0.4668	0.04676	2.2185	0.0106
sampling month:treatment	2	0.1252	0.01254	0.595	0.9219
position:treatment	1	0.185	0.01853	1.7581	0.082
sampling month:position:treatment	2	0.1313	0.01315	0.6239	0.8938
Residual	48	5.0496	0.50589		
Total	59	9.9817	1		
rbcL					
	Df	**Sum Of Sqs**	**R2**	**F**	**Pr(>F)**
sampling month	2	2.2924	0.28476	15.3917	0.0001
position	1	1.6007	0.19884	21.4957	0.0001
treatment	1	0.1033	0.01283	1.3875	0.1902
sampling month:position	2	0.2485	0.03087	1.6686	0.0668
sampling month:treatment	2	0.1002	0.01244	0.6725	0.8002
position:treatment	1	0.0637	0.00791	0.8556	0.5033
sampling month:position:treatment	2	0.0669	0.00831	0.4494	0.9776
Residual	48	3.5745	0.44402		
Total	59	8.0502	1		
16S Universal					
	Df	**Sum Of Sqs**	**R2**	**F**	**Pr(>F)**
sampling month	2	2.405	0.10959	3.5921	0.0001
position	1	0.859	0.03914	2.566	0.0001
treatment	1	0.351	0.016	1.0486	0.3115
sampling month:position	2	0.7156	0.03261	1.0688	0.2294
sampling month:treatment	2	0.6318	0.02879	0.9437	0.6636
position:treatment	1	0.3352	0.01527	1.0012	0.4276
sampling month:position:treatment	2	0.579	0.02638	0.8648	0.9155
Residual	48	16.0685	0.73221		
Total	59	21.9451	1		

Table S17. Effects of position, treatment, and their interaction on overall community structure, determined using two-way PERMANOVA

16S Cyanobacteria					
April					
	Df	**Sum of Sqs**	**R2**	**F**	**Pr(>F)**
Treatment	1	0.0586	0.0207	0.578	0.710
Position	1	1.0201	0.360	10.058	0.0001
Treatment:Position	1	0.131	0.0462	1.291	0.224
Residual	16	1.623	0.573		
Total	19	2.832	1.000		
July					
	Df	**Sum of Sqs**	**R2**	**F**	**Pr(>F)**
Treatment	1	0.117	0.0404	0.999	0.373
Position	1	0.788	0.273	6.756	0.0001
Treatment:Position	1	0.115	0.0399	0.988	0.382
Residual	16	1.867	0.647		
Total	19	2.887	1.000		
September					
	Df	**Sum of Sqs**	**R2**	**F**	**Pr(>F)**
Treatment	1	0.123	0.0487	1.259	0.223
Position	1	0.768	0.304	7.870	0.0001
Treatment:Position	1	0.0700	0.0278	0.718	0.637
Residual	16	1.560	0.619		
Total	19	2.521	1.000		
rbcL					
	Df	**Sum Of Sqs**	**R2**	**F**	**Pr(>F)**
Treatment	1	0.103	0.0128	0.921	0.455
Position	1	1.601	0.199	14.269	0.0001
Treatment:Position	1	0.0637	0.00792	0.568	0.796
Residual	56	6.282	0.780		
Total	59	8.050	1.000		
16S Universal					
	Df	**Sum Of Sqs**	**R2**	**F**	**Pr(>F)**
Treatment	1	0.351	0.0160	0.9636	0.527
Position	1	0.859	0.0391	2.358	0.0001
Treatment:Position	1	0.335	0.0153	0.920	0.664
Residual	56	20.400	0.930		
Total	59	21.945	1.000		

FIGURES AND TABLES: CHAPTER 2

FIGURES

Figure 1. Sampling sites within the Guana Tolomato Matanzas National Estuarine Research Reserve

A) Map of the southeastern United States, showing location of the Guana Tolomato Matanzas National Estuarine Research Reserve (GTMNERR) in northeastern Florida (inset), and locations of the sample collection sites within GTMNERR. B-D) Images of the WETFEET Middle (B), Guana Dam South (C), and Shell Bluff (D) sample collection sites. Images courtesy of Gabriela Canas.

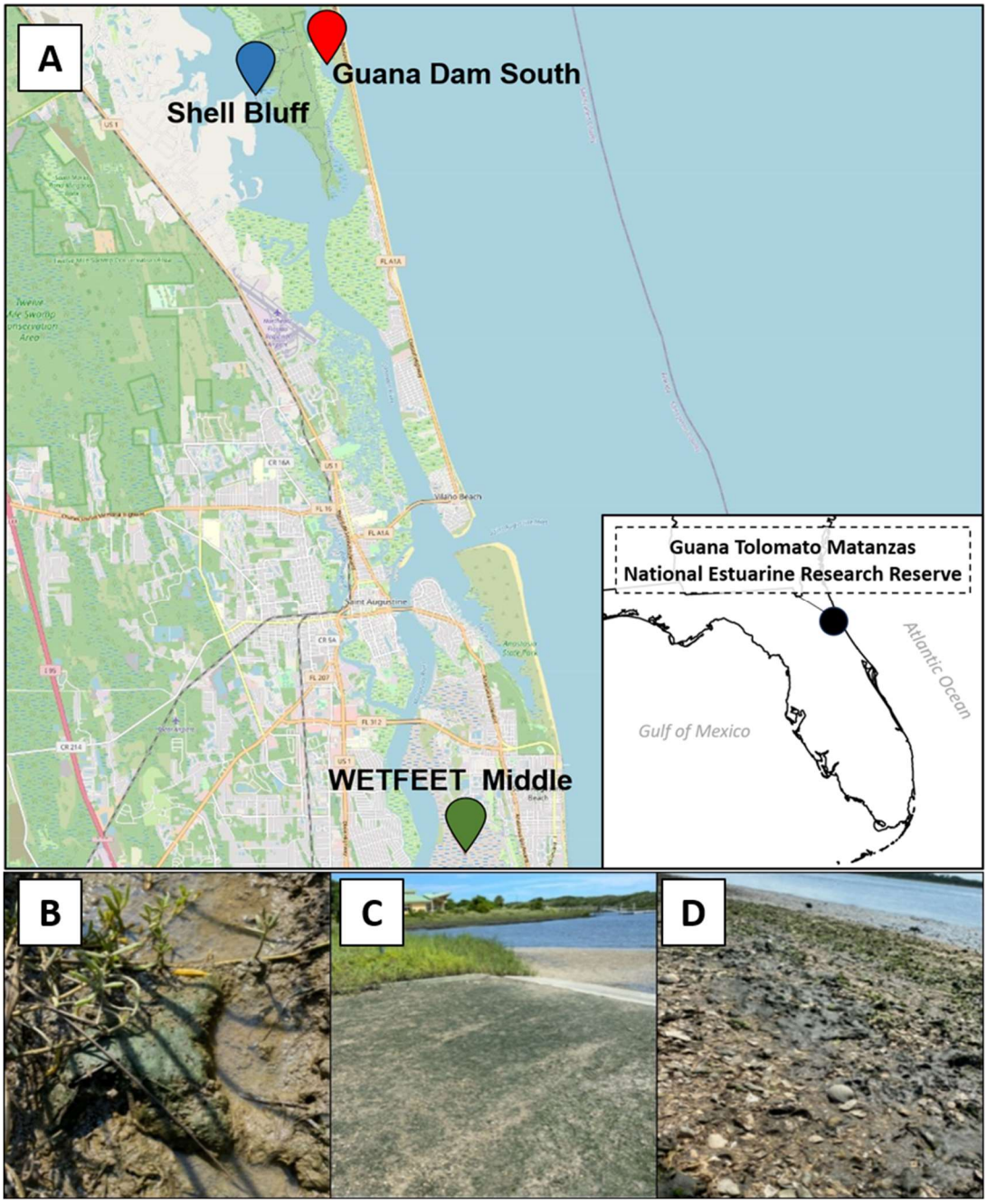

Figure 2. Photomicrographs of strain GTM2
Scale bars: 10 μm.

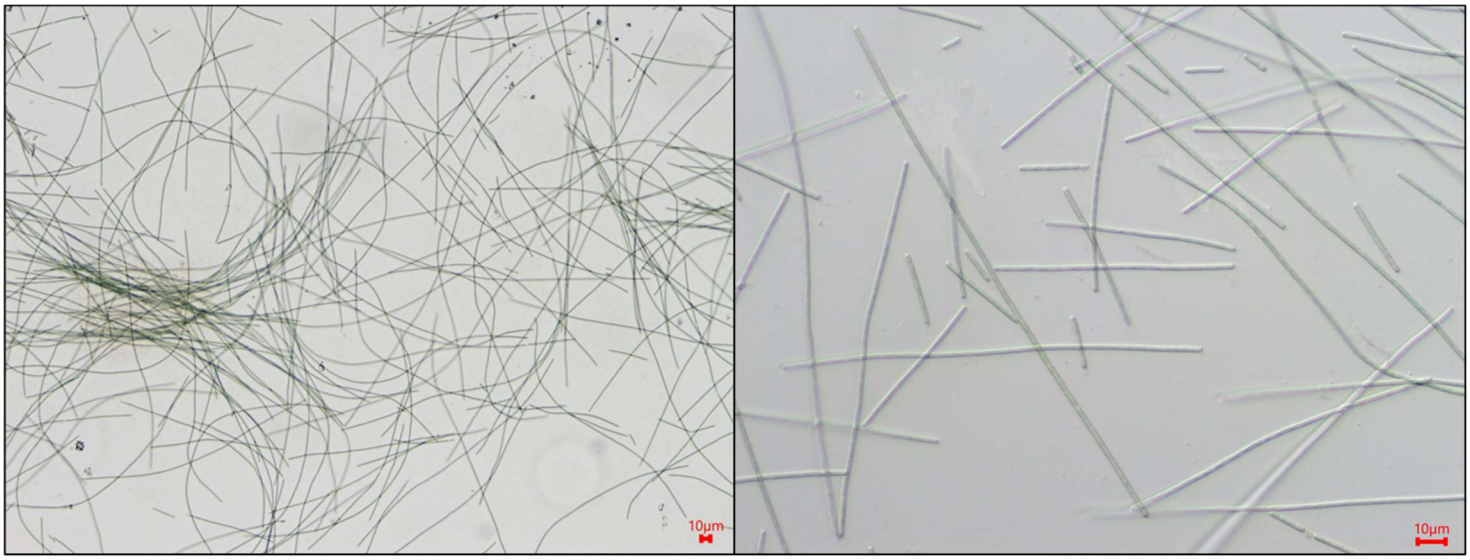

Figure 3. Photomicrographs of strain GTM5
Scale bars: 10 μm.

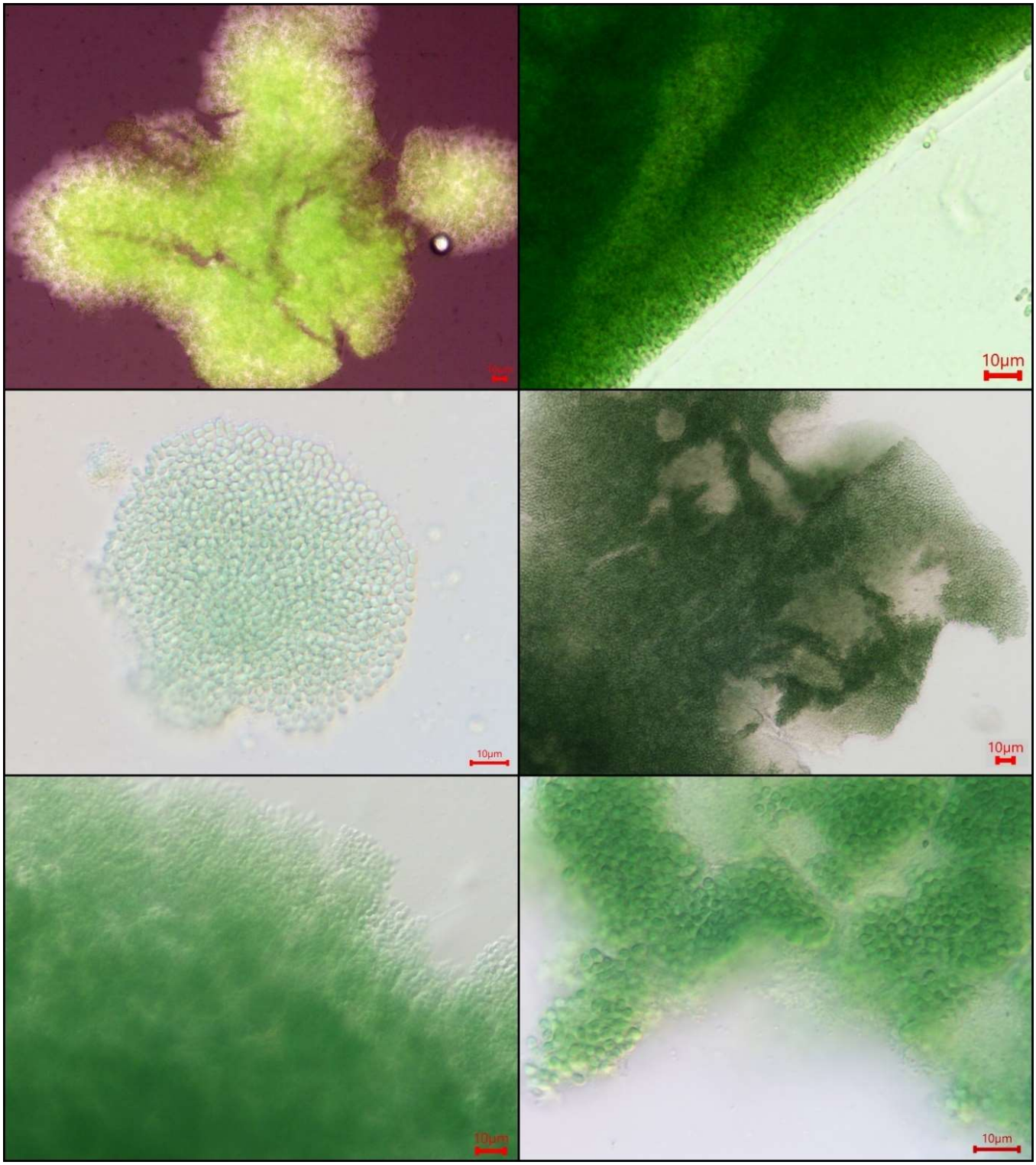

Figure 4. Photomicrographs of strain GTM6
Scale bars: 10 μm.

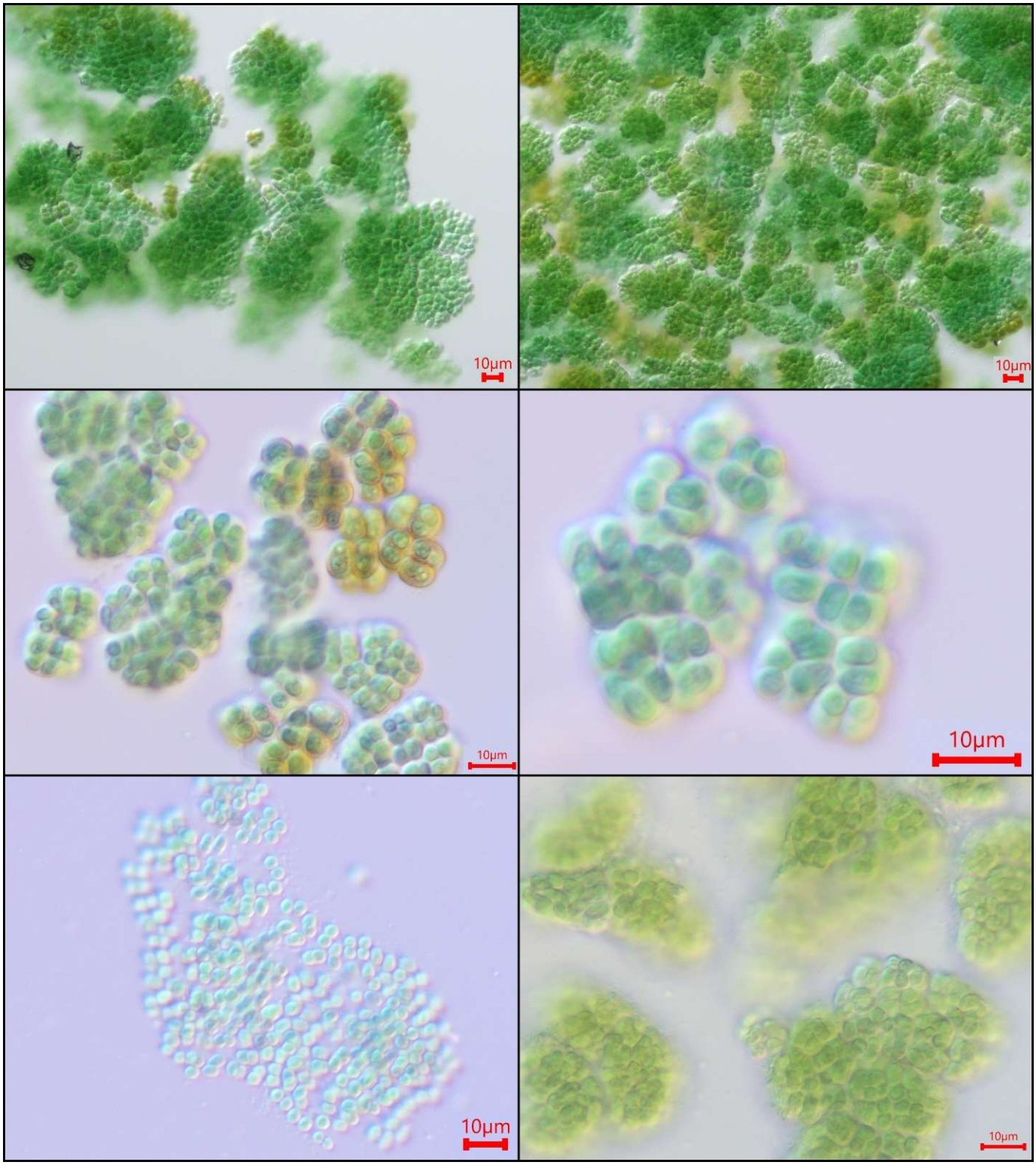

Figure 5. Photomicrographs of strains GTM1, GTM4, and GTM7
Scale bars: 10 μm.

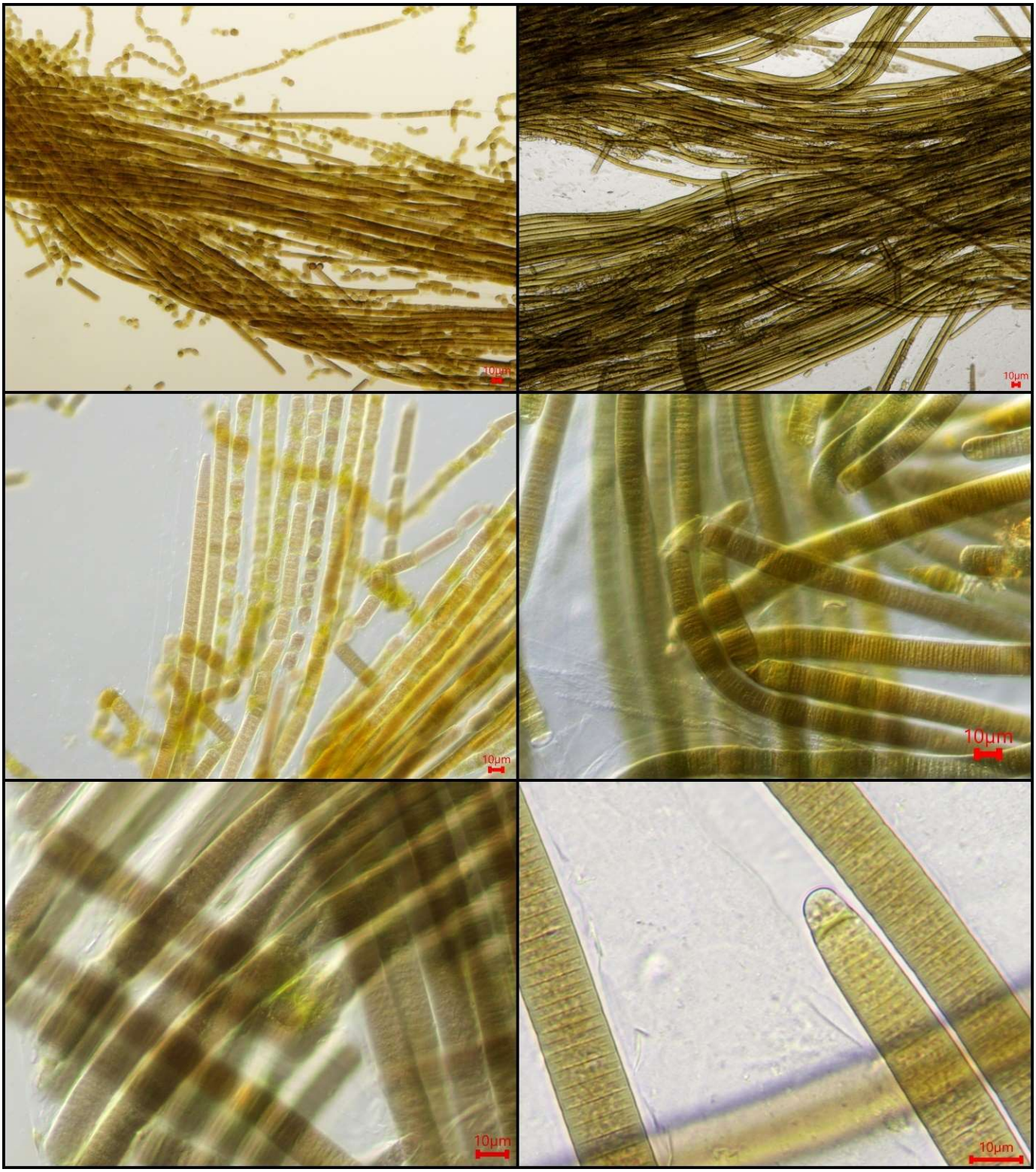

Figure 6. Photomicrographs of strain GTM3
Scale bars: 10 μm.

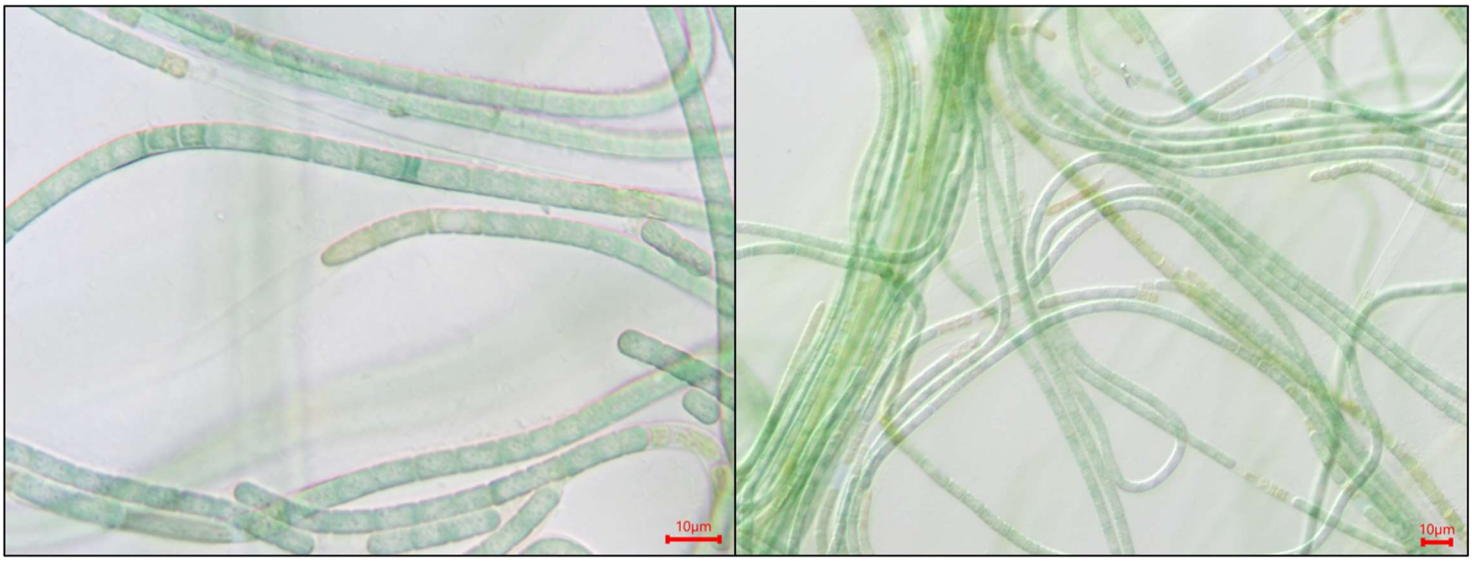

Figure 7. Photomicrographs of strains GTM12 and GTM13
Images in left column: strain GTM12. Images in right column: strain GTM13. Scale bars: 10 µm.

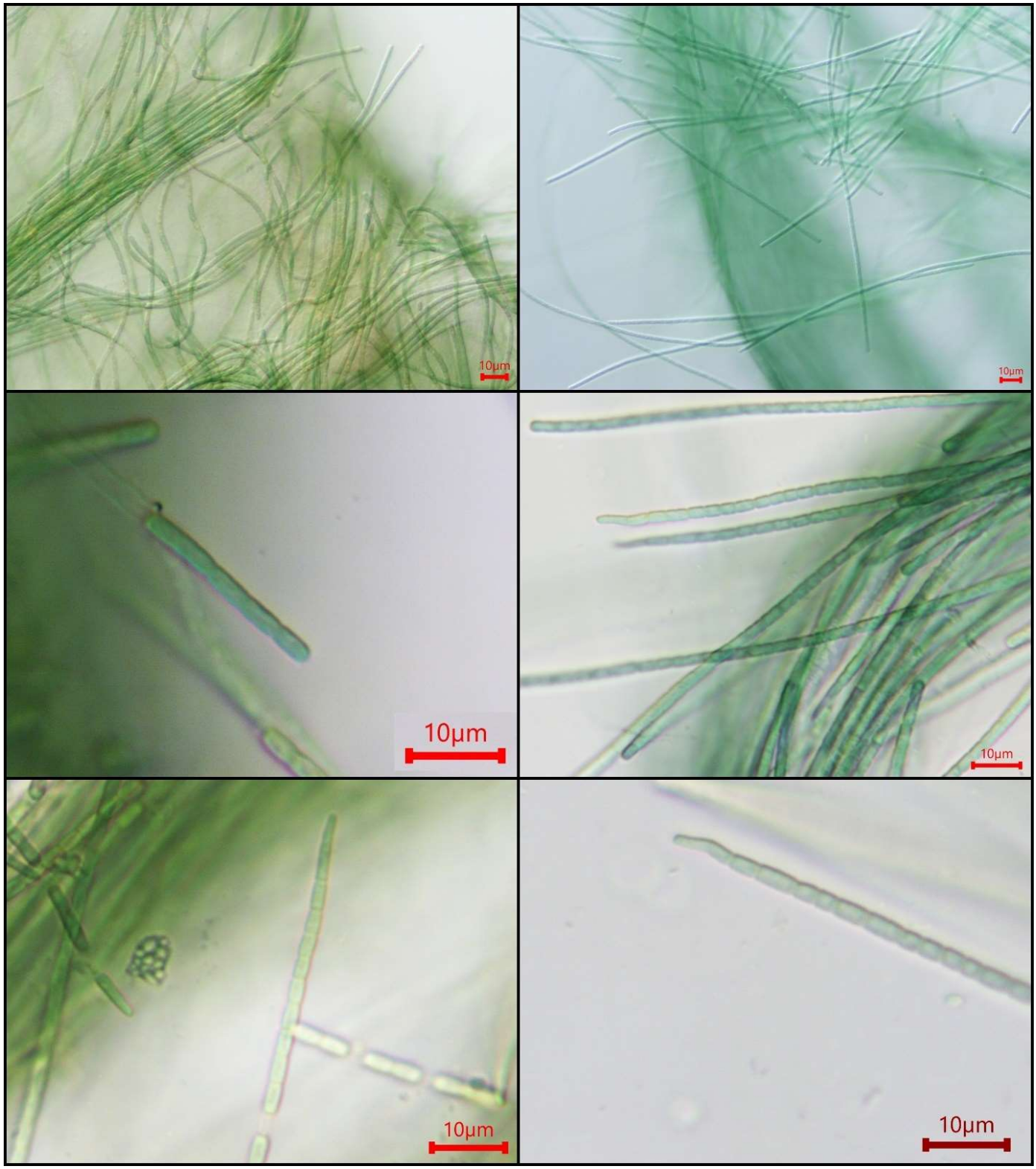

Figure 8. Photomicrographs of strain GTM19
Scale bars: 10 μm.

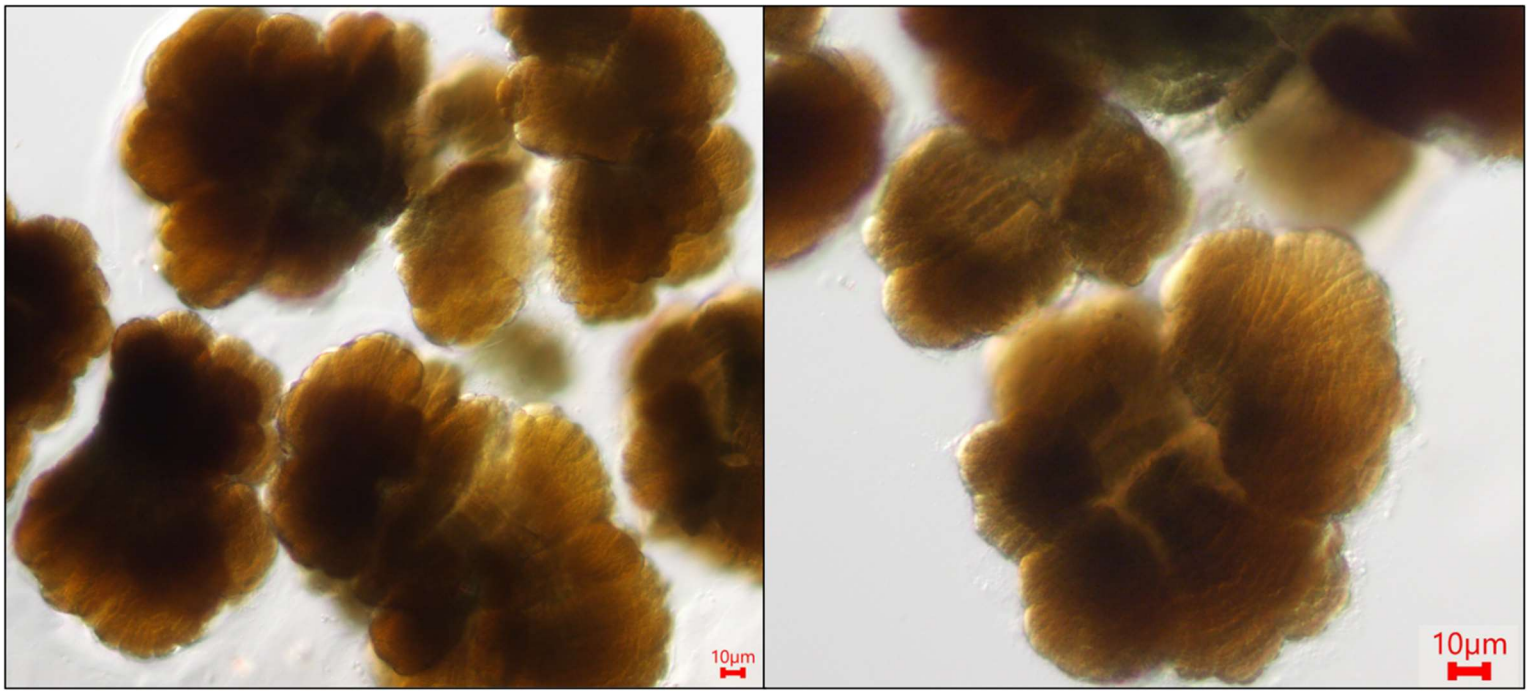

Figure 9. Photomicrographs of strains GTM20, GTM21, and GTM22
Scale bars: 10 μm.

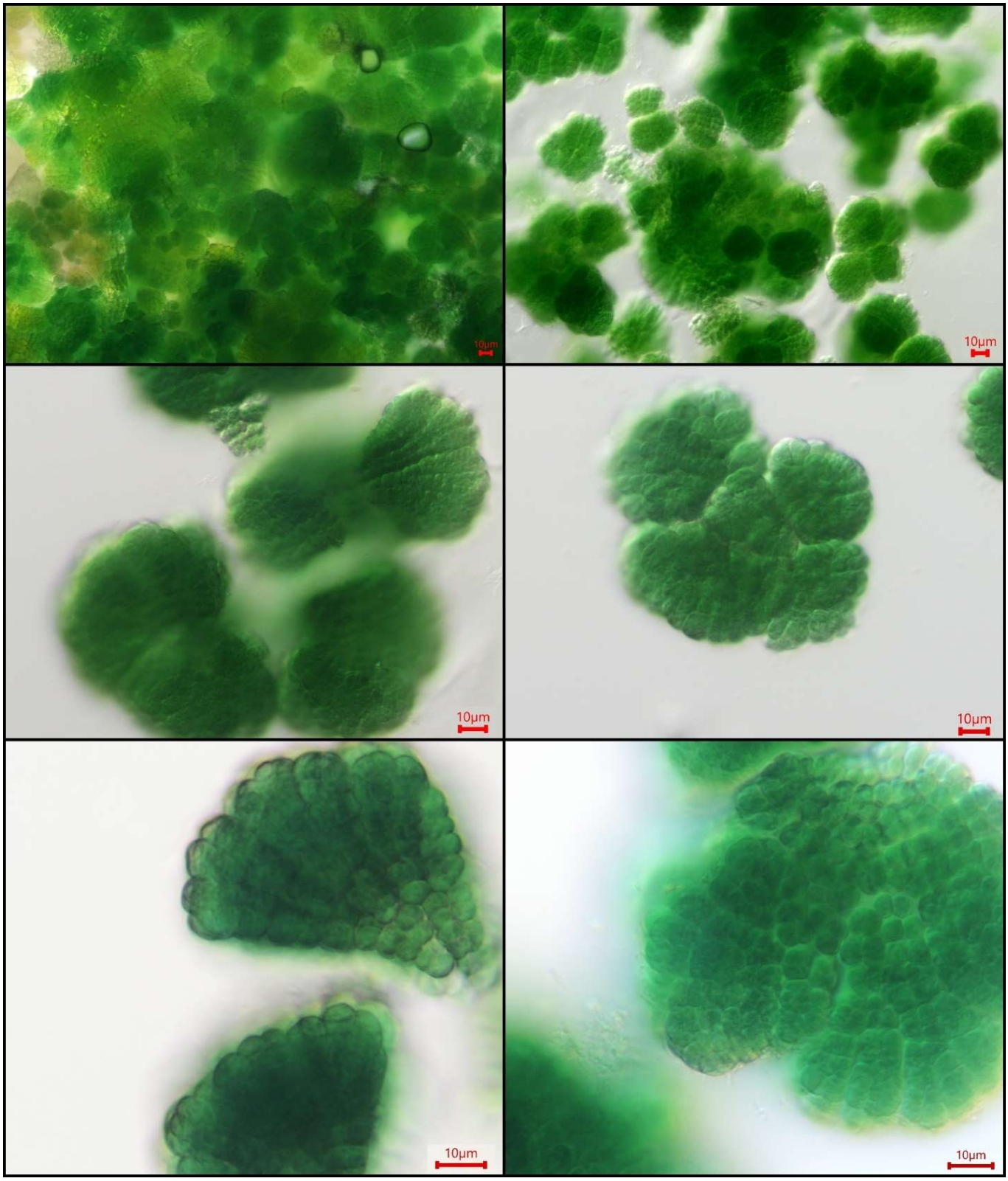

Figure 10. Photomicrographs of strains GTM14 and GTM15
Scale bars: 10 µm.

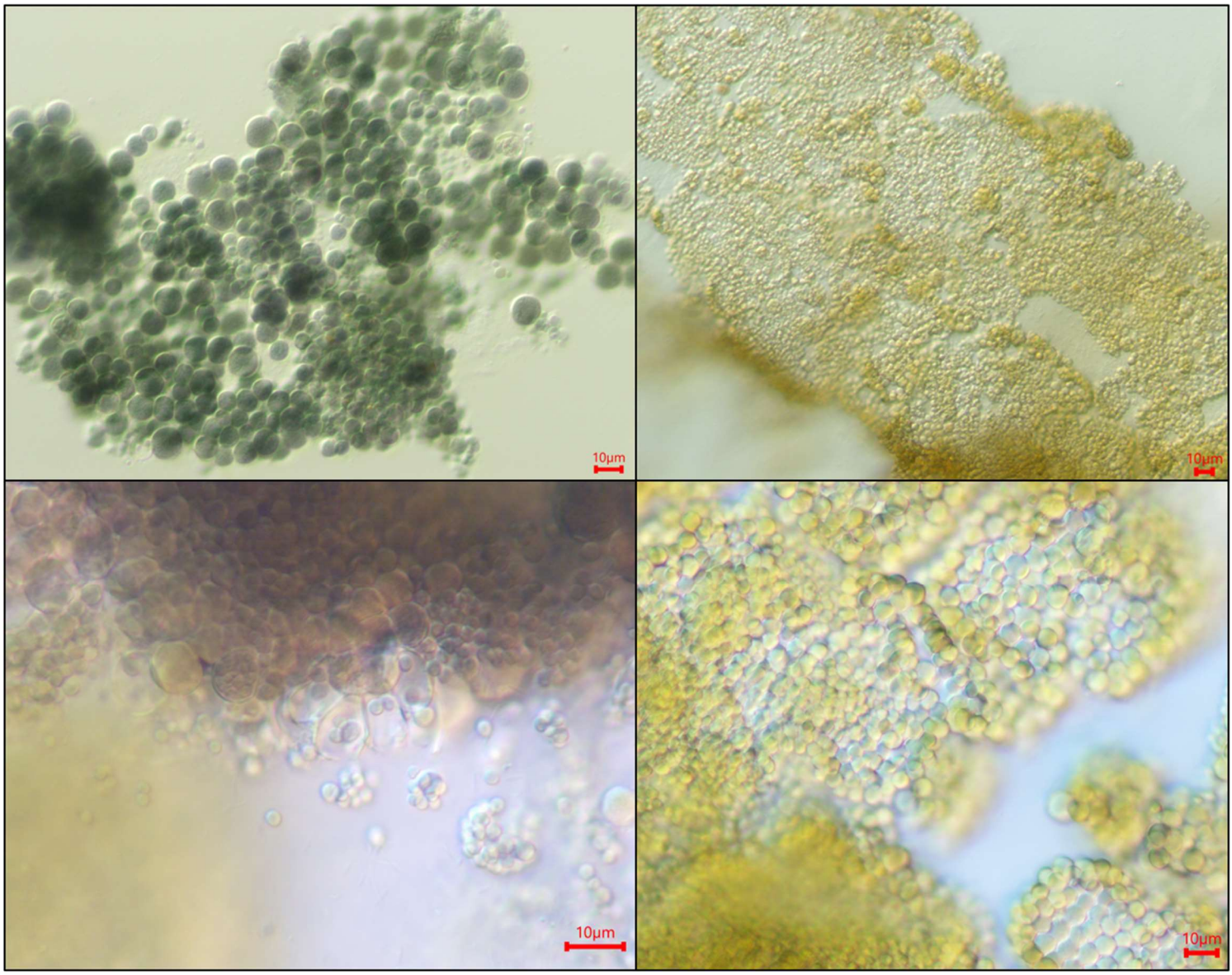

Figure 11. Photomicrographs of strain GTM10
Scale bars: 10 μm.

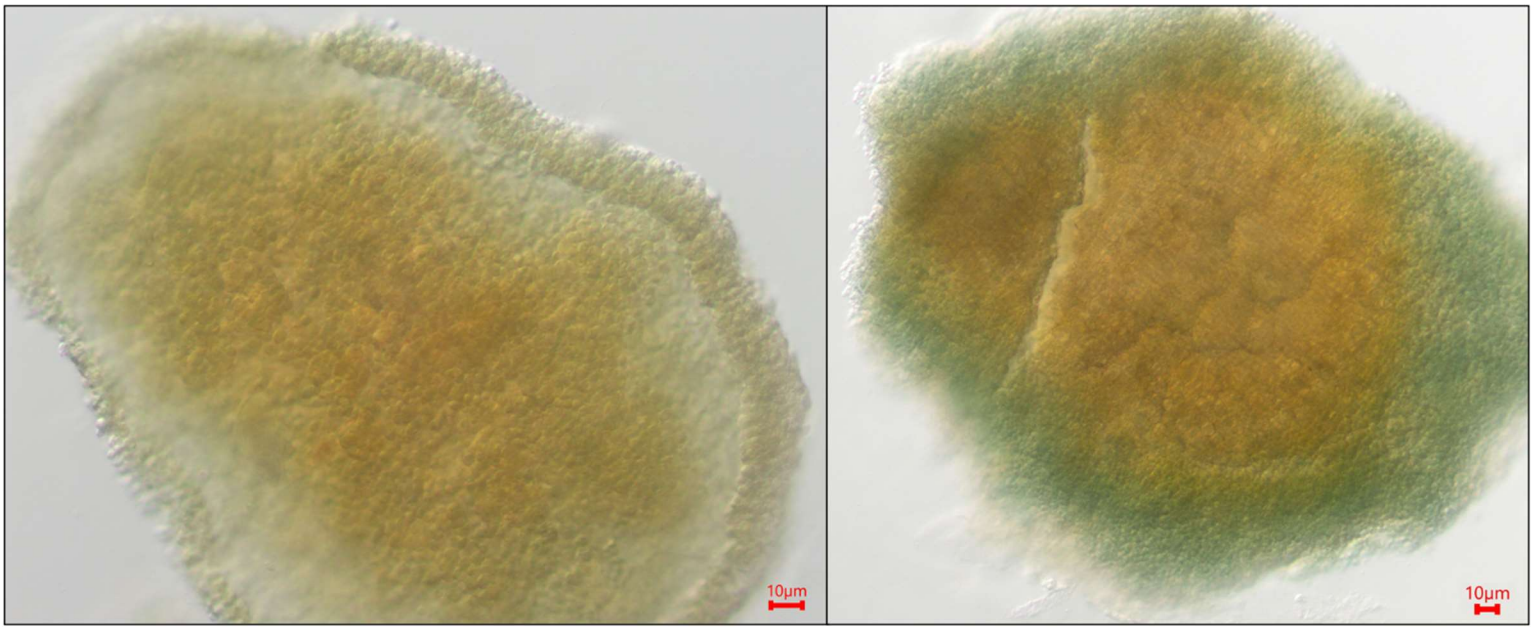

Figure 12. 16S rRNA phylogenetic tree containing strains GTM1, GTM2, GTM3, GTM4, and GTM7. Maximum likelihood (ML) tree based on aligned partial 16S rRNA gene sequences. Bold font indicates strains isolated and sequenced in this study. ML branch support values <50 not shown. Support values >0.9 from Bayesian tree also shown for select branches. ML and Bayesian branch support values are shown in the following order Bayesian/ML.

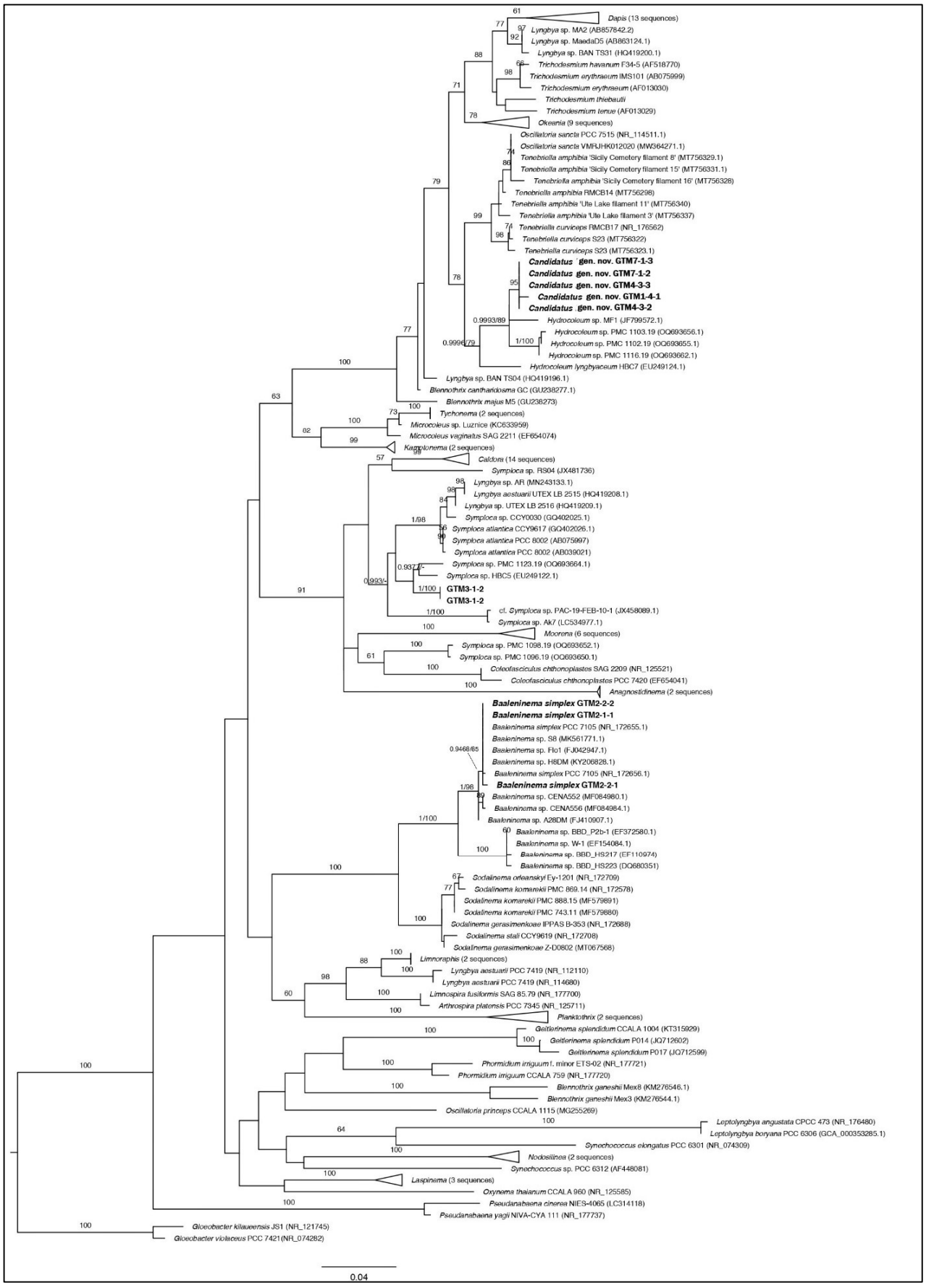

Figure 13. 16S rRNA phylogenetic tree containing strains GTM5 and GTM6.
Maximum likelihood (ML) tree based on aligned partial 16S rRNA gene sequences. Bold font indicates strains isolated and sequenced in this study. ML branch support values <50 not shown. Support values >0.9 from Bayesian tree also shown for select branches. ML and Bayesian branch support values are shown in the following order Bayesian/ML.

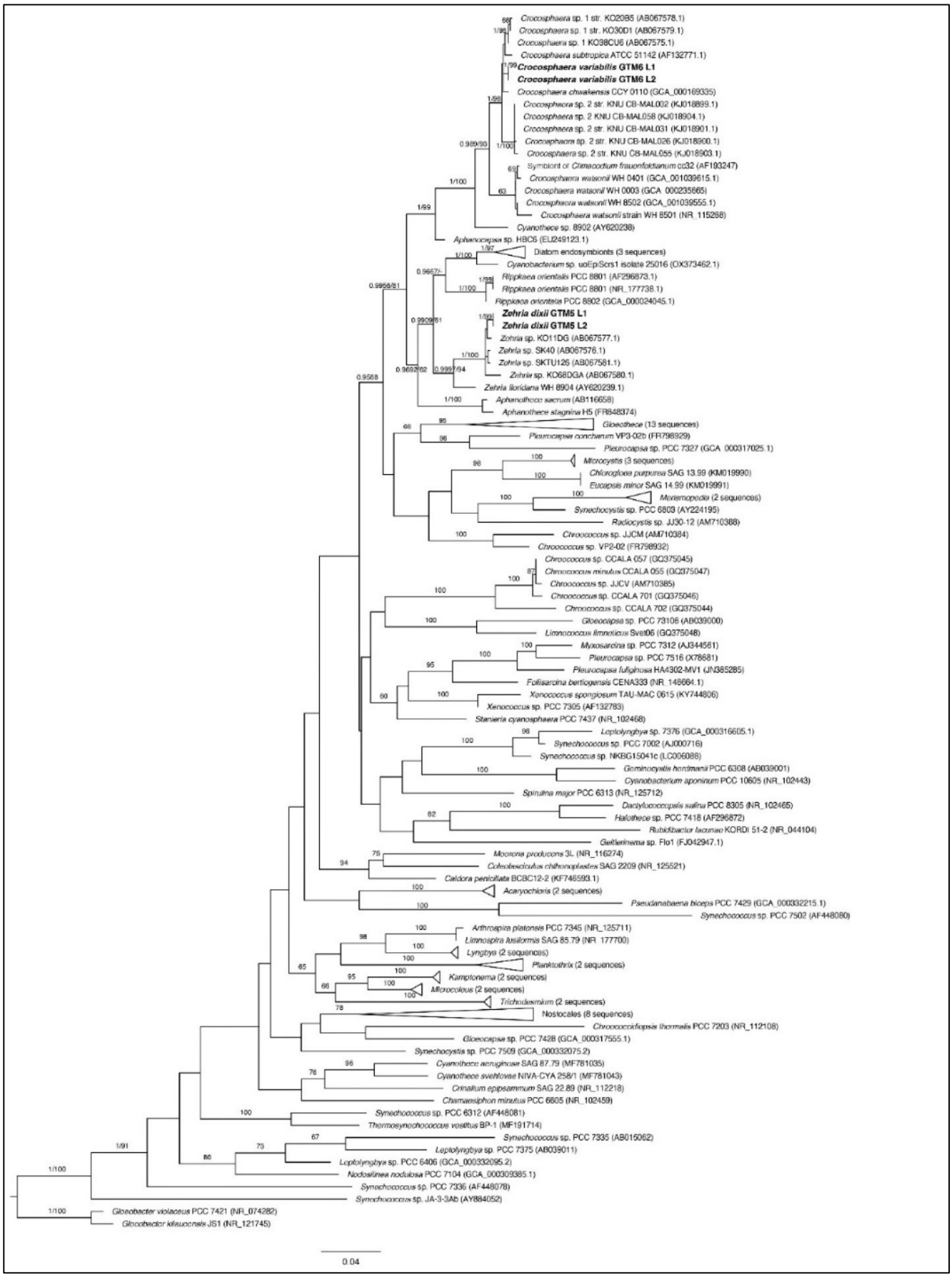

Figure 14. 16S rRNA phylogenetic tree containing strains GTM12 and GTM13.
Maximum likelihood (ML) tree based on aligned partial 16S rRNA gene sequences. Bold font indicates strains isolated and sequenced in this study. ML branch support values <50 not shown. Support values >0.9 from Bayesian tree also shown for select branches. ML and Bayesian branch support values are shown in the following order Bayesian/ML.

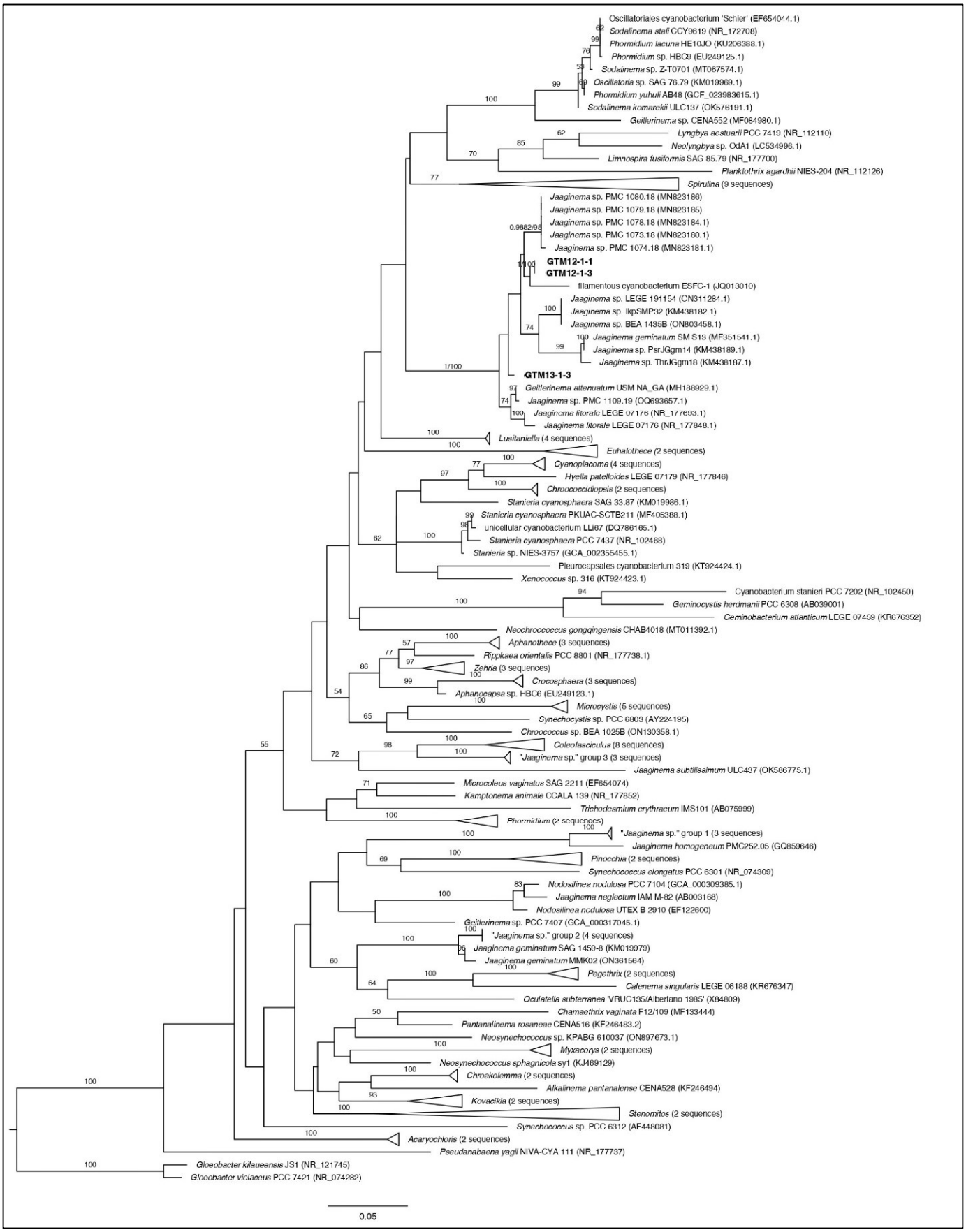

Figure 15. 16S rRNA phylogenetic tree containing strains GTM10, GTM14, GTM15, GTM19, GTM20, GTM21, and GTM22.

Maximum likelihood (ML) tree based on aligned partial 16S rRNA gene sequences. Bold font indicates strains isolated and sequenced in this study. ML branch support values <50 not shown. Support values >0.9 from Bayesian tree also shown for select branches. ML and Bayesian branch support values are shown in the following order Bayesian/ML.

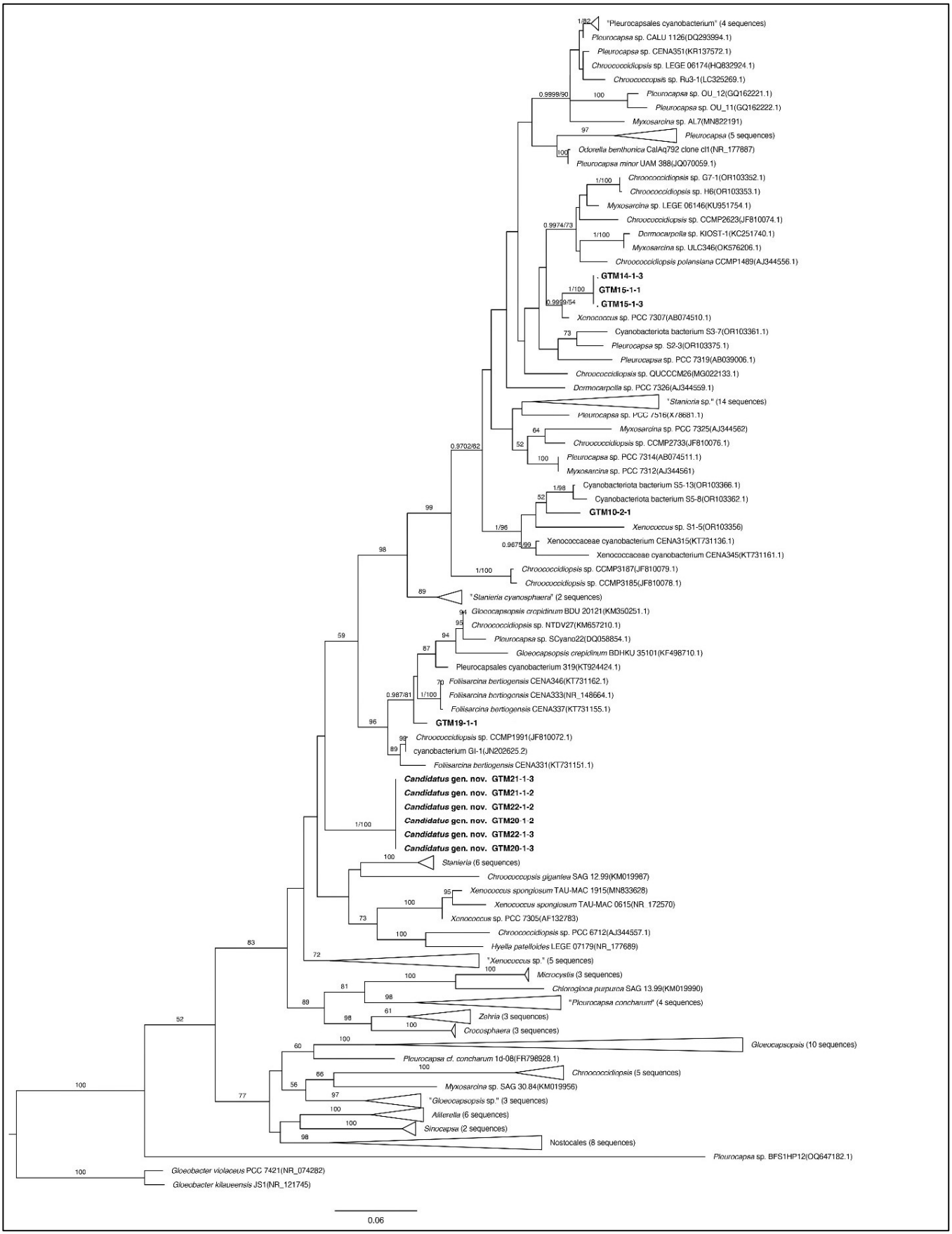

Figure 16. Predicted RNA structures for ITS region D1-D1` for strain GTM2 and closely related strains

Predicted RNA secondary structures for the D1-D1` region of the 16S-23S ITS region for strain GTM2 and closely related strains Flo1, PCC 7105, CENA 552, and CENA 556. Nucleotide sequences for the D1-D1` region were identical for strains GTM2, Flo1, and PCC 7105 (left), and were identical for strains CENA 552 and CENA 556 (right).

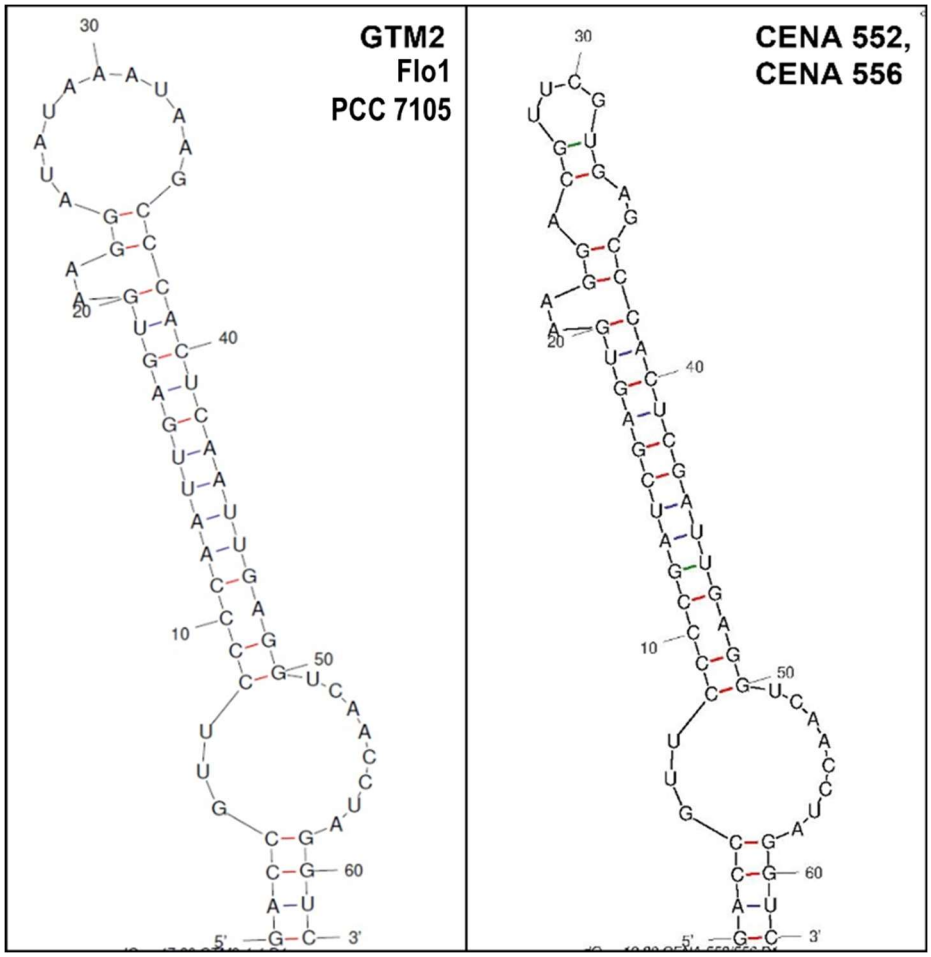

Figure 17. Predicted RNA structures for ITS region BoxB for strain GTM2 and closely related strains

Predicted RNA secondary structures for the BoxB region of the 16S-23S ITS region for strain GTM2 and closely related strains Flo1, PCC 7105, CENA 552, and CENA 556. Nucleotide sequences for the BoxB region were identical for all five strains.

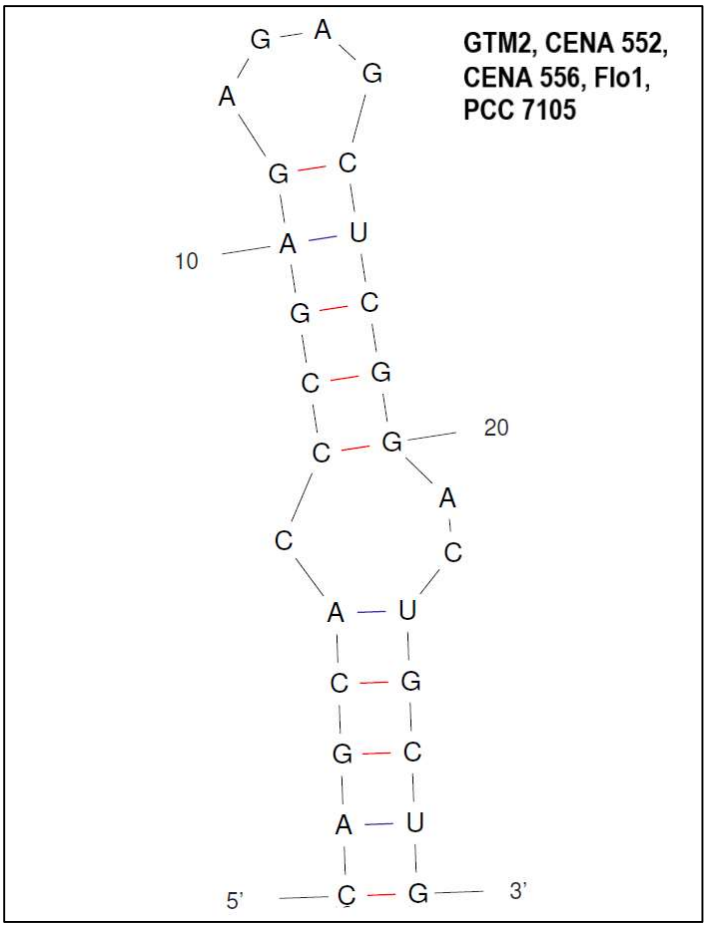

Figure 18. Predicted RNA structures for ITS region D1-D1` for strain GTM5 and closely related strains

Predicted RNA secondary structures for the D1-D1` region of the 16S-23S ITS region for strain GTM5 and closely related strains SKTU126, SK40, KO11DG, and KO68DGA.

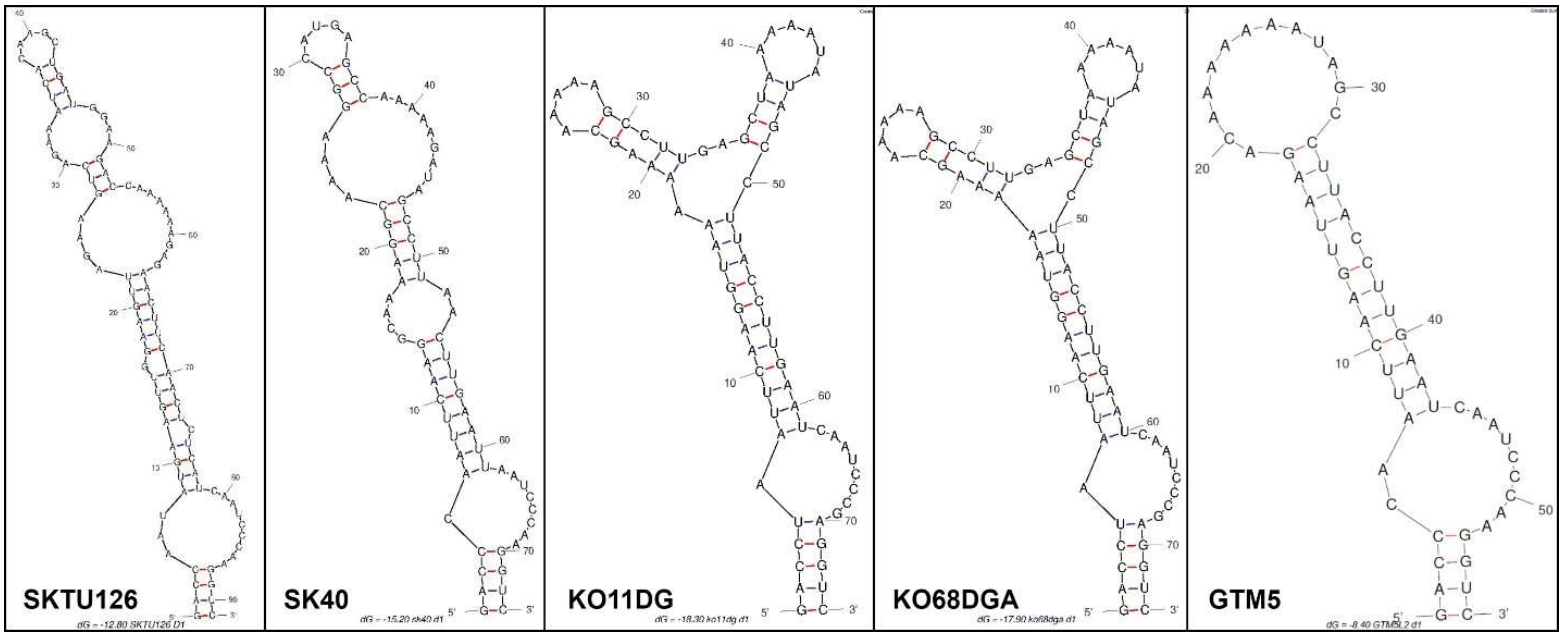

Figure 19. Predicted RNA structures for ITS region BoxB for strain GTM5 and closely related strains

Predicted RNA secondary structures for the BoxB region of the 16S-23S ITS region for strain GTM5 and closely related strains SKTU126, SK40, KO11DG, and KO68DGA. Nucleotide sequences for the BoxB region were identical for strains SKTU126 and SK40 (left) and for strains KO11DG and KO68DGA (middle).

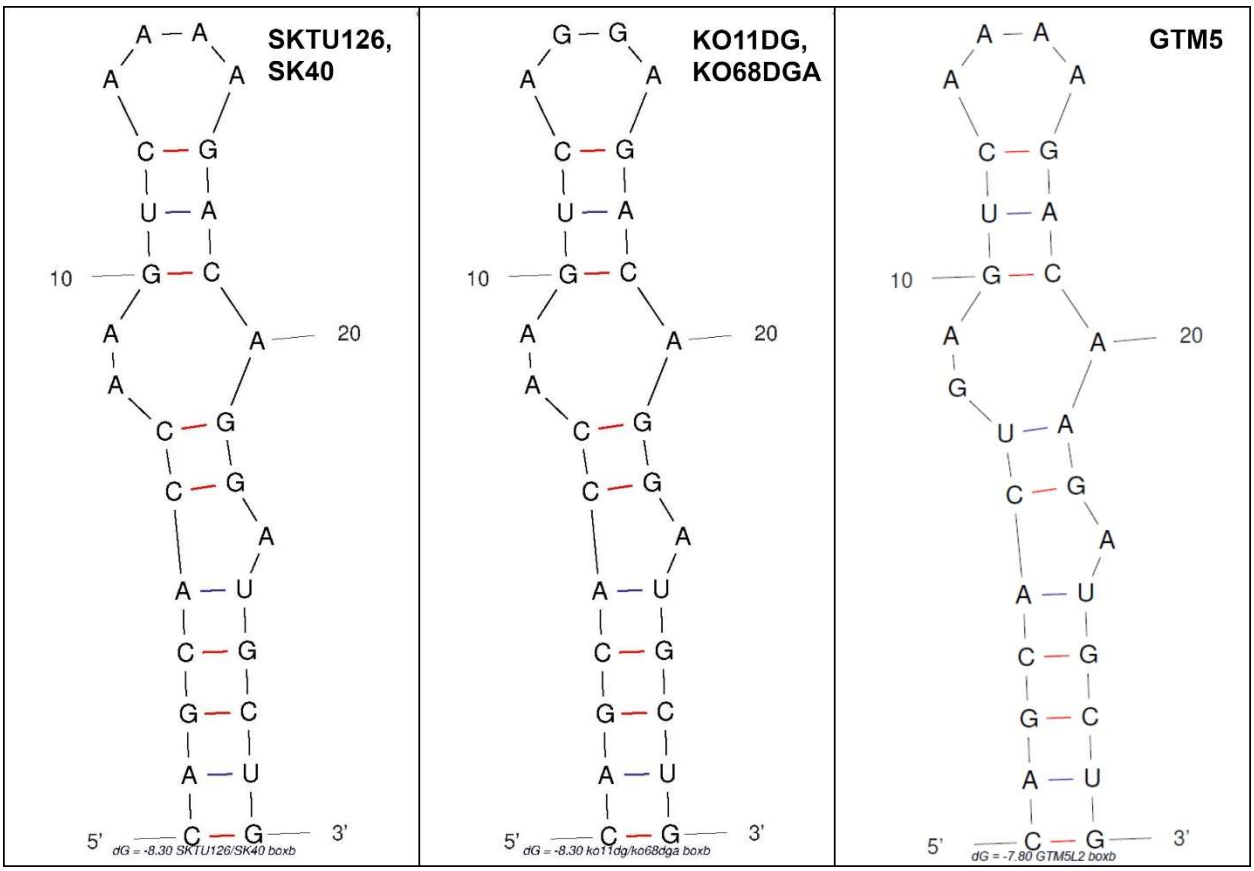

Figure 20. Predicted RNA structures for ITS region D1-D1` for strain GTM6 and closely related strains
Predicted RNA secondary structures for the D1-D1` region of the 16S-23S ITS region for strain GTM6 and closely related strains WH 8502, WH 0401, WH 0003, WH 8501, ATCC 51142, KO20B5, KO30D1, KO38CU6, and CCY 0110. Nucleotide sequences for the D1-D1` region were identical for strains WH 8502, WH 0401, and WH 0003 (top middle), and for strains KO20B5, KO30D1, and KO38CU6 (bottom middle).

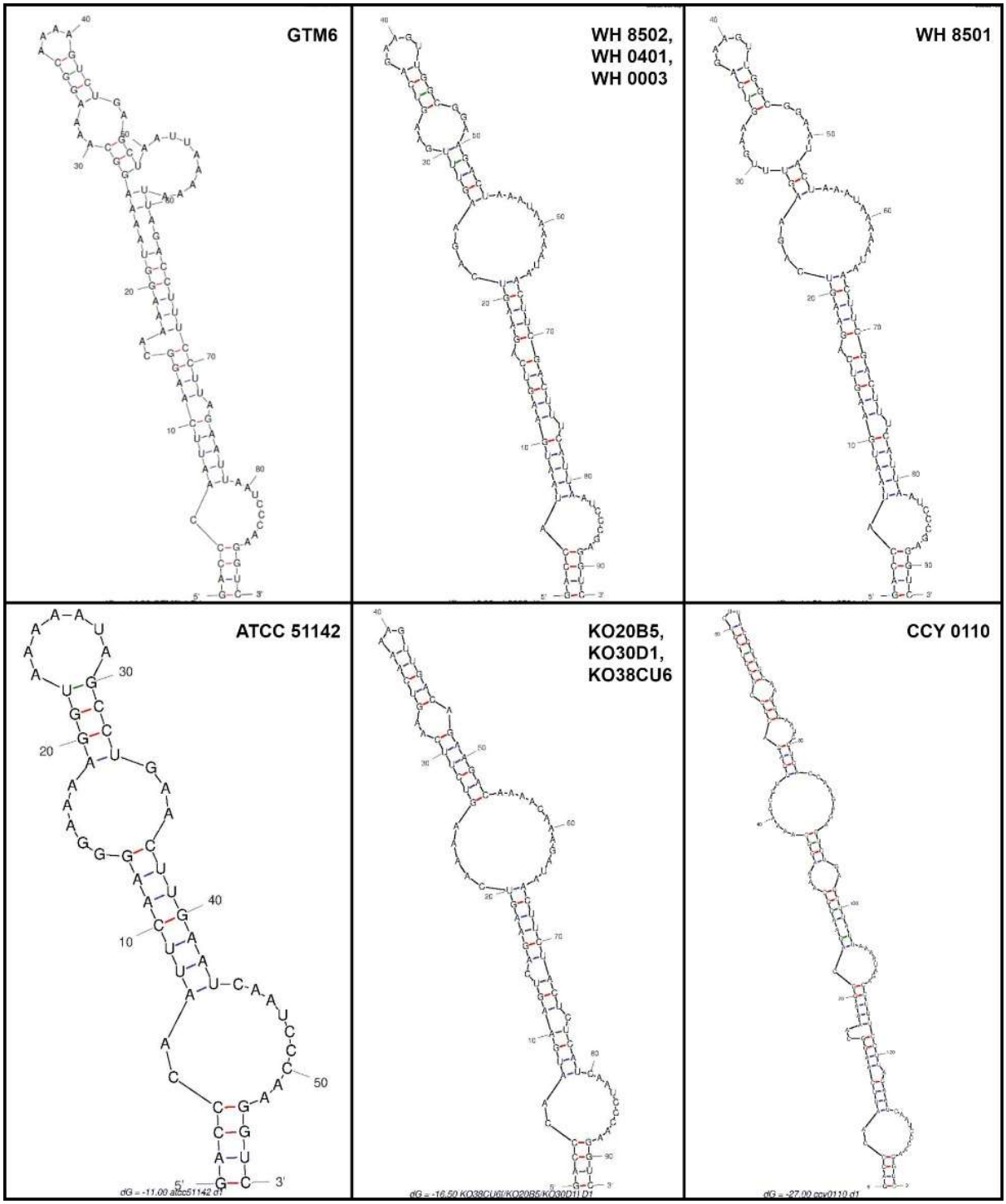

Figure 21. Predicted RNA structures for ITS region BoxB for strain GTM6 and closely related strains

Predicted RNA secondary structures for the BoxB region of the 16S-23S ITS region for strain GTM6 and closely related strains WH 8502, WH 0401, WH 0003, WH 8501, ATCC 51142, KO20B5, KO30D1, KO38CU6, and CCY 0110. Nucleotide sequences for the BoxB region were identical for strains WH 8502, WH 0401, WH 8501, and WH 0003 (second from left), and for strains KO20B5, KO30D1, and KO38CU6 (second from right).

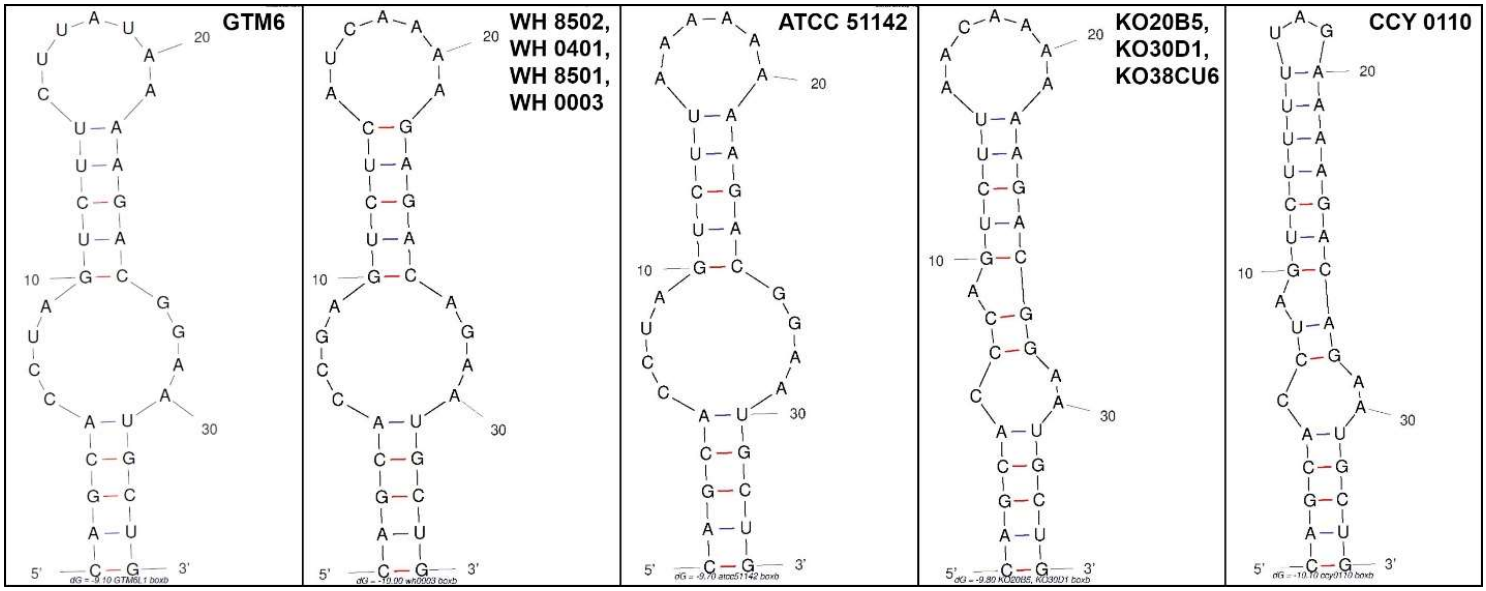

TABLES

Table 1. Summary of morphological characteristics of filamentous cyanobacterial isolates

Morphotype	Strain ID	Growth habit	Cell size (µm)	Apical cells	Constrictions at crosswalls	Sheath	Cell color	Necridia	Motility
1	GTM1	Filaments in fascicle-like colonies	14.2-18.1 wide by 2.5-4.5 long	Widely rounded, sometimes narrowed; sometimes with thickened outer wall; occasionally calyptrate	Absent	Present; sometimes layered	Yellow-brown to greyish-green	+	Immotile or with very slow to nearly imperceptible gliding/creeping
	GTM4		14.7-18.0 wide by 2.3-5.3 long						
	GTM7		13.3-18.7 wide by 2.3-4.4 long						
2	GTM2	Solitary filaments, loosely aggregated in culture	1.7-2.0 wide by 2.5-4.8 long	Rounded	Mostly absent; sometimes slightly constricted	Present; very thin	Blue-green	-	Gliding, sometimes waving/bending
3	GTM3	Loosely entangled filaments, sometimes in ± thin, fascicle-like bundles	4.3-5.9 wide by 2.1-6.7 long	Rounded or narrowed and conical-rounded; last 1-3 cells in a trichome often yellowish-brown	Sporadically with constrictions at crosswalls	Present; thin	Mostly blue-green, sometimes olive-green	+	Immotile or with nearly imperceptible gliding/creeping
4	GTM12	Filaments loosely and irregularly aggregated, or in fascicle-like bundles.	1.7-2.8 wide by 3.3-6.3 long	Rounded or narrowed and bluntly pointed; sometimes narrowed and slightly bent	Slightly to distinctly constricted	Present; very thin	Pale blue-green to greyish olive-green	-	Occasional bending/waving
	GTM13		2.2-2.8 wide by 2.7-5.9 long	Rounded, or narrowed and bluntly pointed, or narrowed and distinctly bent			Pale blue-green; vibrant blue-green in young cultures		Bending/waving; possibly also with very slow creeping/gliding

Table 2. Summary of morphological characteristics of coccoid cyanobacterial isolates

Morphotype	Strain ID	Growth habit	Cell shape	Cell size (µm)	Mucilage	Cell color	Cell division
5	GTM5	Cells aggregated in mostly amorphous colonies.	± spherical to oval or widely cylindrical with rounded ends	1.9-3.5 wide by 2.7-4.7 long	Colonial mucilage present, usually visible only with staining.	Blue-green	Binary fission in a single plane, transverse to long axis of the cell.
6	GTM6	Mostly in aggregations of cells or 2-8-celled groups; highly variable.	Mostly oval to rounded-cylindrical, sometimes subspherical; highly variable.	2.7-4.1 wide by 3.6-5.2 long; sometimes up to 7.7 long.	Usually with delimited mucilage around cells or small groups of cells; colorless or yellowish-brown. Variable.	Mostly blue-green, usually vividly so.	Cell division in multiple planes, regular or irregular.
7	GTM10	Colonial, with complex and variable colony morphology. Often forming ± dome-shaped colonies of densely aggregated cells.	Mostly spherical	(2.4-)3.0-6.7(-9) in diameter	Cells with firm, colorless mucilaginous sheaths	Pale blue-green, greyish olive-green, or reddish-brown.	Produces baeocytes; usually ± few in number.
8	GTM14	Colonial, with complex and variable colony morphology. Often in irregularly dome-shaped masses of densely aggregated cells.	Spherical	Variable, up to 14.8 in diameter	Cells with firm, thin, colorless mucilaginous envelopes.	Greyish blue-green, brownish, or purplish in young cultures; later pale yellowish-brown.	Baeocytes frequently produced.
	GTM15			Variable, up to 16.2 in diameter			
9	GTM19	Colonial, with complex colony morphology. Cells in colonies in radially or fan-like arranged rows.	Cells in colonies ± hemispherical or in the form of a segment of a sphere, rounded-polygonal, or nearly rectangular in outline.	2.2-5.1 wide by 3.4-6.7 long	Firm, thin, colorless mucilaginous envelopes surrounding colonies and individual cells within colonies.	Greyish yellow-brown to orange-brown; sometimes blue-green in parts of colonies.	Cell division in multiple planes; baeocyte formation not observed, but may occur.
10	GTM20	Colonial, with complex colony morphology. Cells in colonies in radially or fan-like arranged rows.	Usually hemispherical or in the form of a segment of a sphere, or rounded-polygonal to nearly rectangular in outline; occasionally spherical.	3.1-7.7 wide by 3.8-10.1 long	Cells with ± thin and delimited mucilaginous envelopes; sometimes with visible colonial mucilage.	Blue-green	Cell division in multiple planes; baeocyte formation not observed, but may occur.
	GTM21			3.8-7.6 wide by 5.0-7.9 long			
	GTM22			3.4-6.6 wide by 3.8-7.9 long			

Table 3. Taxonomic classifications of isolated strains

		Taxonomic Classification[1]				
Strain ID	**Isolation source (sample name)**	**Order**	**Family**	**Genus**	**Species**	**Provisional Classification**
GTM6	Guana Dam South 3	Chroococcales	Microcystaceae	*Crocosphaera*	*C. variabilis*, sp. nov.	
GTM5	Shell Bluff 3	Chroococcales	Microcystaceae	*Zehria*	*Z. dixii*, sp. nov.	
GTM19	Guana Dam South 3	Chroococcales	Pleurocapsaceae	*Foliisarcina*		*Foliisarcina* sp.
GTM20	Guana Dam South 1	Chroococcales	Pleurocapsaceae			Pleurocapsaceae cyanobacterium[2] (sp. 1)
GTM21	Guana Dam South 1	Chroococcales	Pleurocapsaceae			Pleurocapsaceae cyanobacterium[2] (sp. 1)
GTM22	Guana Dam South 1	Chroococcales	Pleurocapsaceae			Pleurocapsaceae cyanobacterium[2] (sp. 1)
GTM10	Guana Dam South 3	Chroococcales	Pleurocapsaceae			Pleurocapsaceae cyanobacterium (sp. 2)
GTM14	Guana Dam South 3	Chroococcales	Pleurocapsaceae			Pleurocapsaceae cyanobacterium (sp. 3)
GTM15	Guana Dam South 3	Chroococcales	Pleurocapsaceae			Pleurocapsaceae cyanobacterium (sp. 3)
GTM3	Guana Dam South 5	Coleofasciculales	Coleofasciculaceae	cf. *Symploca*		cf. *Symploca* sp.
GTM1	WETFEET Middle 6	Oscillatoriales	Microcoleaceae			Microcoleaceae cyanobacterium[3] (sp. 1)
GTM4	WETFEET Middle 3	Oscillatoriales	Microcoleaceae			Microcoleaceae cyanobacterium[3] (sp. 1)
GTM7	WETFEET Middle 1	Oscillatoriales	Microcoleaceae			Microcoleaceae cyanobacterium[3] (sp. 1)
GTM2	WETFEET Middle 4	Oscillatoriales	Oscillatoriaceae	*Baaleninema*	*B. simplex*	
GTM12	WETFEET Middle 5					Filamentous cyanobacterium (sp. 1)
GTM13	Guana Dam South 2					Filamentous cyanobacterium (sp. 2)

[1]Family and Order level classification of genera according to Strunecký et al. (2023)

[2]Strains GTM20, GTM21, and GTM22 are suspected to represent a novel genus and species within Pleurocapsaceae; genus and species to be described in a future work.

[3]Strains GTM1, GTM4, and GTM7 are suspected to represent a novel genus and species within Microcoleaceae; genus and species to be described in a future work.

Table 4. Closest GenBank sequence matches to 16S rRNA sequences obtained from isolated strains

	Closest BLAST match			
Strain	**Scientific Name**	**Query Coverage**	**Percent Identity**	**Accession**
GTM1	*Hydrocoleum* sp. PMC 1116.19	100%	98.54%	OQ693662.1
GTM2	*Baaleninema simplex*	97%	100.00%	NR_172655.1
GTM3	*Symploca* sp. HBC5	100%	98.33%	EU249122.1
GTM4	*Hydrocoleum* sp. PMC 1116.19	94%	98.69%	OQ693662.1
GTM5	*Zehria* sp. SK40	100%	99.43%	AB067576.1
GTM6	*Crocosphaera* sp. 1 str. KO38CU6	100%	99.43%	AB067575.1
GTM7	*Hydrocoleum* sp. PMC 1116.19	99%	98.82%	OQ693662.1
GTM10	Cyanobacteriota bacterium S5-8	95%	98.58%	OR103362.2
GTM12	*Jaaginema* sp. PMC 1073.18	93%	99.05%	MN823180.1
GTM13	*Jaaginema* sp. PMC 1073.18	89%	98.66%	MN823180.1
GTM14	*Xenococcus* sp. PCC 7307	96%	98.23%	AB074510.1
GTM15	*Xenococcus* sp. PCC 7307	99%	98.22%	AB074510.1
GTM19	*Foliisarcina bertiogensis*	98%	98.41%	NR_148664.1
GTM20	Pleurocapsales cyanobacterium 319	97%	95.61%	KT924424.1
GTM21	Pleurocapsales cyanobacterium 319	99%	95.61%	KT924424.1
GTM22	Pleurocapsales cyanobacterium 319	99%	95.61%	KT924424.1

SUPPLEMENTARY FIGURES

Figure S1. Predicted RNA structures for ITS regions D1-D1` and BoxB for strains GTM1, GTM4, and GTM7

Predicted RNA secondary structures for the D1-D1` (left) and BoxB (right) regions of the 16S-23S ITS region for strains GTM1, GTM4, and GTM7. Nucleotide sequences for both regions were identical for all three strains.

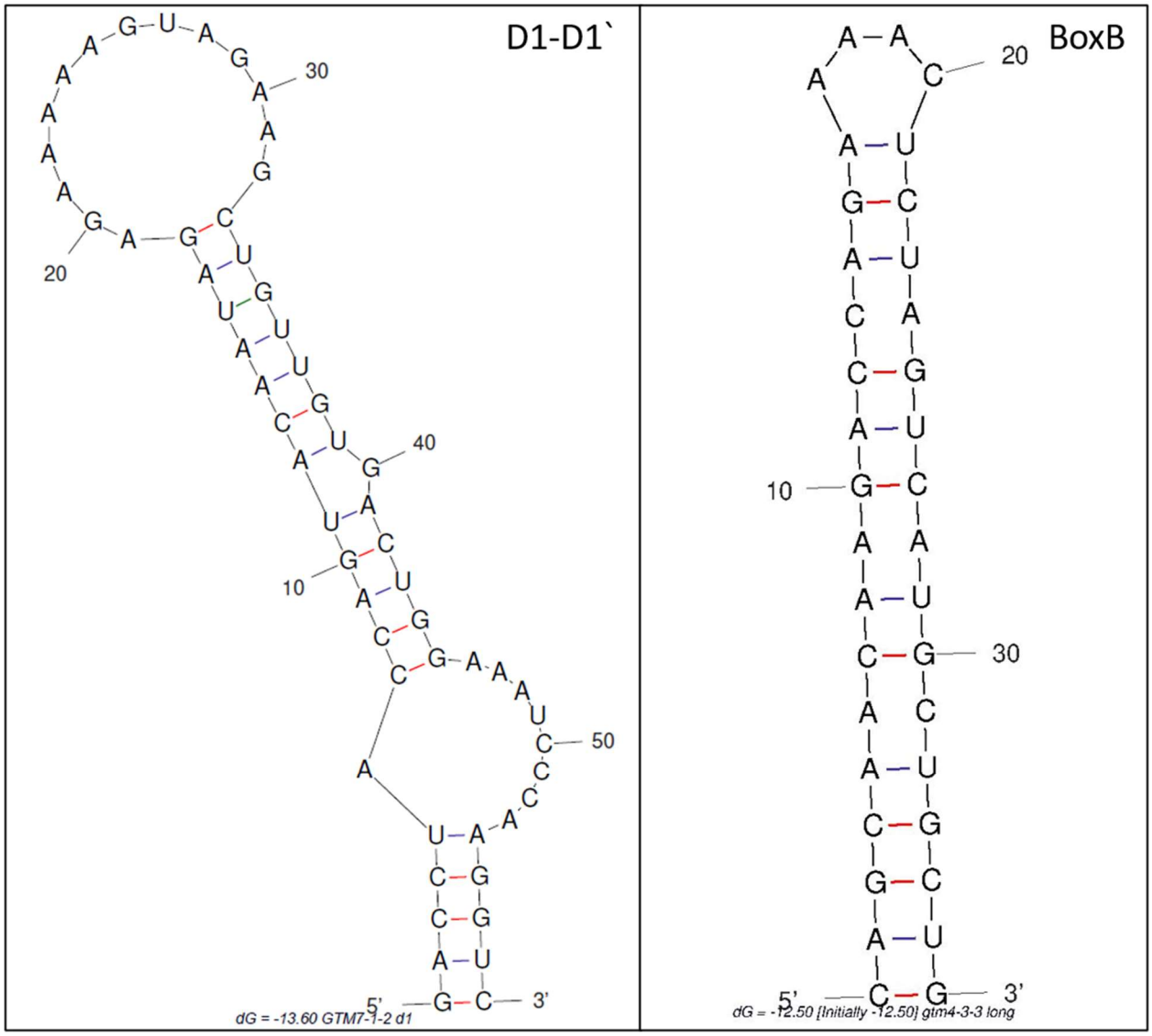

Figure S2. Predicted RNA structures for ITS regions D1-D1` and BoxB for strain GTM3
Predicted RNA secondary structures for the D1-D1` (left) and BoxB (right) regions of the 16S-23S ITS region for strains GTM3.

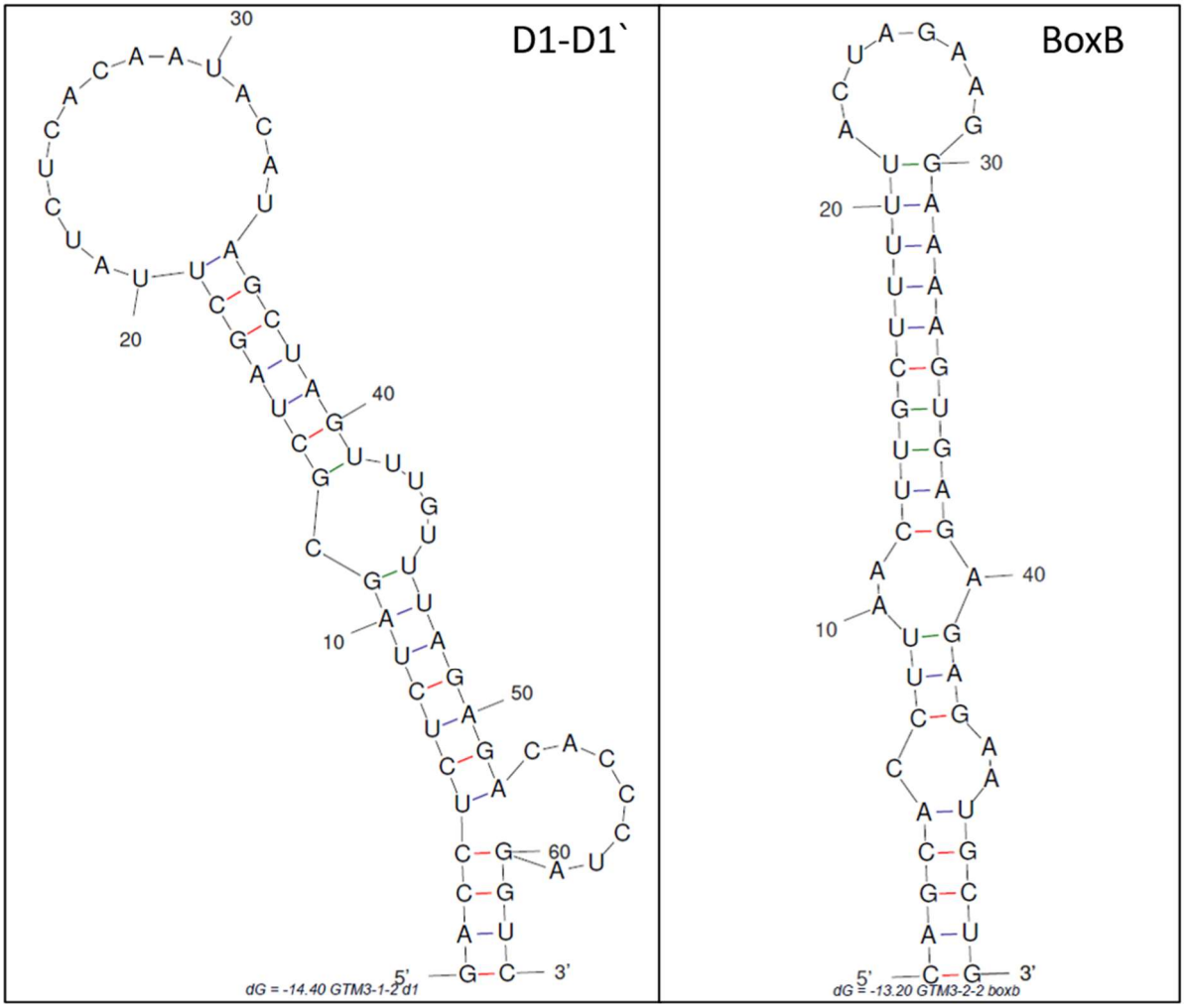

Figure S3. Predicted RNA structures for ITS regions D1-D1` and BoxB for strains GTM12 and GTM13
Predicted RNA secondary structures for the D1-D1` (left) and BoxB (right) regions of the 16S-23S ITS region for strains GTM12 (top) and GTM13 (bottom).

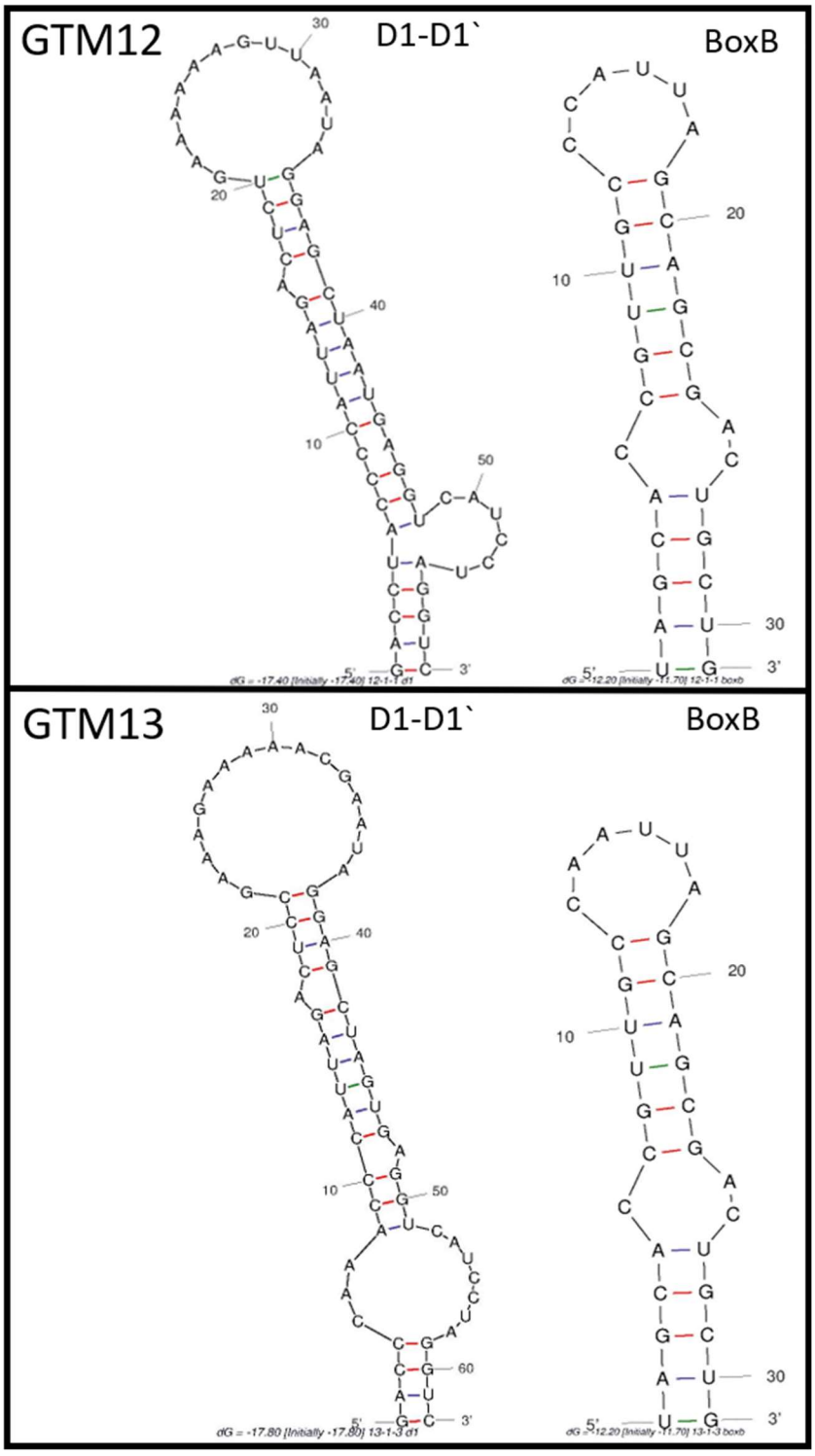

Figure S4. Predicted RNA structures for ITS regions D1-D1` and BoxB for strain GTM19
Predicted RNA secondary structures for the D1-D1` (left) and BoxB (right) regions of the 16S-23S ITS region for strains GTM19.

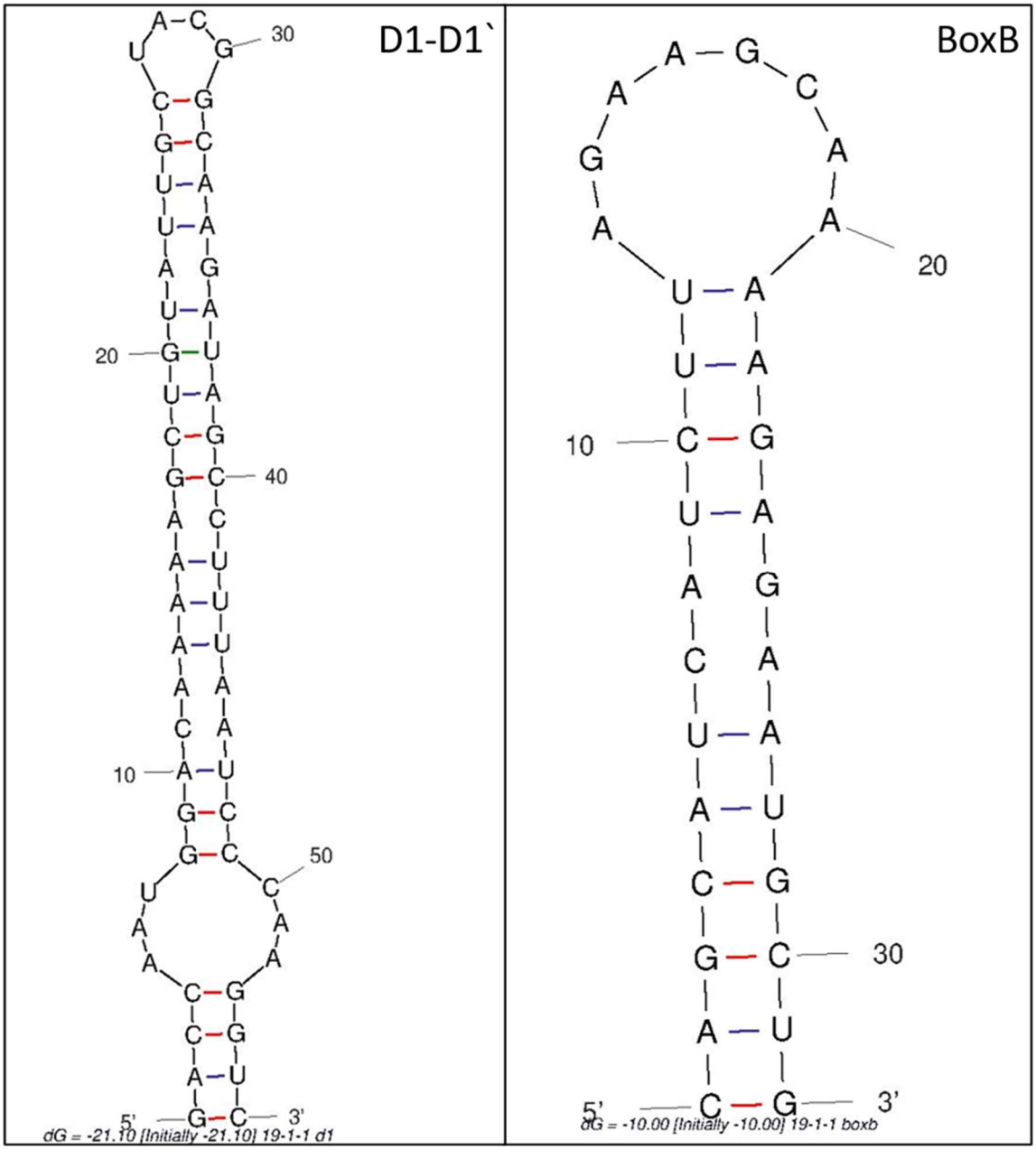

Figure S5. Predicted RNA structures for ITS regions D1-D1` and BoxB for strains GTM20, GTM21, and GTM22

Predicted RNA secondary structures for the D1-D1` (left) and BoxB (right) regions of the 16S-23S ITS region for strains GTM20, GTM21, and GTM22. Nucleotide sequences for both regions were identical for all three strains.

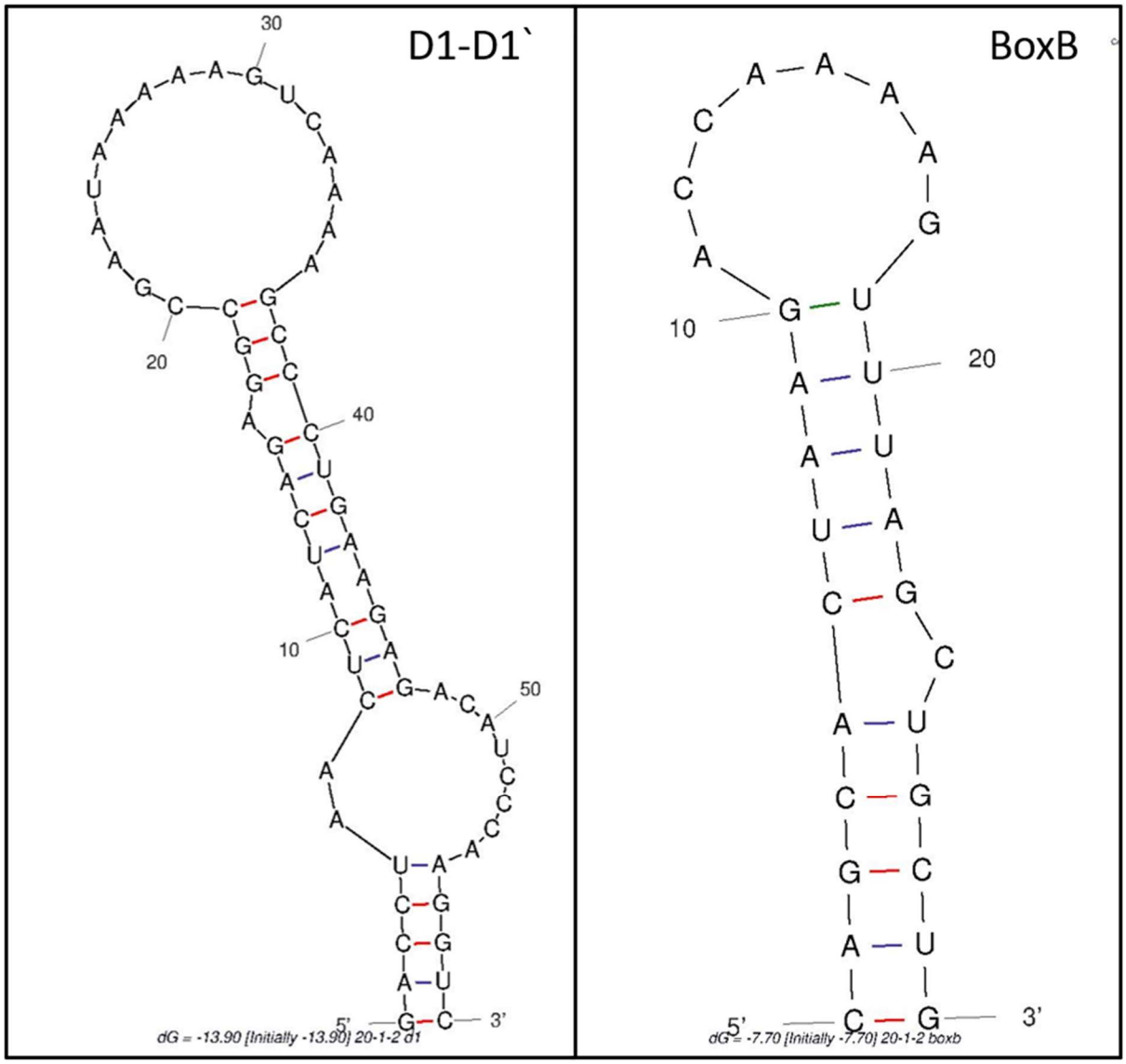

Figure S6. Predicted RNA structures for ITS regions D1-D1` and BoxB for strains GTM14 and GTM15

Predicted RNA secondary structures for the D1-D1` (left) and BoxB (right) regions of the 16S-23S ITS region for strains GTM14 and GTM15. Nucleotide sequences for both regions were identical for both strains.

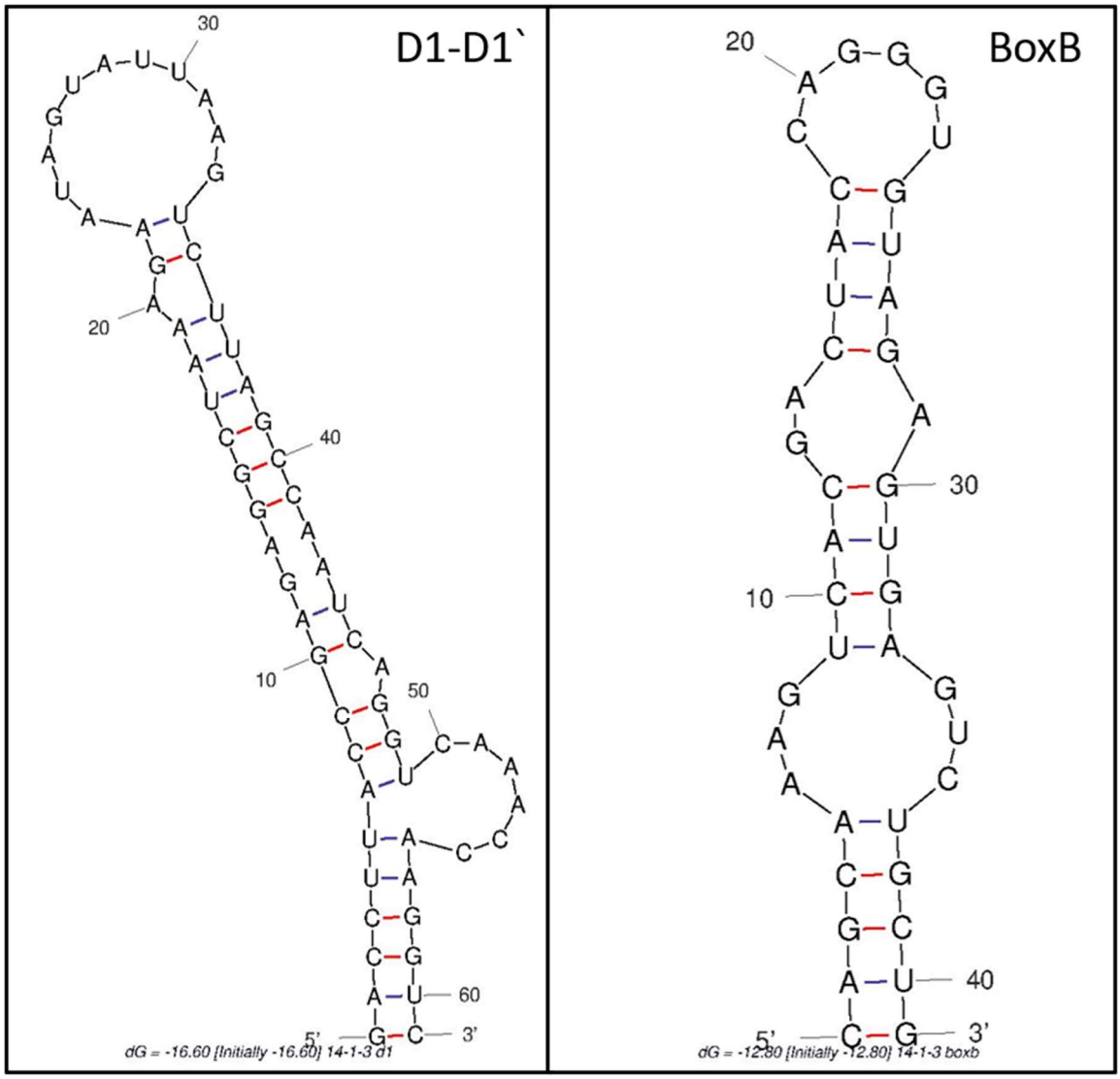

Figure S7. Predicted RNA structures for ITS regions D1-D1` and BoxB for strain GTM10
Predicted RNA secondary structures for the D1-D1` (left) and BoxB (right) regions of the 16S-23S ITS region for strains GTM10.

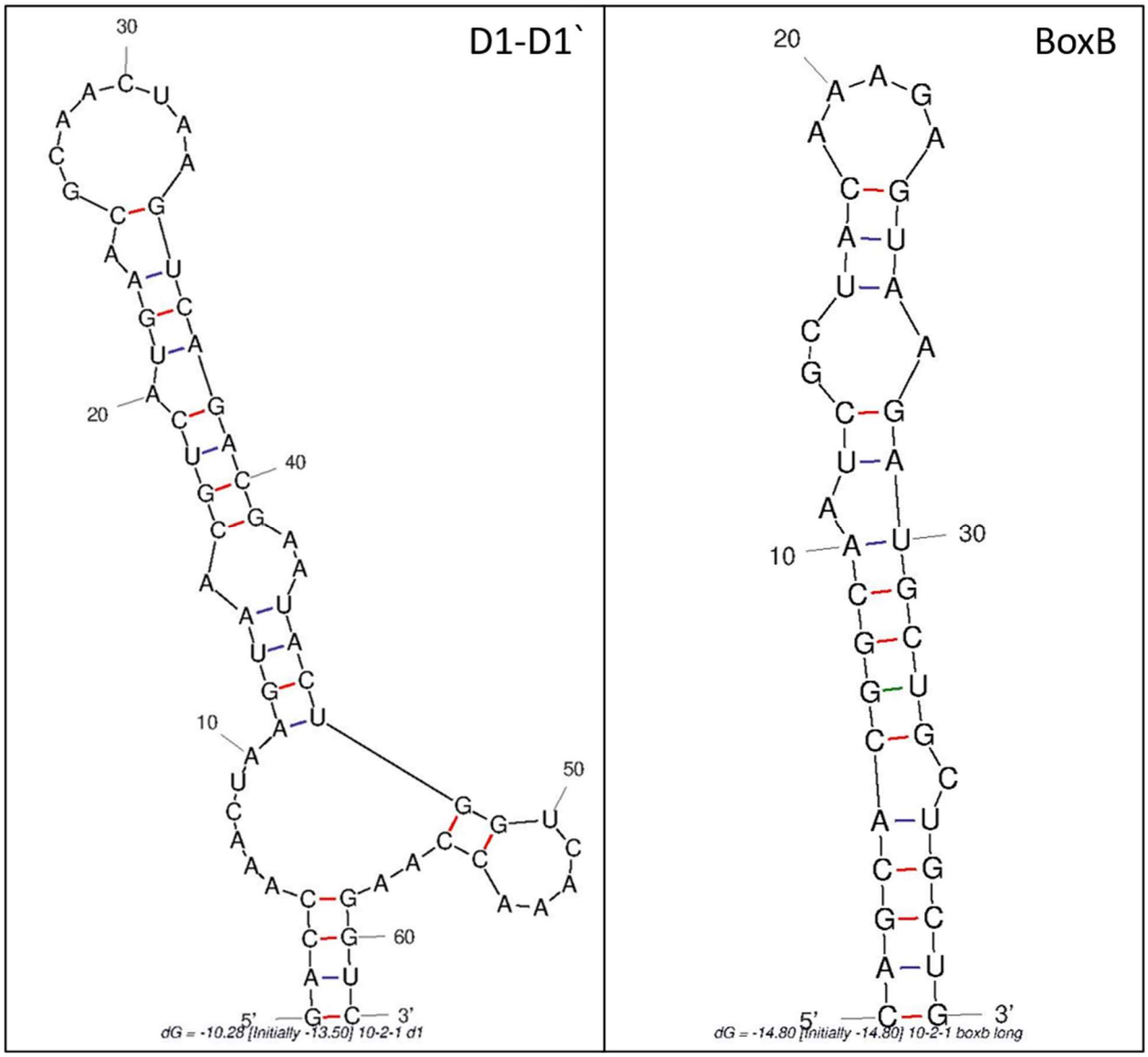

SUPPLEMENTARY TABLES

Table S1. List of sample collection site names, coordinates, and cyanobacterial strains isolated from each sample

Sampling Site	Coordinates	Sample ID	Isolated Strains
Guana Dam South	30.02274° N, 81.32784° W	Guana Dam South 1	GTM20, GTM21, GTM22
		Guana Dam South 2	GTM13
		Guana Dam South 3	GTM6, GTM10, GTM14, GTM15, GTM19
		Guana Dam South 4	
		Guana Dam South 5	GTM3
		Guana Dam South 6	
Shell Bluff	30.01223° N, 81.34519° W	Shell Bluff 1	
		Shell Bluff 2	
		Shell Bluff 3	GTM5
		Shell Bluff 4	
		Shell Bluff 5	
		Shell Bluff 6	
WETFEET Middle	29.83634° N, 81.29553° W	WETFEET Middle 1	GTM7
		WETFEET Middle 2	
		WETFEET Middle 3	GTM4
		WETFEET Middle 4	GTM2
		WETFEET Middle 5	GTM12
		WETFEET Middle 6	GTM1

Table S2. 16s rRNA gene sequence similarity matrix for strain GTM2

16s rRNA gene sequence similarity matrix for *Baaleninema simplex* strain GTM2 and other *Baaleninema* strains, with *Sodalinema komarekii* as outgroup taxon. Strains isolated in this study are bolded.

	1	2	3	4	5	6	7	8	9	10	11	12
1. *Baaleninema simplex* GTM2-1-1												
2. *Baaleninema simplex* PCC 7105^{T} (NR_172656.1)	100.0											
3. "*Geitlerinema* sp."[1] A28DM (FJ410907.1)	99.9	99.9										
4. "*Geitlerinema* sp."[1] BBD HS217 (EF110974.1)	98.9	98.8	98.9									
5. "*Geitlerinema* sp."[1] BBD HS223 (DQ680351.1)	98.9	98.8	98.9	99.9								
6. "*Geitlerinema* sp."[1] BBD P2b-1 (EF372580.1)	98.9	98.9	99.0	99.9	99.9							
7. "*Geitlerinema* sp."[1] CENA552 (MF084980.1)	99.9	99.8	99.9	98.9	98.9	98.9						
8. "*Geitlerinema* sp."[1] CENA556 (MF084984.1)	99.8	99.8	99.9	98.9	98.8	98.9	100.0					
9. "*Geitlerinema* sp."[1] Flo1 (FJ042947.1)	100.0	100.0	99.9	98.9	98.9	98.9	99.9	99.8				
10. "*Geitlerinema* sp."[1] H8DM (KY206828.1)	100.0	100.0	99.9	98.9	98.9	99.0	99.9	99.8	100.0			
11. "*Geitlerinema* sp."[1] W-1 (EF154084.1)	99.0	98.9	99.0	99.9	99.9	100.0	99.0	98.9	98.9	99.0		
12. "*Oscillatoria* sp."[1] S8 (MK561771.1)	100.0	100.0	99.9	98.9	98.9	99.0	99.9	99.8	100.0	100.0	99.0	
13. *Sodalinema komarekii* PMC 869.14^{T} (NR_172578.1)	97.9	97.8	97.9	97.4	97.4	97.5	97.8	97.7	97.8	97.8	97.5	97.8

^{T} denotes type species for a given genus

[1]"*Geitlerinema* sp." and "*Oscillatoria* sp." strains are suspected to belong to the genus *Baaleninema*, but have yet to be formally designated as such.

Table S3. 16s rRNA gene sequence similarity matrix for strain GTM5

16s rRNA gene sequence similarity matrix for *Zehria dixii,* sp. nov., strain GTM5 and other *Zehria* strains, with *Rippkaea orientalis* as outgroup taxon. Strains isolated in this study are bolded.

	1	2	3	4	5	6	7
1. *Zehria dixii*, sp. nov., GTM5-L2							
2. *Zehria floridana* WH 8904^{T} (AY620239.1)	97.5						
3. *Zehria* sp. SKTU126 (AB067581.1)	99.3	97.6					
4. *Zehria* sp. SK40 (AB067576.1)	99.4	97.6	99.7				
5. *Zehria* sp. KO11DG (AB067577.1)	99.4	97.7	99.6	99.4			
6. *Zehria* sp. KO68DGA (AB067580.1)	98.9	97.3	99.1	99.1	99.3		
7. *Rippkaea orientalis* PCC 8801^{T} (NR_177738.1)	95.7	96.0	95.8	96.0	95.5	95.3	
^{T} denotes type species for a given genus							

Table S4. 16s rRNA gene sequence similarity matrix for strain GTM6

16s rRNA gene sequence similarity matrix for *Crocosphaera variabilis,* sp. nov., strain GTM6 and other *Crocosphaera* strains, with *Zehria floridana* as outgroup taxon. Strains isolated in this study are bolded.

	1	2	3	4	5	6	7	8	9	10	11	12	13	14	15	16	17
1. Crocosphaera variabilis, sp. nov., GTM6-L2																	
2. *Zehria floridana* WH 8904[T] (AY620239.1)	94.1																
3. *Crocosphaera watsonii* WH 8501[T] (NR_115288.1)	97.2	94.7															
4. *Crocosphaera watsonii* WH 0003 (GCA_000235665)	98.1	94.5	99.2														
5. *Crocosphaera watsonii* WH 0401 (GCA_001039615.1)	97.9	94.3	99.0	99.8													
6. *Crocosphaera watsonii* WH 8502 (GCA_001039555.1)	98.1	94.4	99.3	99.9	99.7												
7. "*Cyanothece* sp."[1] WH 8902 (AY620238.1)	97.4	94.5	97.2	97.1	96.9	97.0											
8. "*Aphanocapsa* sp."[1] HBC6 (EU249123.1)	97.1	96.0	97.0	97.4	97.2	97.3	96.5										
9. *Crocosphaera chwakensis* CCY0110[R] (GCA_000169335)	99.6	94.1	97.2	98.1	97.9	98.1	97.6	97.2									
10. *Crocosphaera* sp. 1 KO38CU6[R] (AB067575.1)	99.5	94.3	97.2	98.1	97.8	98.0	97.3	97.1	99.5								
11. *Crocosphaera* sp. 1 KO20B5[R] (AB067578.1)	99.4	94.1	97.0	97.9	97.7	97.8	97.1	96.9	99.4	99.9							
12. *Crocosphaera* sp. 1 KO30D1 (AB067579.1)	99.4	94.2	97.1	98.0	97.8	97.9	97.2	97.0	99.4	99.9	99.9						
13. *Crocosphaera* sp. 2 MAL CB058[R] (KJ018904.1)	99.0	94.4	96.9	97.7	97.4	97.6	96.8	97.2	99.0	99.1	98.9	99.0					
14. *Crocosphaera* sp. 2 MAL CB002 (KJ018899.1)	98.6	94.2	96.9	97.2	97.0	97.1	96.8	96.7	98.6	98.6	98.5	98.6	99.6				
15. *Crocosphaera* sp. 2 MAL CB026 (KJ018900.1)	98.8	94.4	96.8	97.3	97.1	97.2	96.7	96.8	98.8	98.9	98.8	98.8	99.9	99.9			
16. *Crocosphaera* sp. 2 MAL CB031[R] (KJ018901.1)	99.0	94.6	96.9	97.6	97.4	97.6	96.8	97.2	99.0	99.1	98.9	99.0	100.0	100.0	99.9		
17. *Crocosphaera* sp. 2 MAL CB055 (KJ018903.1)	98.4	94.2	96.7	97.0	96.9	97.0	96.6	96.6	98.4	98.5	98.3	98.4	99.4	99.9	99.8	99.8	
18. *Crocosphaera subtropica* ATCC 51142[R] (AF132771.1)	99.3	93.9	97.2	98.0	97.8	97.9	97.1	96.9	99.3	99.6	99.4	99.5	99.1	98.6	98.9	99.1	98.5

[T] denotes type species for a given genus

[R] denotes reference strain for a given species

[1]The current names assigned to strains WH 8902 ("Cyanothece sp.") and HBC6 ("Aphanocapsa sp.") are not considered to be indicative of the strains' true generic identities.

APPENDIX A. MORPHOLOGICAL DESCRIPTIONS OF ALL CYANOBACTERIAL STRAINS ISOLATED

GTM1

Filamentous. Thallus a network of macroscopic, prostrate filaments, initially greyish-green to greyish-brown in color, later becoming yellowish-brown.

Individual filaments (meaning individual ensheathed trichomes) mostly gathered into pseudobranched fascicle-like colonies, with filaments more or less parallel to one another and/or entangled, or occasionally rope-like coiled; false branching more or less sparse. Trichomes ensheathed; sheaths colorless, often lengthwise lamellated (layered), apparently sometimes containing bits of precipitate; sheath layers usually more or less firm and thin, sometimes slightly widened and mucilaginous, sometimes appearing ragged. Probably also with irregularly layered outer sheath and/or common mucilage surrounding fascicle-like colonies. Trichomes more or less straight to curved or slightly waved, often slightly attenuated near ends, unconstricted at cell crosswalls. Trichomes immotile or with nearly imperceptible gliding/creeping motility. Cells discoid, 14.2-18.1 μm wide by 2.5-4.5 μm long; cell content yellow-brown to greyish yellow-brown, finely granular, without aerotopes. End cells widely rounded or narrowed and rounded; sometimes with thickened outer cell wall, occasionally calyptrate.

Reproduction by trichome fragmentation into sometimes motile hormogonia, with necridia; entire trichomes sometimes disintegrating into hormogonia. Hormogonia often with a characteristic appearance: attenuated and calyptrate at both ends, short and lemon-shaped or somewhat longer and with an elongated-elliptical shape, similar in outline to a *Navicula*-like diatom frustule. Heterocytes and akinetes absent.

GTM4

Filamentous. Thallus a network of macroscopic, prostrate, filaments, initially greyish-green to greyish-brown in color, later becoming yellowish-brown.

Individual filaments (meaning individual ensheathed trichomes) mostly gathered into pseudobranched fascicle-like colonies, with filaments more or less parallel to one another and/or entangled; false branching more or less sparse. Trichomes ensheathed; sheaths colorless, firm and thin or somewhat mucilaginous and widened, sometimes lengthwise lamellated (layered), apparently sometimes containing bits of precipitate. Probably also with irregularly layered outer sheath and/or common mucilage surrounding fascicle-like colonies. Trichomes straight to curved, sometimes slightly attenuated near ends, unconstricted at cell crosswalls, immotile. Cells discoid, 14.7-18.0 μm wide by 2.3-5.3 μm long; cell content yellow-brown to greyish-brown or greyish-green, finely granular, without aerotopes. End cells mostly widely rounded, sometimes narrowed and rounded; sometimes with thickened outer cell wall, occasionally calyptrate.

Reproduction by fragmentation of trichomes into sometimes motile hormogonia, with necridia; entire trichomes often disintegrating into numerous few-celled hormogonia. Heterocytes and akinetes absent.

GTM7

Filamentous. Thallus a network of macroscopic, prostrate, filaments, initially greyish-green to greyish-brown in color, later becoming yellowish-brown.

Individual filaments (meaning individual ensheathed trichomes) mostly gathered into pseudobranched fascicle-like colonies, with filaments more or less parallel to one another and/or entangled; false branching more or less sparse. Trichomes ensheathed; sheaths colorless, more or less firm and thin or somewhat mucilaginous and widened, sometimes lengthwise lamellated (layered), apparently

sometimes containing bits of precipitate. Probably also with irregularly layered outer sheath and/or common mucilage surrounding fascicle-like colonies. Trichomes straight to curved, sometimes slightly attenuated near ends, unconstricted at cell crosswalls. Trichomes immotile or occasionally with very slow, creeping movement. Cells discoid, 13.3-18.7 μm wide by 2.3-4.4 μm long; cell content yellow-brown to greyish-olive-green, finely granular, without aerotopes. End cells mostly widely rounded, sometimes narrowed and rounded; sometimes with thickened outer cell wall, occasionally calyptrate.

Reproduction by fragmentation of trichomes into sometimes motile hormogonia, with necridia; entire trichomes often disintegrating into numerous few-celled hormogonia. Heterocytes and akinetes absent.

GTM2

Filamentous. Thallus initially in the form of a fine, thin layer, later with irregularly waved filaments visible (macroscopic) throughout, not forming distinct coils/spirals; thallus bright blue-green at first, later becoming more olive-green.

Filaments solitary, in culture loosely and irregularly aggregated; sometimes arranged more or less parallel in bundles of numerous filaments surrounded by common mucilage. Trichomes with very thin, firm, colorless sheaths. Trichomes narrow, short or long, mostly more or less straight to curved or sometimes slightly wavy, not attenuated near ends, mostly unconstricted at crosswalls or sometimes slightly constricted. Trichomes with gliding motility, sometimes also with waving/bending. Cells cylindrical to very slightly barrel-shaped, 1.7-2.0 μm wide by 2.5-4.8 μm long, mostly longer than wide (2-2.5 times longer than wide), sometimes almost isodiametric (slightly longer than wide). End cells rounded to roundly flattened. Cell content blue-green, mostly homogeneous, without aerotopes; usually with one or two prominent granules, mostly localized near cell crosswalls.

Reproduction by trichome fragmentation, without necridia. Heterocytes and akinetes absent.

GTM3

Filamentous. Thallus fine and diffuse, spreading on surface of agar and into agar, not forming a compact mat; initially bright blue green, later becoming olive-green to dirty yellowish-brown.

Filaments loosely entangled or gathered into fairly thin, irregularly anastomosing fascicle-like bundles. Filaments (not fascicles) mostly unbranched; occasionally with double (geminate) or single false branching. Trichomes with firm, thin, colorless sheaths. Trichomes mainly long and many-celled, irregularly curved, bent, or waved, not attenuated or only very slightly attenuated at the ends, unconstricted or sporadically constricted at cell crosswalls. Trichomes immotile or with nearly imperceptible gliding/creeping motility. Cells 4.3-5.9 μm wide by 2.1-6.7 μm long, mostly more or less isodiametric, or shorter or longer than wide (from 0.4-1.3 times longer than wide), cylindrical to slightly barrel-shaped or sometimes distinctly shortly barrel-shaped; actively dividing cells tending to be shorter than wide. End cells rounded or narrowed and conical-rounded; last 1-3 cells in a trichome often yellowish-brown. Cell content mostly blue-green, sometimes olive-green to yellowish-green, finely granular, without aerotopes, sometimes with distinguishable chromatoplasma and centroplasma.

Reproduction by fragmentation of trichomes into hormogonia, sometimes only 1-2 cells long; necridia present; pale yellowish cell remnants, usually resembling contracted and/or irregularly-shaped cells, are sometimes visible between trichome fragments. Heterocytes and akinetes absent.

GTM12

Filamentous. Thallus a somewhat diffuse, spreading layer of irregularly anastomosing filaments, occasionally forming coils, not forming a compact mat; filaments becoming thicker and more mucilaginous-looking with age; bright blue-green initially, later becoming dirty olive- or yellowish-green.

Filaments loosely and irregularly aggregated and entangled, or gathered in irregular elongate clusters, or arranged in irregularly anastomosing fascicle-like bundles of several to many filaments; filaments in bundles arranged more or less parallel to one another or somewhat rope-like coiled. Trichomes with very thin, firm, colorless sheaths (mainly visible only where sheaths are empty). Trichomes narrow, short or long, irregularly curved, bent, or wavy, slightly to distinctly constricted at crosswalls, sometimes attenuated near ends. Trichomes somewhat motile, with occasional bending/waving motility. Cells 1.7-2.8 μm wide by 3.3-6.3 μm long, mostly 1.5-3 times longer than wide, sometimes almost isodiametric (slightly longer than wide), cylindrical to slightly barrel-shaped; sometimes not of uniform size and shape along length of trichome. End cells rounded, or narrowed and bluntly pointed, or sometimes narrowed and slightly bent. Cell content pale blue-green to greyish olive-green, often with distinguishable chromatoplasma and centroplasma.

Reproduction by fragmentation of trichomes into variably long or short hormogonia, sometimes only 1-2 cells long; necridia absent; colorless to pale yellowish-brown remnants of cells often visible between trichome fragments. Heterocytes and akinetes absent.

GTM13

Filamentous. Thallus a somewhat diffuse, spreading layer of irregularly anastomosing filaments, occasionally forming coils, not forming a compact mat; filaments becoming thicker and more mucilaginous-looking with age; bright blue-green initially, later becoming dirty olive- or yellowish-green.

Filaments loosely and irregularly aggregated and entangled, or arranged in irregularly anastomosing fascicle-like bundles of several to many filaments; filaments in bundles arranged more or less parallel to one another, or sometimes densely rope-like coiled. Trichomes with very thin, firm, colorless sheaths (mainly visible only where sheaths are empty). Trichomes narrow, short or long, irregularly curved, bent, or wavy, slightly to distinctly constricted at crosswalls, sometimes attenuated near the ends. Trichomes motile, with bending/waving motility, possibly also with very slow creeping/gliding motility. Cells cylindrical to slightly barrel-shaped, 2.2-2.8 μm wide by 2.7-5.9 μm long, longer than wide (up to 2.3 times longer than wide) to nearly isodiametric (only slightly longer than wide); sometimes not of uniform size and shape along length of trichome. End cells rounded, or narrowed and bluntly pointed, or narrowed and distinctly bent. Cells pale blue-green (or vibrant blue-green in younger cultures) to greyish olive-green, often with distinguishable chromatoplasma and centroplasma.

Reproduction by fragmentation of trichomes into variably long or short hormogonia, sometimes only 1-2 cells long; necridia absent; occasionally with colorless to pale yellowish-brown remnants of cells visible between trichome fragments. Heterocytes and akinetes absent.

GTM5

Coccoid. In culture, thallus initially forming bright blue-green to green spots and/or films on surface of agar, later aggregating into larger, more or less hemispherical, dark blue-green, gelatinous-looking masses.

Cells aggregated in mostly amorphous colonies, occasionally somewhat lobate or clathrate. Cells in colonies somewhat densely to very densely aggregated, irregularly arranged or sometimes exhibiting an indistinct parallel row-like arrangement; in smaller colonies and near margins of larger colonies, cells are often closely and irregularly arranged in a sheet-like single layer. Cells sometimes loosely arranged in short chains, mostly evident only near colony borders or in very small colonies. Colonial mucilage colorless, usually indistinct (only visible with staining); large masses of cells occasionally with distinctly delimited, slightly widened common mucilage. Cells more or less spherical to oval or widely cylindrical with rounded ends, 1.9-3.5 μm wide by 2.7-4.7 μm long (dividing cells up to 5.3 μm long), without

individual mucilaginous envelopes. Cell content blue-green, sometimes with one to a few solitary granules.

Cells divide by binary fission in a single plane, transverse to long axis of the cell; cells sometimes in pairs following division.

GTM6

Coccoid. In culture, thallus forms very dark blue-green (nearly black) masses on surface of agar; masses irregularly hemispherical, with a warty or bumpy texture and irregular margins.

Cells of markedly different shapes/sizes, and associated with somewhat different colony structures or other morphological characteristics, have been observed; these forms probably represent different phases of the growth cycle and/or are related to overall age and condition of the culture. The relationships between these various forms are presently unclear (e.g., which forms represent younger colony stages and which represent older colony stages), so the most commonly observed form is described first and in the most detail, and the less frequently observed forms are described briefly in separate paragraphs; the less frequent forms are described largely in terms of their morphological differences compared to the most frequently observed form.

Cells mostly in irregular, formless colonies, consisting of aggregations of cells or small 2-4-8-celled groups. Cells or small groups of cells surrounded by mucilaginous envelopes with clearly delimited margins; common mucilage surrounding groups of cells usually indistinctly to distinctly concentrically layered, with inner layers more or less following the cell outline; colorless or yellowish-brown, and in the latter case sometimes with a rough or bumpy-looking outer surface. Cells mostly oval to rounded-cylindrical, sometimes subspherical, 2.7-4.1 μm wide by 3.6-5.2 μm long. Cell content blue-green, often vividly so; sometimes with one to several very prominent granules in cells surrounded by yellowish-brown envelopes. Cell division in multiple planes, either regular or irregular, likely sometimes in planes perpendicular to one another.

Observed in young cultures (8 days old) only: cells sometimes fairly loosely aggregated in formless colonies, with cells irregularly arranged in a sheet-like single layer; cells in these colonies are not in 2-4-8-celled groups, and sheet-like arrangement is mainly apparent only in small colonies or near margins of larger colonies (similar to strain AHGTM5). Small irregularly rounded colonies consisting of cells very tightly packed together were also observed in young cultures.

Cells sometimes markedly more elongate than usual (up to 7.7 μm long) and kidney-bean shaped, with more olive- to yellow-green cell content (not vivid blue-green). Cells of this shape are not in distinct groups of 2-4-8 cells, and are sometimes tightly packed together in small irregularly-shaped colonies, usually with scarcely discernible to indiscernible (or absent) mucilaginous envelopes around cells within these small colonies.

Cells sometimes more irregularly and variably shaped; hemispherical, somewhat pyriform, or irregular polygonal-rounded, with dividing cells sometimes gently tapered-pointed at the ends. Cells of this form are aggregated in small to large, irregular, formless colonies, consisting of cells or small packet-like groups of cells, but without cells in distinct groups of 2-4-8. Mucilaginous envelopes around cells or small packet-like groups of cells in these colonies are sometimes clearly discernible, otherwise indistinct (or absent), and are always colorless.

GTM10

Coccoid. Initially forming more or less flat (slightly raised) spots on substrate, roughly circular to irregularly rounded in outline, spots later becoming continuous with one another and forming a somewhat granular-looking and crust-like layer on agar; initially greyish-brownish-green to slightly purplish-brown, later becoming paler reddish-brown to greyish-orange.

Cells mainly in colonies, only rarely occurring as irregularly and sparsely dispersed solitary cells (likely in early/initial growth stages); may occasionally form pseudofilaments (also early/initial form?). Colonies dome-like, more or less circular to irregularly rounded in outline, later becoming continuous with one another; colonies sometimes appear somewhat crust-like, with visible cracks/fractures in the colony. Cells densely and irregularly aggregated in colonies, possibly arranged in one or more (not uniform) layers; a somewhat linear or row-like arrangement of cells (or their empty sheaths?) within colonies is sometimes distinguishable. Colonies greyish blue-green, yellowish-brown, or pale reddish-brown to yellowish-grey in color, often with concentrically arranged (ring-like) regions of different coloration; colony color sometimes different at the margin than at the center, other times with multiple concentrically arranged regions.

Cells mostly spherical, (2.4?)3.0-6.7(9?) μm in diameter, with firm colorless sheaths. Cell content pale blue-green, greyish olive-green, or greyish-reddish-brown, sometimes very pale. Cell division pattern requires further observation; apparently divides mainly by binary fission in multiple planes in successive generations, forming a relatively small number of baeocytes which are liberated by rupturing (or gelatinization?) of the surrounding sheath, less commonly (only in certain parts of colonies?) with numerous baeocytes formed by enlarged cells. Unreleased baeocytes 1.4-1.9 μm wide by 2.0-2.4 μm long. Sheaths surrounding dividing cells (or surrounding baeocytes) sometimes slightly elongate and widened at one end, somewhat pyriform or cup-shaped. The occurrence of many cup-shaped to pyriform sheaths (possibly empty) prominently visible in some parts of colonies may indicate that different types of cell division prevail in certain parts of colonies.

Note: due to slow growth rate in culture, all observations come from cultures ~120-260 days old.

GTM14

Coccoid. Initially forming small flat to slightly raised specks or spots on agar, dark greyish-green in color, later becoming larger, slightly raised, roughly spherical in outline, and reddish-orange to orange-brown in color; later also forming a somewhat crust-like layer of growth on agar, pale yellowish-green to yellowish-brown in color.

Cells in younger cultures sparsely dispersed to densely aggregated in amorphous colonies; in older cultures attached to the substrate and arranged in a single layer in circular colonies, with colonies becoming continuous in places, forming a sheet-like layer of cells, or (also in older cultures) very densely aggregated in larger, possibly layered(?) masses. Cells spherical, variable in size, up to 14.8 μm in diameter, in colonies flattened along points of contact with neighboring cells; cells are possibly slightly narrowed at one-end, but this is usually not evident if it is the case. Cells with firm, thin, colorless mucilaginous envelopes. Cell content homogeneous to very finely granular, greyish blue-green to greyish-brown or purplish-grey in younger cultures, pale yellowish-brown to pale greyish-gold in older cultures. Baeocytes frequently produced, 2.0-3.3 μm in diameter, liberated by splitting (or sometimes gelatinization?) of the surrounding sheath; form of cell division may be exclusively baeocytic division (successive rounds of binary fission).

GTM15

Coccoid. Initially forming small flat to slightly raised specks or spots on agar, dark greyish-green in color, later becoming larger, slightly raised, roughly spherical in outline, and reddish-orange to orange-brown in color; later also forming a somewhat crust-like layer of growth on agar, pale yellowish-green to yellowish-brown in color, with the edge of the thallus having a darker purplish-brown color.

Cells in younger cultures sparsely dispersed to densely aggregated in amorphous colonies; in older cultures attached to the substrate and arranged in a single layer in circular colonies, with colonies

becoming continuous in places, forming a sheet-like layer of cells, or (also in older cultures) very densely aggregated in larger, possibly layered(?) masses. Cells spherical, variable in size, up to 16.2 μm in diameter, in colonies flattened along points of contact with neighboring cells; cells are possibly slightly narrowed at one-end, but this is usually not evident if it is the case. Cells with firm, thin, colorless mucilaginous envelopes. Cell content homogeneous to very finely granular, greyish blue-green to greyish-brown or purplish-grey in younger cultures, pale yellowish-brown to pale greyish-gold in older cultures. Baeocytes frequently produced, 1.8-3.6 μm in diameter, liberated by splitting (or sometimes gelatinization?) of the surrounding sheath; form of cell division may be exclusively baeocytic division (successive rounds of binary fission).

GTM19

Coccoid. Forms small dark spots on substrate, eventually aggregating into larger, irregularly clumpy masses, very dark greyish-brown to essentially black in color.

Colonial. Colonies orange- to reddish-brown, sometimes greyish blue-green in parts furthest from the outer colony margins; mostly compound, consisting of very compact sub-colonies or distinct segments, not easily disintegrating into sub-colonies; (compound) colonies mostly irregularly rounded in outline overall when viewed from above. Firm, thin, colorless mucilaginous envelopes surrounding colony segments and/or entire colonies. When viewed from above, colony segments are mostly rounded in outline along their free edges and flattened along edges in contact with adjacent segments, with adjacent segments usually very close together; cells in each segments are very closely appressed to one another, usually more or less regularly arranged and with a distinct or indistinct tabular (*Merismopedia*-like) appearance. When viewed in cross-section, colony segments appear to be radially arranged to some degree and narrowed towards the colony center; cells in each colony segment also appear to be situated in closely adjacent, radially oriented, irregular rows, such that colonies have an overall fan-like appearance when viewed in cross-section.

Cells 2.2-5.1 μm wide by 3.4-6.7 μm long; cells in colonies more or less hemispherical or in the form of a segment of a sphere (flattened on two sides), rounded-polygonal, or nearly rectangular in outline, flattened at sides adjacent to neighboring cells; with firm, thin, colorless mucilaginous envelopes. Cell content mostly greyish yellow- to orange-brown to greyish olive-green, or more greyish blue-green near the center/base of some colonies; more or less homogeneous to somewhat granular.
Solitary cells and small, more or less cubic, packet-like groups of cells liberated/dissociated from within larger (compound) colonies; probably mode of colony reproduction. Cells divide in three or more planes, roughly perpendicular to each other or at irregular angles with respect to each other; possibly in three perpendicular planes in initial divisions (yielding small cubic groups of cells). Baeocytes not observed.

Note: due to very slow growth rate in culture, all observations come from cultures ~150 days old.

GTM20

Coccoid. Forms small, greyish blue-green spots/specks on substrate, eventually aggregating into larger, irregularly clumpy masses, very dark blue-green to almost black in color.

Colonial. Colonies blue-green to green in color, becoming yellowish with age, mostly irregularly rounded to subspherical or spherical; usually compound, composed of segments or sub-colonies, but easily disintegrating into smaller sub-colonies; colonies later becoming aggregated together. When viewed from above, colony segments are mostly rounded in outline along their free edges and flattened along edges bordering adjacent segments; cells in each segment are mostly closely appressed to one another, more or less regularly arranged and with a somewhat distinct or indistinct tabular (*Merismopedia*-like) appearance, later becoming more irregularly arranged. When colonies (or

dissociated segments of colonies) are viewed in cross-section, cells appear to be situated in closely adjacent, radially oriented, irregular rows; rows appear narrower towards the colony center and become widened into double rows or quadruple rows, becoming somewhat lobe-like near colony margin; colony segments have an overall fan-like appearance.

Cells with colorless, more or less thin and delimited or slightly diffluent mucilaginous envelopes; similar mucilaginous envelopes occasionally visible around whole colonies or sub-colonies as well. Cells sometimes spherical, more often hemispherical or in the form of a segment of a sphere (flattened on two sides), or rounded-polygonal to nearly rectangular in outline, flattened at sides adjacent to neighboring cells; 3.1-7.7 μm wide by 3.8-10.1 μm long. Cell content greyish blue-green to blue-green, more or less homogeneous to somewhat granular.

Cells appear to be able to divide in three or more planes, roughly perpendicular to each other or at irregular angles with respect to each other. Baeocytes not observed. Reproduction probably by disintegration of colonies; small numbers of solitary cells occasionally observed, possibly liberated/dissociated from larger colonies as a form of colony reproduction.

Note: due to very slow growth rate, all observations come from cultures ~150 days old.

GTM21

Coccoid. Forms small, greyish blue-green spots/specks on substrate, eventually aggregating into larger, irregularly clumpy masses, very dark blue-green to almost black in color.

Colonial. Colonies blue-green to green in color, becoming yellowish with age, mostly irregularly rounded to subspherical or spherical; usually compound, composed of segments or sub-colonies, but easily disintegrating into smaller sub-colonies; colonies later becoming aggregated together. When viewed from above, colony segments are mostly rounded in outline along their free edges and flattened along edges bordering adjacent segments; cells in each segment are mostly closely appressed to one another, more or less regularly arranged and with a somewhat distinct or indistinct tabular (*Merismopedia*-like) appearance, later becoming more irregularly arranged. When colonies (or dissociated segments of colonies) are viewed in cross-section, cells appear to be situated in closely adjacent, radially oriented, irregular rows; rows appear narrower towards the colony center and become widened into double rows or quadruple rows, becoming somewhat lobe-like near colony margin; colony segments have an overall fan-like appearance.

Cells with colorless, more or less thin and delimited or slightly diffluent mucilaginous envelopes; similar mucilaginous envelopes occasionally visible around whole colonies or sub-colonies as well. Cells sometimes spherical, more often hemispherical or in the form of a segment of a sphere (flattened on two sides), or rounded-polygonal to nearly rectangular in outline, flattened at sides adjacent to neighboring cells; 3.8-7.6 μm wide by 5.0-7.9 μm long. Cell content greyish blue-green to blue-green, more or less homogeneous to somewhat granular.

Cells appear to be able to divide in three or more planes, roughly perpendicular to each other or at irregular angles with respect to each other. Baeocytes not observed. Reproduction probably by disintegration of colonies; small numbers of solitary cells occasionally observed, possibly liberated/dissociated from larger colonies as a form of colony reproduction.

Note: due to very slow growth rate, all observations come from cultures ~150 days old.

GTM22

Coccoid. Forms small, greyish blue-green spots/specks on substrate, eventually aggregating into larger, irregularly clumpy masses, very dark blue-green to almost black in color.

Colonial. Colonies blue-green to green in color, becoming yellowish with age, mostly irregularly rounded to subspherical or spherical; usually compound, composed of segments or sub-colonies, but easily disintegrating into smaller sub-colonies; colonies later becoming aggregated together. When viewed from above, colony segments are mostly rounded in outline along their free edges and flattened along edges bordering adjacent segments; cells in each segment are mostly closely appressed to one another, more or less regularly arranged and with a somewhat distinct or indistinct tabular (*Merismopedia*-like) appearance, later becoming more irregularly arranged. When colonies (or dissociated segments of colonies) are viewed in cross-section, cells appear to be situated in closely adjacent, radially oriented, irregular rows; rows appear narrower towards the colony center and become widened into double rows or quadruple rows, becoming somewhat lobe-like near colony margin; colony segments have an overall fan-like appearance.

Cells with colorless, more or less thin and delimited or slightly diffluent mucilaginous envelopes; similar mucilaginous envelopes occasionally visible around whole colonies or sub-colonies as well. Cells sometimes spherical, more often hemispherical or in the form of a segment of a sphere (flattened on two sides), or rounded-polygonal to nearly rectangular in outline, flattened at sides adjacent to neighboring cells; 3.4-6.6 μm wide by 3.8-7.9 μm long. Cell content greyish blue-green to blue-green, more or less homogeneous to somewhat granular.

Cells appear to be able to divide in three or more planes, roughly perpendicular to each other or at irregular angles with respect to each other. Baeocytes not observed. Reproduction probably by disintegration of colonies; small numbers of solitary cells occasionally observed, possibly liberated/dissociated from larger colonies as a form of colony reproduction.

Note: due to very slow growth rate in culture, all observations come from cultures ~150 days old.